# UNDERSTANDING ACTIN FUNCTION DURING CYTOKINESIS IN FISSION YEAST

**JUNQI HUANG**

B.Sc., Sun Yat-sen University

**A THESIS SUBMITTED FOR THE DEGREE OF DOCTOR OF PHILOSOPHY**

**DEPARTMENT OF BIOLOGICAL SCIENCES**

**NATIONAL UNIVERSITY OF SINGAPORE**

**2013**

## DECLARATION

I hereby declare that the thesis is my original work and it has been written by me in its entirety. I have duly acknowledged all the sources of information which have been used in the thesis.

This thesis has also not been submitted for any degree in any university previously.

_____

Junqi Huang

21st February 2014

## ACKNOWLEDGEMENTS

I would like to express the depth of my gratitude to my supervisor *Prof.* Mohan Balasubramanian, for giving me the precious opportunity to study in his laboratory, leading my way in the science world with his everlasting enthusiasm and always inspiring me with his great wisdom. I appreciate it more than any word could express.

I would also like to take this opportunity to thank Dr. Xie Tang, for teaching me plenty of experiments when I joint the lab four years ago without any experience in doing science. His infinite diligence and scrupulousness keep on encouraging me to do better in my experiments.

I am also much obliged to Dr. Yinyi Huang. Her conscientiousness and diligence always reminds me the important character of a good scientist. It was a great pleasure working, studying and discussing with her. Many thanks for her contribution to the lifeact project.

I am extremely grateful to my good friend and lab member Ms. Dhivya Subramanian. She helped me a lot in and outside my PhD study. Without her help, I would not have reached so far.

My sincere appreciation also goes to *Prof.* Roland Wedlich-Soldner and Dr. Haochen Yu. Their discussions and suggestions really helped a lot in the lifeact project. I would like to specially thank *Prof.* Roland Wedlich-Soldner for helping and teaching me image-processing techniques.

Another special thank to my QE thesis committee members (Dr. Snezhana Oliferenko, Dr. Uttam Surana and Dr. Davis Ng), their supervision and suggestions really aided my PhD studies.

I am indebted to all the past and current members of the cell division lab for their helpful discussions, especially Mr. Sevugan Mayalagu for his help in some of the experiments and Dr. Meredith Calvert for teaching me some

imaging techniques. I also gratefully acknowledge National University of Singapore and Department of Biological Sciences for the scholarship and Temasek Life Sciences Laboratory.

Many thanks to Dr. Yinyi Huang, Dr. Singh Nongmaithem Sadananda, Dr. Ramanujam Srinivasan, Dhivya Subramanian, Shao Nan and Yaqiong Tao for critical reading of this thesis.

Finally, I want to specially thank my families. My parents (Father: Jinren Huang & Mother: Qiuying Huang) always taught me to be a good man and earn things through my own hard work. Their unconditional support has filled my life with love. I would like to thank my grandparents (Gengjiu Huang, Pengchang Huang, Amei Chen, Ying Chen) for their love and care when I was a kid. And I want to thank my little brother (Gongyi Huang) who sacrificed a lot and supports me as always. Lastly, I also much appreciate Shuiqing Lai for her support in the last seven years.

Without all these people, I would not have accomplished my PhD study.

## TABLE OF CONTENTS

## SUMMARY

Many eukaryotes utilize a conserved actomyosin based contractile ring for cell division. How actin filaments of the actomyosin ring are nucleated/assembled at the division site remains poorly understood. In recent years fission yeast *Schizosaccharomyces pombe* has emerged as an attractive model organism to study actomyosin ring dependent cytokinesis. In this thesis, a recently developed technology named lifeact was applied to study fission yeast F-actin dynamics. Moreover, a novel fission yeast actin mutant *act1*-j28 was recovered from a reverse genetic screen and was characterized to aid further understanding of actin function during cytokinesis. Previous work suggested that F-actin for cytokinesis was nucleated *de novo* at the division site in fission yeast. However, our analysis showed that a significant fraction of F-actin was recruited from formin-Cdc12p nucleated F-actin cables located throughout the cell and these actin cables migrated towards the cell middle in a type II (Myo2p) and type V myosin (Myo51p) dependent manner. In a complementary approach to understand actin assembly during cytokinesis, we isolated a bank of fission yeast actin mutants. Partial characterization of one of these, *act1*-j28, is reported in this thesis. A high copy suppressor screen identified a putative 12 transmembrane protein as a suppressor of *act1*-j28. Interestingly, this suppressor protein Aap1p localized to a ring-like structure during cytokinesis in fission yeast. Taken together, by studying mitotic F-actin dynamics and characterizing a novel actin mutant *act1*-j28, this thesis assists further understand actin assembly during cytokinesis.

## LIST OF TABLES

## LIST OF FIGURES

## LIST OF ILLUSTRATIONS

## LIST OF ABBREVIATIONS

**ade-,** Edinburgh minimal medium without adenine

**AOTF,** acousto-optic tunable filter

**atb2,** tubulin alpha 2

**CHD,** calponin homology domain

**DPSS,** diode pumped solid state

**dd$H_2O$,** double-distilled water

**EM,** electron microscopy

**EMM,** Edinburgh minimal medium

**F-BAR,** FCH (Fer and CIP4 Homology) and BAR (Bin1 Amphiphysin Rvs161/167p)

**FRAP,** fluorescence recovery after photobleaching

**his-,** Edinburgh minimal medium without histidine

**HU,** hydroxyurea

**LA,** Lifeact

**LAGFP,** Lifeact-GFP

**LAmCh,** Lifeact-mCherry

**LatA,** Latrunculin A

**leu-,** Edinburgh minimal medium without leucine

**LiAc,** lithium acetate

**µM,** micromolar

**mCh,** mCherry

**mGFP,** monomeric GFP

**P*act1*,** act1 promoter

**PEG,** polyethylene glycol

**Pfu,** Pfu DNA polymerase

**P*nmt*,** nmt promoter

**rlc1,** myosin II regulatory light chain

**SIN,** septation initiation network

**TE,** Tris-EDTA

**TIRF,** total internal reflection

**UCS,** UNC-45/CRO1/She4

**ura-,** Edinburgh minimal medium without uracil

**Utr-CH,** calponin homology domain of utrophin

**VALAP,** vaseline, lanolin and paraffin

**wt,** wild-type

**YES,** yeast extract with supplements

**YPD,** yeast extract-peptone-dextrose

## LIST OF PUBLICATIONS

**Huang J***, Huang Y*, Yu H, Subramanian D, Padmanabhan A, Thadani R, Tao Y, Tang X, Wedlich-Soldner R, Balasubramanian MK. 2012. Nonmedially assembled F-actin cables incorporate into the actomyosin ring in fission yeast. *The Journal of Cell Biology*. 199(5):831-47. (*** Equal Contribution; Article; Highlighted by the journal in text and biosights video**)

Subramanian D*, **Huang J***, Sevugan M, Robinson RC, Balasubramanian MK, Tang X. 2013. Insight into Actin Organization and Function in Cytokinesis from Analysis of Fission Yeast Mutants. *Genetics*. 194:435-446. (*** Equal Contribution; Article**)

Tang X, **Huang J**, Padmanabhan A, Bakka K, Bao Y, Tan BY, Cande WZ, Balasubramanian MK. 2011. Marker reconstitution mutagenesis: a simple and efficient reverse genetic approach. *Yeast*. 28(3):205-12. (**Article**)

Mishra M, **Huang J**, Balasubramanian MK. 2014. The Yeast Actin Cytoskeleton. FEMS Microbiol Rev. doi: 10.1111/1574-6976.12064. (**Review**)

# CHAPTER I GENERAL INTRODUCTIONS

## 1.1 OVERVIEW OF CELL DIVISION AND CYTOKINESIS

### 1.1.1 Cell division

Cell division is a complicated proliferation process during which a cell is divided into two nascent daughter cells. Cell division happens in every organism but differs in detail (e.g. timing and assembly of the physical apparatuses) from one species to another (Balasubramanian et al., 2012; Bennett, 1977; Pollard and Wu, 2010). In spite of the differences, cell division contains many common steps such as DNA replication and segregation, redistribution of cytoplasmic materials, membrane deposition and scission. According to the reproductive cycle stage, eukaryotic cell division can be categorized into mitotic cell division and meiotic cell division (Miller et al., 2013). Cell division can also be grouped into symmetric cell division or asymmetric cell division based on the spatial relationship between the division site and cell center (Gomez-Lopez et al., 2013; Li, 2013). Furthermore, cell division in polarized cells could be classified into longitudinal binary fission and transverse binary fission, depending on the relationship between division plane and cell long axis (Peckova and Lom, 1990). Cell division is important for the growth, development, proliferation as well as the evolution of an organism. During cell division, mitotic or meiotic recombination could occur hence may promote species evolution (Didelot and Maiden, 2010). In summary, cell division is a complicated but important process essential for all living organisms.

### 1.1.2 Cytokinesis

Cytokinesis is the last step of the cell division cycle in which a cell positions and assembles a physical apparatus to partition two prospective daughter cells following chromosome segregation. Although cytokinesis machineries are different from one organism to another, it is highly ordered and strictly controlled. Orchestration between cytoskeleton, genetic material and cell cycle events are required for successful and efficient cytokinesis. Additional cellular processes such as membrane trafficking, lipid metabolism and protein synthesis are also important for cytokinesis (Normand and King, 2010). Most

of the eukaryotic cells assemble and constrict an actomyosin based contractile ring to split the daughter cells whereas plant and some prokaryotic cells utilize microtubules or microtubule-like proteins to execute cytokinesis (Balasubramanian et al., 2012). Failure in cytokinesis could lead to serious problems for the living organism, such as production of tetraploid cells, centrosome amplification and development of cancer (Fujiwara et al., 2005; Normand and King, 2010). Although cytokinesis has been studied for around half a century and a lot has been achieved (Duraiswami, 1953; Pollard and Wu, 2010), more work is yet to be done in the future to understand the exact mechanism regulating cytokinesis.

## 1.2 CYTOKINESIS IN DIFFERENT ORGANISMS

### 1.2.1 Cytokinesis in budding yeast

Budding yeast *Saccharomyces cerevisiae* is a round/ovoid shape microorganism which undergoes asymmetric cell division known as budding. During cytokinesis, budding yeast assembles an actomyosin based contractile ring at the division site (also called bud neck). Proteins in the budding yeast actomyosin ring are highly conserved and have counterparts in other eukaryotic cells (Balasubramanian et al., 2004). Bni1 and Bnr1 are two budding yeast formins essential for linear actin filament nucleation and actomyosin ring assembly (Wloka and Bi, 2012). While both formins play a role in actin ring assembly, Bni1 is more crucial for this process (Vallen et al., 2000). Interestingly, myosin II motor activity is not essential for cytokinesis in budding yeast as cytokinesis can happen in mutants lacking the motor domain of myosin II (Lord et al., 2005; Mendes Pinto et al., 2012). Primary septum formation, which eventually divides the cell, may also contribute to cytokinetic force generation in budding yeast (Schmidt et al., 2002).

### 1.2.2 Cytokinesis in animals

In animals, cytokinesis begins in anaphase with the assembly of an actomyosin based, cleavage furrow associated contractile ring (Green et al., 2012; Mabuchi et al., 1988). During anaphase, mitotic spindles have multiple functional regions: central spindles and astral spindles. Signaling between the anaphase spindles and the cell medial cortex recruits the lipid-modified GTP

bound form active RhoA (together with Rac1 and Cdc42 constitute the Rho family proteins in mammalian cells) in the equator of the dividing cell (Jordan and Canman, 2012). Active RhoA together with centralspindlin, CPC (Chromosomal Passenger Complex) and PRC1, promote the assembly of an actomyosin based contractile ring beneath the cell membrane (Green et al., 2012). It is believed that the contraction of the actomyosin based cytokinetic ring results in the ingression of the medial cell membrane and hence forms the cytokinetic cleavage furrow. Interestingly, a substantial number of actomyosin molecules remains outside of the equatorial furrow and are believed to generate resistant forces that regulate furrow ingression (Sedzinski et al., 2011). The final stage of animal cytokinesis after actomyosin ring constriction is called abscission. During abscission, the condensation of the midzone central spindles forms an intercellular bridge between the prospective daughter cells. This ~1 μm wide, 3-5 μm long intracellular structure is known as midbody (Hu et al., 2012; Mullins and McIntosh, 1982). Moreover, membrane abscission in the midbody involves helices of ESCRT-II-dependent filaments (Guizetti et al., 2011).

One major question in animal cytokinesis is how F-actin and myosin accumulate in the cleavage furrow. No directional type II myosin flow is detected during early mitosis and its equatorial localization is believed to be controlled by multiple regulatory pathways (Uehara et al., 2010; Zhou and Wang, 2008). As for F-actin, two prevailing hypotheses are proposed to explain its medial accumulation. The first one is called cortical flow hypothesis (Bray and White, 1988; Cao and Wang, 1990a; Cao and Wang, 1990b; Guha et al., 2005; Zhou and Wang, 2008), in which “pre-existing” F-actin filaments from the cell poles are used preferentially to congregate F-actin in the cleavage furrow. This hypothesis is mainly derived from two sets of experiments. Firstly, injection of rhodamine conjugated phalloidin (to label the pre-existing actin filaments before cytokinesis) into prometaphase or metaphase cells showed medial fluorescence accumulation during cytokinesis. But rhodamine conjugated phalloidin signal was depleted from the poles when these cells proceed into anaphase (Cao and Wang, 1990a; Cao and Wang, 1990b). On the contrary, injection of rhodamine conjugated G-actin shortly

before cytokinesis only led to a slight increase of fluorescence in the contractile ring, suggesting a less pronounced role of *de novo* nucleation in the cell middle (Cao and Wang, 1990a; Cao and Wang, 1990b). Secondly, "pre-existing" actin filaments (labeled by rhodamine-phalloidin, Alexa Fluor 488 phalloidin or fluorophore-actin) are found to translocate towards the cleavage furrow (Alsop et al., 2009; Cao and Wang, 1990b; Chen et al., 2008; Zhou and Wang, 2008). Different from the cortical flow hypothesis, the second hypothesis argues that *de novo* F-actin nucleation also plays a role in animal cytokinesis (Noguchi and Mabuchi, 2001; Zhou and Wang, 2008). Work in *Xenopus* egg cytokinesis seems to support this idea (Noguchi and Mabuchi, 2001). Rhodamine conjugated G-actin was injected away from the cleavage furrow and time-lapse recording was applied in this study. During the first cleavage of the *Xenopus* egg, small F-actin clusters were found at the growing end of the cleavage furrow. These tandem aligned F-actin clusters could grow and merge to form short actin bundles, which later incorporated into the forming actomyosin ring (Noguchi and Mabuchi, 2001). However, the evidence presented in this paper could not rule out the possibility that part of (if not all) these "*de novo* nucleated F-actin structures" are derived from cortical flow of even smaller F-actin structures outside the division plane. Other indirect evidence also support this *de novo* nucleation hypothesis (Zhou and Wang, 2008). In this work, blebbistatin, an inhibitor of myosin motor, seemed to abolish the pre-existing F-actin flow during cytokinesis. Surprisingly, even though actin flow seemed to be inhibited, medial concentration of fluorescent actin filaments (labeled by mCherry-actin) still occurred, indicating a significant role of *de novo* nucleation in the cell middle. However, the time-lapse movies in this experiment were not clear enough to totally rule out the participation of actin flow. Shortly before the accumulation of fluorescent actin signals at the division site, bright signal was observed outside the cleavage furrow and seemed to move towards the middle in the blebbistatin treated cells (supplemental video 9 and 10 in Zhou and Wang, 2008). Interestingly, instead of being mutually exclusive, the experiments above indicate that these two mechanisms may exist/function simultaneously during animal cytokinesis.

### 1.2.3 Cytokinesis in plants and bacteria

Unlike animal cells, higher plants (hereafter called plants for simplicity) do not assemble an actomyosin based contractile ring during cytokinesis. In plants such as *Arabidopsis*, proteins like type II myosin and septin are absent in the genome (Arabidopsis Genome, 2000). Animal cells divide by centripetal ingression of the cleavage furrow. By contrast, cytokinesis in plant somatic cells starts from the center and progress outward laterally. But similar to animal cells, plant cells also utilize protein polymers to execute cytokinesis. In plants, microtubules are used instead of F-actin. At late anaphase, plant cells form a specialized structure called phragmoplast which contains bundles of antiparallel microtubule arrays (Heese et al., 1998; Jurgens, 2005). Vesicles derived from Golgi are transported to the division site and fuse with each other via SNARE proteins to form a structure called cell plate. In later stages, the medially localized cell plate undergoes dramatic maturation and expands laterally towards the peripheral cell wall. This inside-out maturation and reorganization finally separates a cell into two. During plant cytokinesis, a mitogen-activated protein kinase (MAPK) cascade is believed to control the turnover of the microtubules. Interestingly, F-actin is also found in the phragmoplast.

Similar to plants, most bacteria also use microtubule-like protein for cell division. The bacterial tubulin homolog is called FtsZ (the Filamentous temperature sensitive protein Z). FtsZ is a cytosolic GTPase which assembles into short protofilaments (~125 nm) at the edge of constricting bacterial membrane during cytokinesis (Li et al., 2007; Osawa et al., 2008). FtsZ is anchored to the bacteria cell membrane by its C-terminal region, which interacts with different domains of ZipA (an integral membrane protein) and FtsA (a membrane associated protein) (Pichoff and Lutkenhaus, 2002; Pichoff and Lutkenhaus, 2005). Interestingly, unlike eukaryotes, myosin and dynein motor proteins are not identified in bacteria (Mingorance et al., 2010). Surprisingly, FtsZ can self-assemble into ring structures *in vitro* and can constrict without the presence of other proteins, indicating FtsZ conformational changes may be enough for cytokinesis in bacteria (Osawa et al., 2008).

## 1.3 FISSION YEAST AS A MODEL FOR ACTOMYOSIN RING DEPENDENT CYTOKINESIS

Fission yeast *Schizosaccharomyces pombe*, a rod shape single-celled organism was first used in an experiment studying cell cycle in the 1950s (Nurse, 2002). Fission yeast haploid cells are around 12-15 μm in length and 3-4 μm in width, with only three chromosomes (with genome size ~ 12.57 mega base pairs) containing ~5,123 protein coding genes (http://www.pombase.org/). In the past few decades, fission yeast has become a popular model organism for cell biology studies, including cytokinesis. A few but not limited reasons could account for this. First, fission yeast utilizes an actomyosin based contractile ring for cytokinesis, which shares similarity with animal cytokinetic machinery. Second, unlike diploid animal cells in which mutation in one allele could be recessive due to the dominance of the wt allele on the sister chromosome, mutation phenotypes could be easily revealed in the haploid fission yeast cells. Third, easy genetic manipulation allows precise deletion, replacement or ectopic tagging of any protein of interest. Fourth, fission yeast is not motile, making it easy for microscopy imaging. Fifth, whole genome deletion data and whole proteome localization data are available. In all, fission yeast is a good model organism for studying cytokinesis.

## 1.4 ACTIN CYTOSKELETON IN FISSION YEAST

### 1.4.1 Actin patches

Actin patches are one of the prominent F-actin structures commonly found in fungi (Kovar et al., 2011; Waddle et al., 1996). Similar actin patch structures are also found in animal cells (Collins et al., 2011). These sphere-like (around 250 nm in diameter) actin patches are assembled at the endocytotic sites and their distribution is correlated with region of polarized growth (Arai et al., 1998; Waddle et al., 1996; Wu and Pollard, 2005) (see Illustration 1). Studies in budding yeast *Saccharomyces cerevisiae* and fission yeast *Schizosaccharomyces pombe* found that more than 50 proteins are recruited at the sites of endocytosis (Arasada and Pollard, 2011). The patch components arrive in a defined order (Chen and Pollard, 2013; Kaksonen et al., 2003; Kaksonen et al., 2006). Clathrin arrives in actin patches at ~100 s before internalization and forms a coated pit on the inner surface of the cell

membrane (Ferguson et al., 2009; Kovar et al., 2011). After the other early patch components (Ede1, Ent1, Yap1801, Syp1 etc.) are recruited, adaptor proteins (Pan1, Sla1, End3, End4 etc.) arrive at the endocytotic site at ~30-40 s before internalization. Then regulators (Bbc1, Lsb1, Lsb4, Ldb17 etc.) and actin binding proteins (Arp2/3, App1, Fim1, Cdc15, Hob1/3, Acp1 and Acp2 etc.) accumulate to promote invagination and scission of the endocytic vesicle (Kaksonen et al., 2003; Kovar et al., 2011). After internalization, in around 10 s, actin signal would disappear to allow the fusion between vesicle and endosomes (Kovar et al., 2011).

Actin polymerization is found to be important for the formation and movement of these actin patches (Kaksonen et al., 2003; Pelham and Chang, 2001). F-actin filaments on the actin patches are nucleated by Arp2/3 complex, which nucleate a new F-actin filament on another preexisting F-actin filament with an angle of $70^{o}$ (Campellone and Welch, 2010). The existing actin filament may be nucleated by other formins or from the Adf1p-cofilin severed actin patches (Chen and Pollard, 2013; Collins et al., 2011). The length of actin filament on the actin patches is controlled by barbed end capping proteins (Nakano and Mabuchi, 2006a). Molecule counting using fluorescence microscopy and mathematical models suggest that fission yeast actin patch contains ~2,700 actin molecules and ~150 branched F-actin filaments, each around 100-200 nm long (Berro et al., 2010; Wu and Pollard, 2005). By myosin subfragment 1 (myosin S1) decoration, electron microscopy study in cultured mouse cells shows that the actin filament barbed ends are oriented towards the clathrin-coated invagination/vesicle (Collins et al., 2011). Branched actin network may expand and gradually circle around the clathrin-coated pit through multiple cycles of dendritic nucleation. Clathrin-coated invaginations/vesicles may move laterally (not perpendicular to the plasma membrane) at this stage because of the force generated by the laterally positioned branched F-actin network (Collins et al., 2011). The branched actin circles the neck of the deeply invaginated clathrin-coated structure and the continuous polymerization may contribute to the scission of the invaginated tubules (Arasada and Pollard, 2011; Collins et al., 2011).

After formation of the sphere-like actin patches, actin patches become highly dynamic. According to the speed of the moving actin patches, patch movement could be divided into two stages: restrictive movement (slow movement) near the site where the actin patch is formed and long distance movement (higher speed) before they disappear (Kaksonen et al., 2003). Based on the directionality of movement and their relationship with F-actin cables, actin patches movement could be separated into undirected movement in the cytosol and directed movement along F-actin cables (Feierbach and Chang, 2001). But on average, the speed of both movement is similar (fission yeast~0.32 μm/s; budding yeast~0.31 μm/s) (Feierbach and Chang, 2001; Waddle et al., 1996). Studies in budding yeast showed that the movement of actin patches may be independent of myosins but requires the polymerization of F-actin (Feierbach and Chang, 2001; Waddle et al., 1996). The lifetime of a patch varies from 5s to 20 s (Smith et al., 2001; Wu and Pollard, 2005). Interestingly, actin patches depolymerize slower compared to F-actin cables upon LatA treatment (Feierbach and Chang, 2001) and actin patches could be partially purified in budding yeast (Young et al., 2004).

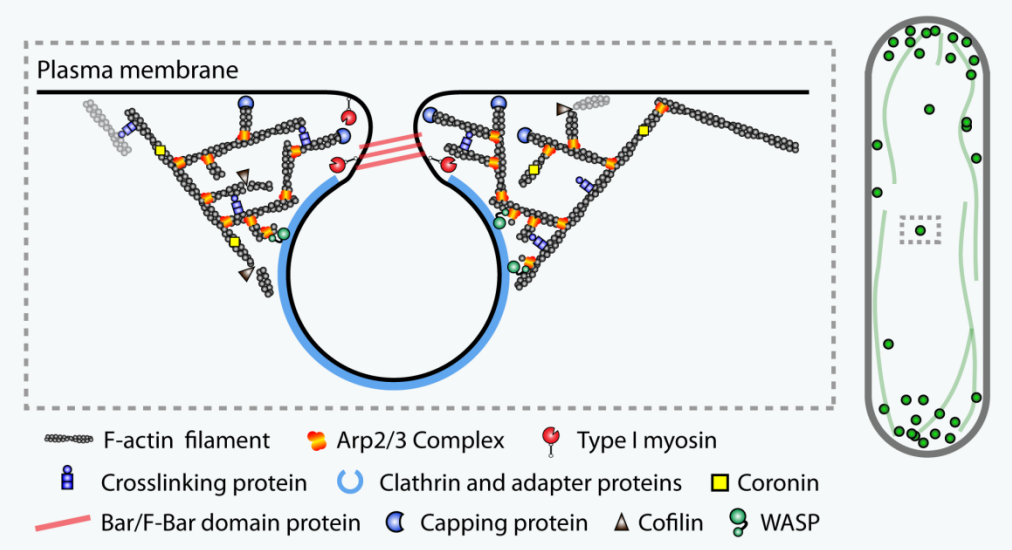


**Illustration 1.** A cross section schematic of an actin patch (modified from Mishra et al, 2014).

Actin filament barbed ends are oriented towards the clathrin-coated invagination/vesicle. Arp2/3 complex nucleates a new F-actin filament on another preexisting actin filament with an angle of 70°. The representation of each component is indicated at the bottom.

### 1.4.2 Actin cables

Actin cables are bundles of short F-actin filaments and are predominantly presented longitudinally in interphase fission yeast cells (Feierbach and Chang, 2001; Kamasaki et al., 2005) (see Illustration 2). Electron microscopy studies in fission yeast have shown that the average thickness of actin cables is ~0.06 µm in wild-type cells and ~0.09 µm in cells synchronized by *cdc25*-22 arrest-release (Kamasaki et al., 2005). Actin cables are two times longer after G2 phase blocking by *cdc25*-22 (Kamasaki et al., 2005). Although actin cables contain F-actin filaments of both directionalities, most filaments are coherent in one direction (Kamasaki et al., 2005). Actin cables are involved in intracellular cargo transport, serving as a track for type V myosins (Lo Presti et al., 2012; Snaith et al., 2011). The barbed ends of most (but not all) F-actin filaments in the interphase actin cables are oriented towards the cell tips, consistent with the tip localization of actin cable nucleator formin-For3p (Kamasaki et al., 2005; Martin and Chang, 2006). EM studies showed that the

direction of actin cables reverses during mitosis, presumable coordinating cell wall material deposition in the division site (Kamasaki et al., 2005).

Fission yeast longitudinal actin cables exhibit dynamic behaviors and their equivalent in budding yeast flow at a rate of 0.3 um/s (similar to formin-For3p retrograde flow on actin cables in fission yeast) (Martin and Chang, 2006; Yang and Pon, 2002). Formin-For3p is the nucleator of actin cables in fission yeast and its regulator Bud6p and profilin-Cdc3p are supposed to affect F-actin polymerization in actin cables (Martin and Chang, 2006). Very few proteins are found to distribute evenly on fission yeast actin cables, with the exception of tropomyosin-Cdc8p (acetylated) and Coronin-Crn1p (Kovar et al., 2011; Skoumpla et al., 2007). It is also unknown which protein is responsible for crosslinking actin filaments in the actin cable, candidates including but not limited to Fim1p, α-actinin Ain1p and transgelin-Stg1p (Kovar et al., 2011). Turnover of the actin cables are demonstrated by LatA treatment (Pelham and Chang, 2001) and cofilin-Adf1 may involve in the severing of actin cables (Okada et al., 2006). Overexpression of the formin-For3p interaction protein Tea4p leads to thicker actin cable assembly in a formin-For3p dependent manner (Martin et al., 2005b). Moreover, cells expressing excess amount of Fim1p A2 domain (369-614 AAs) also generate thicker F-actin cables in a formin-For3p independent manner (Nakano et al., 2002; Nakano et al., 2001). Since actomyosin rings were intact and actin cables were not observed by phalloidin staining in the *for3*Δ cells, actin cables are considered dispensable for actomyosin ring assembly or cell survival (Feierbach and Chang, 2001). Formin-For3p mediated actin cable assembly and elongation could be computer modeled, allowing quantitative predictions of the functional relationships between actin cables and their interacting proteins (Wang and Vavylonis, 2008).

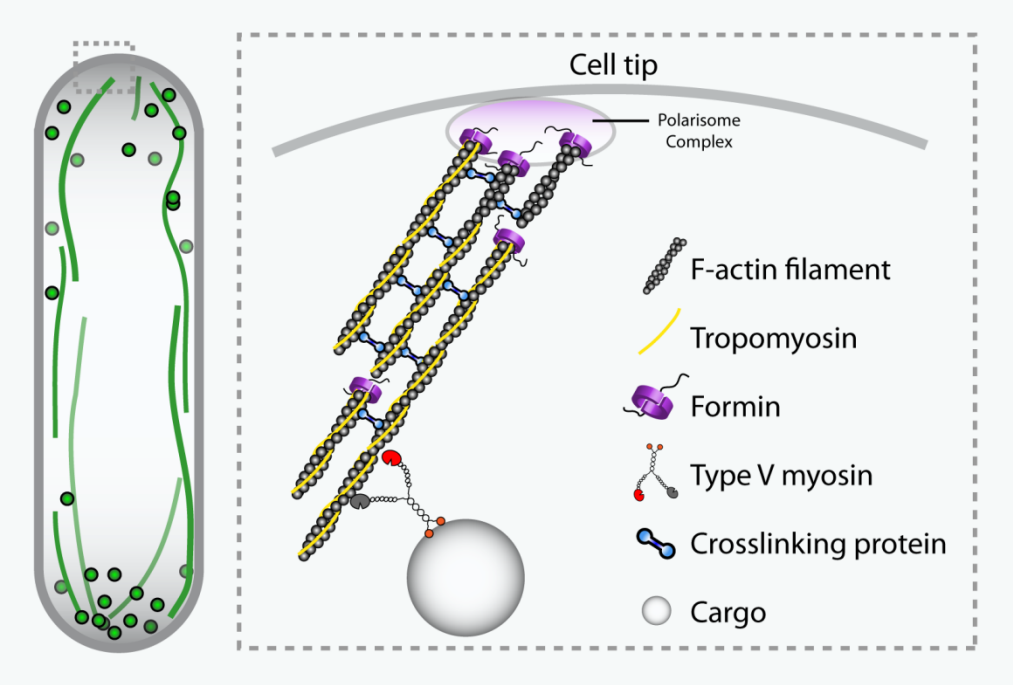


**Illustration 2.** Schematic of part of an actin cable (modified from Mishra et al, 2014).

Actin cables are bundles of short actin filaments. Most of the actin filaments in the cable are parallel, with their pointed ends orient towards the cell center. These actin filaments are nucleated by formins at the barbed end and are bundled by crosslinking proteins. Type V myosin transports cargos along the actin track toward the barbed end. Tropomyosin binds to and stabilizes actin filaments.

### 1.4.3 Actin ring

The third but the most widely studied fission yeast F-actin structure is the actin ring (see Illustration 3). Actin ring together with many other ring proteins such as myosins form a broader concept termed actomyosin ring, which could contract and change its diameter. One electron microscopy study showed that fission yeast actin ring was composed of ~1,000-2,000 short F-actin filaments, each of which was around 0.6 μm long (Kamasaki et al., 2007). The same study also showed that fission yeast actomyosin ring in early stage contained two semicircular F-actin populations, each of which was of opposite direction. However, actin ring became homogenous with F-actin filaments of mixed directionalities in later stage (Kamasaki et al., 2007). In a recent study, fission

yeast actomyosin ring was partially isolated and its contractility was retained (Mishra et al., 2013). Actin rings are also important for proper sporulation in fission yeast (Yan and Balasubramanian, 2012).

To coordinate with cell cycle progression, the actomyosin ring undergoes three stages of genesis: ring assembly, ring maturation and ring constriction. For ring assembly, please refer to section 1.6 in this chapter.

Ring maturation (between the appearance of a full ring and its constriction) takes around 25 min at 25$^{o}$C (fission yeast doubling time: ~3 h at 25$^{o}$C), during which the diameter of the fission yeast ring remains constant (Wu et al., 2003). During this period, the contractile ring matures by recruitment of additional proteins, such as Cdc15p, septins, Ain1p and unconventional type II myosin Myp2p etc (Coffman et al., 2009; Lee et al., 2012). Concentration of some proteins increases several fold during ring maturation, such as ~10 fold increase of the F-BAR protein Cdc15p (Wu and Pollard, 2005). Ring maturation time is shortened or abolished in some temperature sensitive mutants, such as *myo2*-E1, *cdc8*-27 and *mid1*Δ cells (Saha and Pollard, 2012; Stark et al., 2010). On the contrary, cells could also have a longer maturation time (e.g. cells with two copies of Myo2p) (Stark et al., 2010). Furthermore, it is suggested that fission yeast ring undergoes reorganization during ring maturation as ring proteins exhibit different turn over dynamics comparing to earlier ring assembly stage (Lee et al., 2012). However, not much is known about ring maturation and a lot remains to be learned.

Another important stage is ring constriction. During ring constriction, the diameter of the actomyosin ring decreases gradually. Actin concentration remains constant during this process while type II myosin Myo2p becomes denser during this process (Wu and Pollard, 2005). Although actin depolymerization seems to play a major role in budding yeast actomyosin ring constriction *in vivo* (Mendes Pinto et al., 2012), recent work in fission yeast showed that neither actin depolymerization nor nucleation is required for ring constriction *in vitro*. (Mishra et al., 2013). The same work also showed that excessive actin crosslinking blocks ring contraction. There are many

hypotheses attempted to explain the force involved in ring constriction. Most prevalent ones involved myosin motor activity, actin depolymerization or cell wall synthesis (Mendes Pinto et al., 2013).

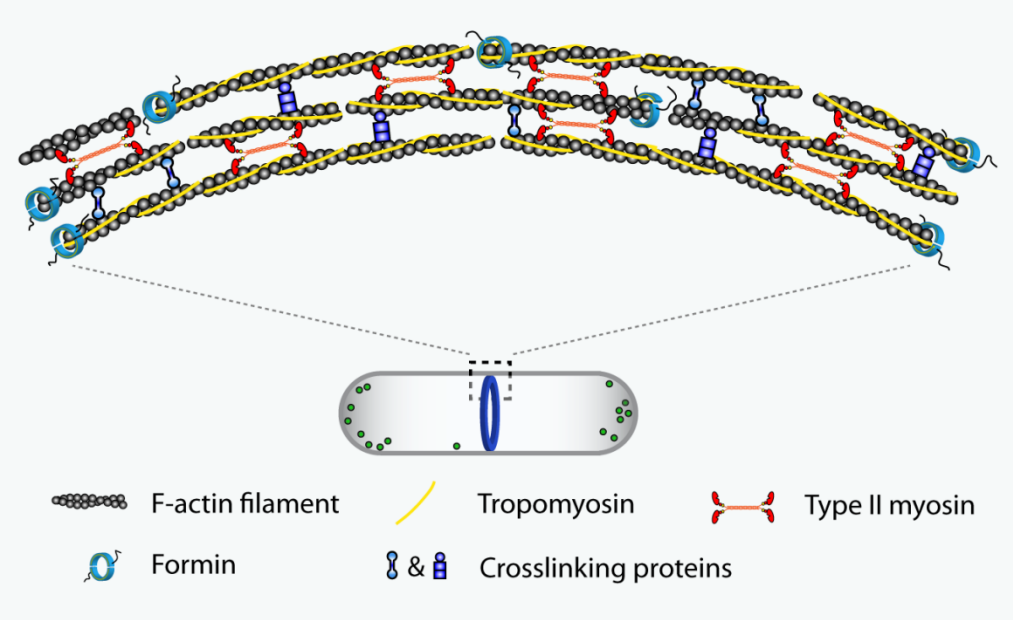


**Illustration 3.** Schematic of part of an actomyosin ring (modified from Mishra et al, 2014).

A mature actomyosin ring is composed of many short anti-parallel actin filaments. These actin filaments are nucleated by formins at the barbed end and are bundled by crosslinking proteins. Type II myosin is believed to form dimmers and generate force during actomyosin ring assembly and constriction. Tropomyosin binds to and stabilizes actin filaments.

## 1.5 FISSION YEAST FORMINS

### 1.5.1 Formin-For3p

Fission yeast formin-For3p is responsible for F-actin cable nucleation in interphase and is involved in cell polarity (Feierbach and Chang, 2001; Nakano et al., 2002). Fission yeast *for3* gene is not essential for viability but *for3*Δ cells exhibit dumpy, round, lemon-like or bent morphological defects (length/width = ~2.0 compared to ~3.0 in wt) at permissive temperature (Martin et al., 2007; Nakano et al., 2002; Scott et al., 2011). F-actin patches are moderately randomized/depolarized in *for3*Δ cells (Feierbach and Chang, 2001; Nakano et al., 2002). F-actin cables are either missing or short in the

*for3*Δ cells (Feierbach and Chang, 2001; Nakano et al., 2002). Microtubule organization/bundling defects are found in cells either depleted of or overexpressing formin-For3p (Feierbach and Chang, 2001; Nakano et al., 2002). Furthermore, overexpression of formin-For3p produces large swollen fission yeast cells (Nakano et al., 2002). Interestingly, expression of a truncated formin-For3p (deletion of 353-406 AAs) under endogenous promoter as a sole copy results in curved and robust F-actin cables (Martin et al., 2007).

For3p localizes to the contractile ring as well as dots near the cell tips (Feierbach and Chang, 2001; Martin and Chang, 2006; Martin et al., 2007; Nakano et al., 2002). It is unclear when exactly For3p localized to the contractile ring. Each For3p dot present near the cell tip contains ~4.2 ± 1.7 molecules of For3p (Martin and Chang, 2006). For3p dots are dynamic, most of them passively move away from the cell tips on F-actin cables with a rate of 0.3 μm/s (Martin and Chang, 2006). This long range retrograde movement of For3p depends on F-actin polymerization. Localization of For3p to the tip depends on the kelch repeat protein Tea1p, the SH3 domain containing protein Tea4p, the small Rho GTPase Cdc42p, Pob1p and Sec3p (Jourdain et al., 2012; Martin and Chang, 2006; Martin et al., 2007; Rincon et al., 2009). Tea1p and Tea4p are transported on microtubules to the cell tips. Primary sequence alignment suggests that formin-For3p lacks canonical N-terminal DAD (diaphanous autoregulatory domain) and C-terminal DID (diaphanous inhibitory domain) sequences, which are important for regulating formin activity (Higgs and Peterson, 2005). However, experiments suggest that DID-like sequence and DAD-like sequence are present in formin-For3p (Martin et al., 2007). Further experiments show that For3p nucleation activity depends on profilin-Cdc3p, Bud6p, Cdc42p and partially on Pob1p (Martin and Chang, 2006; Rincon et al., 2009). Bud6p dots partially colocalize with For3p dots at the tips. Bud6p interacts with the N-terminus of For3p (Feierbach et al., 2004). For3p dots are less distinct and move slower in *bud6*Δ cells. F-actin cables are thinner after *bud6* deletion. Bud6p and Cdc42p regulate For3p activity in parallel pathways (Martin et al., 2007). N-terminal amino acids 149-488 of For3p could interact with active Cdc42p (Nakano et

al., 2002). Cdc42p is believed to activate For3p by relieving its autoinhibition (Martin et al., 2007). Pob1p binds to Cdc42p and therefore facilitates activation of For3p (Rincon et al., 2009).

Formin-For3p lacks F-actin filament bundling activity *in vitro* (same as Cdc12p but not Fus1p) (Scott et al., 2011). Moreover, although the F-actin elongation rate is almost the same as formin-Cdc12p *in vitro*, nucleation efficiency (for one F-actin filament nucleation, the optimal number of formin dimer required) is much lower than formin-Cdc12p (filaments per formin dimer; For3p, 1:170; Cdc12p, 1:3) (Scott et al., 2011). Furthermore, formin-For3p is important for meiotic actomyosin ring assembly (Yan and Balasubramanian, 2012).

### 1.5.2 Formin-Cdc12p

Fission yeast *cdc12* gene is essential for cell viability. It encodes a ~220 KD *Drosophila* diaphanous-like protein known as formin-Cdc12p (Chang et al., 1997). Deletion of *cdc12* gene results in a long and large swollen dumbbell-shaped cells that do not continue cell division and accumulate multiple nuclei (Chang et al., 1997). Formin-Cdc12p localizes to speckles, spot, nodes and the actomyosin ring (Chang et al., 1997; Coffman et al., 2009; Wu et al., 2006; Yonetani et al., 2008). Multiple regions (N-terminal region and the FH1-FH2 domains) in Cdc12p are responsible for ring localization, suggesting that the recruitment of Cdc12p to the contractile ring could be regulated by multiple pathways (Yonetani et al., 2008). Localization of formin-Cdc12p to the medial ring precursor structures (spot or nodes) depends on the PCH family protein Cdc15p as well as the Mid1p-dependent ring assembly pathway (Carnahan and Gould, 2003; Laporte et al., 2011; Padmanabhan et al., 2011). Two-hybrid analysis showed a strong interactions between the N-terminal of Cdc15p (1-282 AAs) and the N-terminal formin-Cdc12p (1-524 AAs, includes the FH3 domain) (Carnahan and Gould, 2003). However, it is unclear how Cdc12p is recruited through the Mid1p-dependent ring assembly pathway (Laporte et al., 2011). Cdc12p speckles are present in interphase (218 ± 46 copies) and their number decreases dramatically (to < 40 copies) during mitosis (Coffman et al., 2009).

Cdc12p speckles could move within a local area at 0.9 ± 0.5 μm/s independent of actin polymerization (Coffman et al., 2009). Cdc12p spot localization depends on its FH3/DID region as well as Cdc15p and Ain1p (Chang et al., 1997; Coffman et al., 2009; Yonetani et al., 2008) whereas Cdc12p node localization is controlled through overlapping pathways (Laporte et al., 2011). Both Cdc12p spot and nodes are believed to initiate contractile ring assembly (Chang et al., 1997; Coffman et al., 2009; Wu et al., 2003; Yonetani et al., 2008). Cdc12p spots exist in interphase, some persist until mitosis and are believed to form the contractile ring by spreading along the *de novo* nucleated F-actin cables (Chang et al., 1997; Yonetani et al., 2008). Cdc12p nodes appear only after cells enter mitosis (0.4 ± 0.9 min or 1.0 ± 2.5 min after SPB separation, mean ± SD) (Coffman et al., 2009; Wu et al., 2003; Wu and Pollard, 2005) and are believed to coalesce into a ring through force generated by actin-myosin interaction (Coffman et al., 2009; Vavylonis et al., 2008). Cdc12p ring possesses ~62% of the total Cdc12p intensity of a cell, while Cdc12p nodes, spot and each speckle occupy ~24%, ~3.6% and ~0.4 %, respectively (Coffman et al., 2009).

Fission yeast formin-Cdc12p resembles a barbed-end capping protein in the absence of profilin (Kovar et al., 2006). It is unclear how F-actin nucleation activity of Cdc12p is controlled. Unlike many other formins, there is no evidence that Cdc12p activity is regulated by Rho-type small GTPases or a DAD-like domain (Yonetani and Chang, 2010; Yonetani et al., 2008). Mutations in the putative DID-like and DAD-like sequences do not affect Cdc12p activity. FH1-FH2 domains are important for the F-actin nucleation activity for Cdc12p. Although FH1-FH2 domains could not complement full length Cdc12p function, deletion of other domain or sequences outside the FH1-FH2 region does not affect cell viability (Yonetani et al., 2008). Moreover, overexpression of the FH1-FH2 domains leads to aberrant thicker F-actin cables (Kovar et al., 2003; Yonetani et al., 2008). Interestingly, it has recently been found that overexpression of a truncated version (cdc12ΔC, 1438-1841AAs deleted) of Cdc12p could lead to the assembly (sometimes also constriction) of an actomyosin ring in interphase (Yonetani and Chang, 2010). This interphase ring induced by cdc12ΔC contains some proteins same

as the mitotic actomyosin ring, such as actin, Rlc1p, For3p, Bud6p, Ain1p and Mid1p (weakly) etc. F-actin nucleation function of FH1-FH2 domains is required for this interphase ring formation, although it could be substituted with FH1-FH2 domains from formin-For3p (Yonetani and Chang, 2010). It is also found that the first 50 AAs in the N-terminal of Cdc12p is also required for the interphase ring assembly. In summary, it is still unclear how Cdc12p incorporated into the actomyosin ring during mitosis and how Cdc12p activity is regulated during cell cycle.

## 1.6 ACTOMYOSIN RING ASSEMBLY IN FISSION YEAST

### 1.6.1 Fission yeast actomyosin ring assembly pathways

Previous work showed that fission yeast actomyosin ring assembles through one of the two pathways: the Mid1p node-dependent pathway and Cdc15p-dependent (also called SIN-dependent) pathway (Hachet and Simanis, 2008; Huang et al., 2008) (see Illustration 4). Under normal circumstance, Mid1p node-dependent pathway works in early mitosis while Cdc15p-dependent pathway works in late mitosis. When SIN is activated during interphase or Mid1p is missing during mitosis, fission yeast cells would bypass the Mid1p dependent nodes and assemble an off-centered but contractile actomyosin ring in interphase or late mitosis, respectively (Huang et al., 2008; Minet et al., 1979; Schmidt et al., 1997; Sohrmann et al., 1996).

SIN (septation initiation network) is a conserved fission yeast pathway that coordinates mitotic exit and cytokinesis in anaphase (McCollum and Gould, 2001; Ray et al., 2010). Similar pathways are also found in budding yeast and metazoans (Bardin and Amon, 2001; Johnson et al., 2012). SIN proteins associate with one or both of the spindle pole bodies (SPB, yeast centrosome counterpart) and their asymmetric localizations on the SPBs are important for cytokinesis completion (Garcia-Cortes and McCollum, 2009). Cdc11p, Sid4p and Ppc89p are the most upstream scaffold proteins in the SIN signaling pathway (Krapp et al., 2001; Rosenberg et al., 2006). Ppc89p interacts with the C-terminus of Sid4p and therefore brings the Cdc11p-Sid4p scaffold to the SPBs (Rosenberg et al., 2006). The SIN component GTPase Spg1p localizes downstream of the scaffold proteins by direct interaction with the N-terminus

of Cdc11p (Morrell et al., 2004). Spg1p overexpression induces actomyosin ring assembly in interphase (Schmidt et al., 1997) and its activity is inhibited by the bipartite GAP Cdc16p-Byr4p (Furge et al., 1999; Furge et al., 1998). In early mitosis, the GTP-bound active form of Spg1p recruits Cdc7p to both SPBs (Sohrmann et al., 1998). Sid1p (kinase) and its binding partner Cdc14p are subsequently recruited to the new SPB during anaphase (Guertin et al., 2000). Downstream of Sid1p and Cdc14p are another SPBs localized kinase Sid2p and its binding partner Mob1p (Hou et al., 2004; Sparks et al., 1999). Sid2p also localizes to the cell division site and this localization is Cdc15p dependent (Sparks et al., 1999). Sid2p phosphorylation of Clp1p leads to the maintenance of Clp1p in the cytoplasm during cytokinesis. Clp1p then possibly dephosphorylates Cdc15p (Johnson et al., 2012). SIN inhibition causes cytokinesis failure and a multi-nucleate phenotype. On the contrary, SIN hyper-activation triggers actomyosin ring formation in interphase and multi-septa formation in fission yeast.

Actomyosin ring assembly could also go through the Mid1p nodes-dependent pathway (Laporte et al., 2011; Padmanabhan et al., 2011; Pollard and Wu, 2010; Wu et al., 2003). Mitotic nodes are considered the precursors of the actomyosin ring and many ring proteins accumulate in nodes before or shortly after mitosis (Wu et al., 2003; Wu et al., 2006). The anillin-like protein Mid1p is the most upstream scaffold node protein (Sohrmann et al., 1996). Mid1p shuttles between nucleus and a cortical medial broad band 1 h before mitosis onset (Paoletti and Chang, 2000; Pollard and Wu, 2010). This cortical broad band contains 63 ± 10 nodes (Vavylonis et al., 2008). Then starting between -10 min to 0 min before SPB separation, Mid1p nodes recruit downstream proteins such as IQGAP protein Rng2p, myosin essential light chain EF hand protein Cdc4p, myosin heavy chain Myo2p, myosin regulatory light chain Rlc1p and F-BAR protein Cdc15p etc (Laporte et al., 2011; Padmanabhan et al., 2011).The formin-Cdc12p is also recruited into the nodes around 0.4 ± 0.9 min or 1.0 ± 2.5 min (mean ± SD) after SPB separation (Coffman et al., 2009; Wu et al., 2003; Wu and Pollard, 2005). In this pathway, Mid1p first recruits Cdc4p and Rng2p by direct interaction. Node localizations of Cdc4p and Rng2p are mutually dependent (Laporte et al., 2011; Padmanabhan et al.,

2011). Meanwhile, Mid1p localization and stabilization on the medial cortex is partially dependent on Cdc4p and Rng2p. Then Rng2p recruits Myo2p and Rlc1p into nodes. Mid1p also recruits Cdc15p into nodes. It is unclear how formin-Cdc12p is recruited into nodes. But physical interaction is observed between Cdc12p and hypophosphorylated Cdc15p (Roberts-Galbraith et al., 2010) and the localization of Cdc12p in the nodes were abolished in *rng2*-D5 *cdc15*-140 double mutant but not the single mutants at 30$^{o}$C (Laporte et al., 2011). Deletion of Mid1p causes a ring-positioning defect with strands of ring proteins assembled into a tilt or off centered actomyosin ring.

Although neither the Mid1p-dependent pathway nor the SIN-dependent pathway is essential for fission yeast actomyosin ring assembly, deletion of both pathways totally abolishes ring assembly (Hachet and Simanis, 2008; Huang et al., 2008). This indicates that these two pathways coordinate in actomyosin ring assembly.

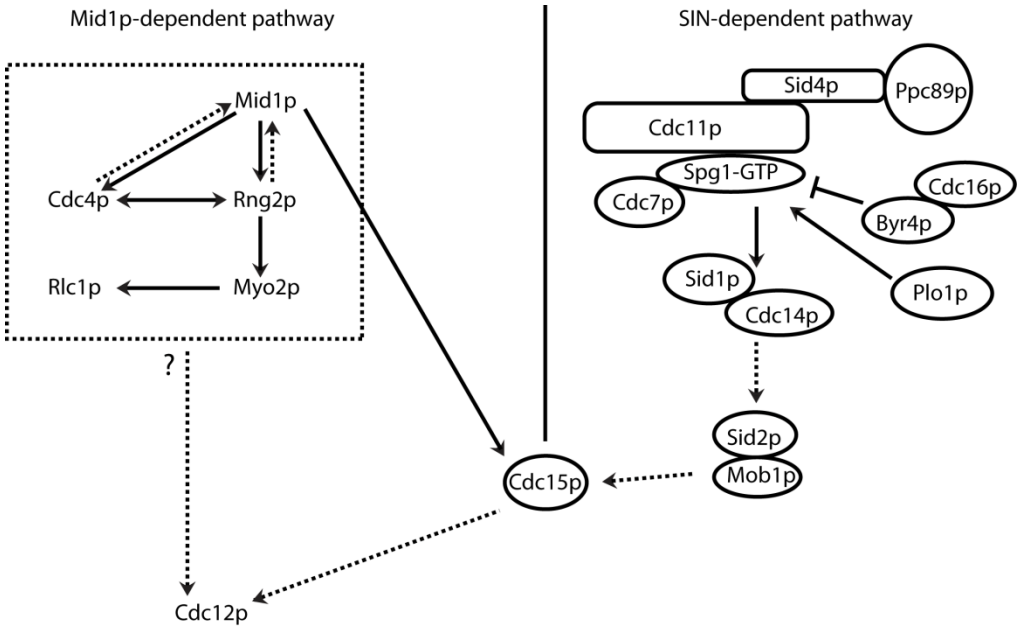


**Illustration 4.** Fission yeast actomyosin ring assembly pathways (modified from Laporte et al., 2011 & Johnson et al., 2012).

Left, Mid1p-dependent pathway. The solid arrow in this pathway indicates the node localization of a protein (near the arrowhead end) is completely dependent on another protein (near the base of the arrow). The dashed arrow in this pathway indicates the node localization of a protein (near the arrowhead end) is partially dependent on another protein (near the base of the arrow). The question mark indicates the protein recruiting Cdc12p is unknown. Right, SIN-dependent pathway. Solid or dashed arrows in this pathway indicated direct or indirect signal transduction. "**T**" means inhibition.

### 1.6.2 Fission yeast actomyosin ring assembly models

Many years of genetics, cell biology and biochemistry studies in fission yeast have led to the proposal of two main models speculating the assembly procedure of the actomyosin ring (Bathe and Chang, 2010; Mishra and Oliferenko, 2008). One is called "leading cable" model or aster model, the other one is called "search, capture, pull and release" model (SCPR model in short) (see Illustration 5).

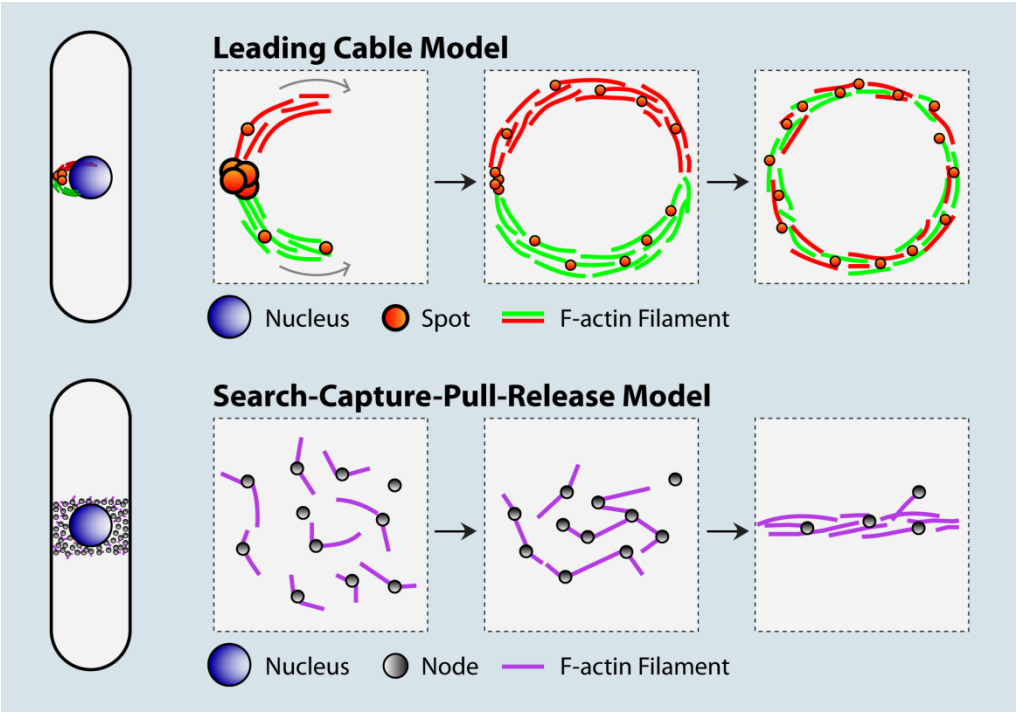


**Illustration 5.** Fission yeast actomyosin ring assembly models (modified from Mishra and Oliferenko, 2008).

Upper panel: Leading cable model. Lower panel: SCPR model. All structures are as indicated in the illustration.

#### 1.6.2.1 Leading cable model

In the "leading cable" model, it is hypothesized that fission yeast formin-Cdc12p forms a big spot structure near the division site during mitosis and from this big spot F-actin filaments are nucleated into two opposite directions. These opposite oriented F-actin filaments could be stabilized or bundled by type II myosin Myo2p to form bidirectional F-actin bundles (Motegi et al., 2004). As a result of the continuous polymerization by formin-Cdc12p, these bidirectional F-actin bundles encircle the cell equator and finally seal up the assembling actomyosin ring. During this encircling process, the F-actin filament barbed end associated protein formin-Cdc12p may also spread from the spot to the whole actomyosin ring. This model is supported by a set of individual observations (Arai and Mabuchi, 2002; Carnahan and Gould, 2003; Chang, 1999; Chang et al., 1997; Kamasaki et al., 2007). First, immunofluorescence staining using anti-Cdc12p antibody showed that formin-Cdc12p accumulates as one or several big "spots" in either interphase or mitotic wild-type (wt) fission yeast cells (Chang, 1999; Chang et al., 1997). Upon overexpression, anti-Cdc12p antibody stained formin-Cdc12p spot was found near the division site or associate with the actomyosin ring (both complete ring and incomplete ring) in either wt or *cdc4*-377 mutant background during mitosis (Chang et al., 1997). Secondly, cells expressing either GFP-Cdc12p or Cdc12p-3GFP under endogenous promoter possess a Cdc12p spot (Chang, 1999; Yonetani et al., 2008). Moreover, it was reported that the intensity and size of the medially localized GFP-Cdc12p spot progressively decreased during actomyosin ring formation and Cdc12p-3GFP spot could physically spread out to form a ring (Chang, 1999; Yonetani et al., 2008). Thirdly, an elegant study using phalloidin staining to directly observe the early mitotic F-actin cytoskeleton seemed to support the leading cable model (Arai and Mabuchi, 2002). Using a deconvolution DeltaVision microscopy and 3D reconstruction, the authors found that some F-actin cables accumulated in the division site seemed to converge at an aster-like actin structure, consistent with another study using GFP-CHD as live cell F-actin marker (Coffman et al., 2009). Furthermore, at metaphase, a single or two leading cables seemed to extend from the aster-like structure and encircled the cell equator during actomyosin ring assembly.

However, this study did not analyze the spatial relationship between the formin-Cdc12p and the leading cables. Fourthly, at least two other ring proteins were also found in the big Cdc12p spot structure, including Cdc15p and Ain1p but not Rlc1p (Carnahan and Gould, 2003; Coffman et al., 2009). Cdc15p and Ain1p are important for Cdc12p spot formation (Chang et al., 1997; Coffman et al., 2009). Fifthly, although Rlc1p spot like structure does not colocalize with Cdc12p spot, close spatial association of Rlc1p spot like structure or Cdc12p spot with strand-like ring precursor proteins are frequently observed in *mid1* mutants (Chang et al., 1997; Hachet and Simanis, 2008; Huang et al., 2008; Zhang et al., 2010). The last but most stunning evidence was from an electron microscopy study (Kamasaki et al., 2007). It was found that the early actomyosin was composed of two semicircular populations of oppositely oriented F-actin filaments while rings at later stages consisted of F-actin filaments with mixed directionality, suggesting that F-actin nucleation may mainly took place at one site.

#### 1.6.2.2 Search-Capture-Pull-Release model

The SCPR model differs from the leading cable model mainly in the organization of formin-Cdc12p, direction of F-actin filaments and myosin motor activity (Coffman et al., 2009; Lee et al., 2012; Pollard and Wu, 2010; Vavylonis et al., 2008; Wu et al., 2006). In the SCPR model, formin-Cdc12p and many other ring proteins (Mid1p, Rng2p, Myo2p, Rlc1p, Cdc15p and Ain1p etc.) form a broad band of nodes (~63 copies) in the cell middle during early mitosis. F-actin filaments nucleated by the formin-Cdc12p emanate from the nodes into random directions. Owing to the close distance between the nodes, the randomly oriented F-actin filaments could be captured by the myosin molecules on the neighboring nodes. Although this connection maybe transient and F-actin filaments may break during this process, F-actin filaments and nodes are compacted into an actomyosin ring through the stochastic mutual interaction between actin and myosin motor. This model is also supported by quite a few observations. Firstly, more and more proteins are found to localize in nodes, some even form nodes long before cells enter mitosis (Coffman et al., 2009; Jourdain et al., 2013; Lee et al., 2012; Moseley et al., 2009; Pollard and Wu, 2010; Vavylonis et al., 2008; Wu et al., 2006).

Secondly, according to time-lapse microscopy using GFP-CHD as an F-actin marker, some F-actin filaments seemed to be nucleated *de novo* from the formin-Cdc12p nodes (Coffman et al., 2009; Vavylonis et al., 2008). Thirdly, in *mid1*-6 cells or cells forced to make an interphase ring, both ring formation and constriction are slower than wt (Hachet and Simanis, 2008; Huang et al., 2008). Since cells in these circumstances did not form rings from any nodes, it is likely that nodes are important for timely assembly of actomyosin ring and proper subsequent constriction. The fourth supporting experiment came from computer simulation (Vavylonis et al., 2008). By applying quantitation data derived from live cell imaging and some necessary speculations, computer simulation seems to support the SCPR model.

However, there are also evidences opposing either of the models. For the leading cable model, it is found by a group that most of the Ain1p or Cdc15p spot structures disappear before actomyosin ring formation, some even vanish before the cell enter mitosis (Coffman et al., 2009). Around 73% of cells assembling the actomyosin ring do not contain any Cdc12p or Ain1p spot. Moreover, the same study also points out that the formin-Cdc12p spot only contains 3.6 ± 2.7% of the total Cdc12p molecules while the formin-Cdc12p nodes occupy ~18% of the Cdc12p total intensity. FRAP experiments also show that Ain1p or Ain1p dependent Cdc12p spot turns over much slower than each protein in the rings. The authors also argue that the spreading of spot into ring is not observed in their study and rings form normally in *ain1*Δ cells possessing no spot structure (Coffman et al., 2009). For the leading cable/aster structure observed by both phalloidin staining and GFP-CHD (Coffman et al., 2009), it is suggested that these structures could be at an intermediate stages resulting from sites where condensation of nodes and F-actin filament is faster. For the SCPR model, one issue is that formin-Cdc12p nodes are not observed in wt cells by other groups (Roberts-Galbraith and Gould, 2008; Yonetani et al., 2008). This could be due to the difference in fluorescent tag or the microscopy (Coffman et al., 2009). Another problem is the GFP-CHD probes used in the time-lapse studies. F-actin filaments or cables marked by GFP-CHD were not clear enough and tended to bleach easily. Cells overexpressing GFP-CHD under inducible promoter became longer, indicating

GFP-CHD may affect cellular processes. In the SCPR model, myosin motor activity is important for nodes and F-actin filament compaction. However, study in animal cells showed that non-muscle myosin motor activity is not important for actomyosin ring assembly in monkey kidney cells (Ma et al., 2012). Although researchers tried to use the *myo2*-E1 mutant (lower motor activity but unclear about its bundling activity) to explain this contradiction (Coffman et al., 2009), it does not rule out the possibility that myosin bundling activity plays a more important role during actomyosin ring. Strangely, neither nodes nor spot structures are observed under electron microscopy. There are also some other models that combine features from both models (Hachet and Simanis, 2008; Roberts-Galbraith and Gould, 2008). It is possible that formin-Cdc12p spot dissolve in the middle to create a higher concentration of Cdc12p and later form nodes (Coffman et al., 2009).

In summary, the current models explain important aspects of the mechanism involved in actomyosin ring assembly but neither is sufficient to address all the questions raised from observations by different groups. New evidence are yet needed to combine or modify the proposed models as so to better understand cytokinesis in fission yeast.

## 1.7 DIFFICULTIES IN STUDYING FISSION YEAST ACTIN AND AVAILABLE ACTIN MONITORING PROBES

### 1.7.1 Direct tagging of fission yeast actin

To detect the localization pattern of F-actin, phalloidin a toxin from the death cap fungus *Amanita phalloides*, has been commonly used for decades (Cooper, 1987; Marks et al., 1986). However, phalloidin staining sometimes does not stain all the F-actin structures and moreover could not reveal F-actin dynamics *in vivo* (Riedl et al., 2008). Another easy and direct method to check the localization/dynamics of a protein of interest is to tag the protein directly with fluorescent fluorophores and subsequently observe under microscopy (Prendergast and Mann, 1978; Wu et al., 2003). In higher eukaryotes, F-actin pattern and its dynamics have been monitored by expressing a second copy of fluorophore tagged actin (Ballestrem et al., 1998; Vishwasrao et al., 2012), despite minor defects (influence differs from organism to organism) being

reported (Aizawa et al., 1997; Deibler et al., 2011; Feng et al., 2005; Westphal et al., 1997). However, direct tagging fission yeast actin in the endogenous locus is lethal (Chen et al., 2012; Wu and Pollard, 2005). Tagged actin has never been incorporated into actin cables or rings (Kovar et al., 2005; Wu and Pollard, 2005). In budding yeast *Saccharomyces cerevisiae*, GFP tagging of actin at the C-terminal also could not complement the actin null mutant and again only labeled the actin patches (Doyle and Botstein, 1996). Recently, a modified version of tetracysteine (12 AAs, original tetracysteine is 6 AAs) was used to tag fission yeast actin (Chen et al., 2012). Tetracysteine is a short peptide motif that binds to the membrane permeable fluorogenic biarsenical labeling reagents FlAsH-$EDT_2$ or ReAsH-$EDT_2$ (Hoffmann et al., 2010). In this work, researchers tagged fission yeast actin at the N-terminus, C-terminus and 8 other carefully selected sites within the actin protein. However, despite the numbers of carefully selected sites and the small size of the modified tetracysteine, none of the fusion protein could replace the native actin protein or incorporate into the contractile ring. But interestingly, weak incorporation of tetracysteine tagged actin into actin cable-like structures was found in two of the constructed stains (N-terminal tagging between methionine 1 and glutamic acid 2; between serine 232 and serine 233). Collectively, it is believed that filtering by the homodimeric formin FH2 ring was responsible for the failure of tagged actin to be detected in cables and the ring (Chen et al., 2012). Although *in vivo* tagging of fission yeast actin did not work as in other organisms, in vitro studies showed that oregon green labeled G-actin (cysteine 374, located within the profilin-actin interaction surface) could be incorporated into F-actin filaments in the presence of native G-actin (Kovar et al., 2006; Kovar et al., 2003).

### 1.7.2 Actin monitoring probes in different organisms

An alternative method to examine the localization/dynamics of a protein of interest is to monitor the behavior of its binding partners. Thus, it may be helpful to tag an F-actin binding protein with fluorophore. Many actin binding proteins are identified to date, some only bind to either G-actin or F-actin while others interact with both forms (dos Remedios et al., 2003; Winder and Ayscough, 2005). These proteins often differ in size and their actin binding

efficiency. Some of them are not capable of binding to all F-actin structures. Actin binding proteins often have homologous sequence within an organism, which could interact with other endogenous proteins. This may affect actin-actin binding protein interaction and hence changes dynamics of actin. Thus, finding an ideal marker for monitoring F-actin dynamics *in vivo* is difficult.

Since 1997, a few probes are generated and applied in different living organisms to study F-actin dynamics *in vivo* (Bretschneider et al., 2004; Burkel et al., 2007; Edwards et al., 1997; Iwano et al., 2007; Johnson and Schell, 2009; Kost et al., 1998; Pang et al., 1998; Patkar et al., 2012; Riedl et al., 2008; Sheahan et al., 2004; Yang and Pon, 2002). Most often, the use of these probes is restricted in one organism or two. Sizes of these probes are different, with the shortest lifeact of 17 AAs (Riedl et al., 2008) to the largest Abp140p of 628 AAs (Yang and Pon, 2002). Fluorophores are either fused to the N- or C-terminus of respective actin binding protein and expressed under various promoters, including actin promoter. Minor defects (e.g. F-actin stabilization or bundling) are found upon expression of some fusion proteins. In some cases, different F-actin organization is observed between tags (Sheahan et al., 2004). Furthermore, sometimes it is unclear how these tags structurally interact with F-actin. To better compare these actin monitoring probes, a few of them are described below.

Moesin is a member of the MER (moesin, ezrin and radixin) protein family. In 1997, N-terminus of a truncated *Drosophila* moesin (hereafter called this truncated version moe) was fused with GFP to visualize F-actin dynamics in fruit flies (Edwards et al., 1997). To our knowledge, this is the first actin binding protein utilized for monitoring actin dynamics. This moe contained 280 AAs and was expressed under hsp70 promoter. *Drosophila* moesin was identified from a genetic screen in fission yeast (Edwards et al., 1994). When moesin was overexpressed in fission yeast, it strongly interrupted fission yeast cytokinesis. In *Drosophila*, GFP-moe transgenic flies became paralyzed for 5-10 min after heatshock induction, although they soon recovered, behave normally and remain fertile for several generations.

Talin is another actin binding protein that has been used to show actin dynamics in plants (Iwano et al., 2007; Kost et al., 1998). In 1998, mouse talin (197 AAs) was expressed under CaMV 35S promoter in tobacco BY-2 suspension cells and 35S promoter in *Arabidopsis thaliana*. GFP was fused to the N-terminal of mouse talin. Human talin was also used in plants to monitor actin dynamics later (Kwok and Hanson, 2004; Takemoto et al., 2003). However, later it was found that GFP-mouse talin could not label all F-actin structures and may cause artificial aggregation of F-actin in plants (Sheahan et al., 2004).

Abp120 (also named Gelation factor, 857 AAs) was also used in *Dictyostelium discoideum* in 1998 (Noegel et al., 1989; Pang et al., 1998). The N-terminus of Abp120 was fused with GFP and the fusion protein was expressed under *Dictyostelium* actin promoter (Pang et al., 1998). Abp120 also worked in NIH 3T3 mouse fibroblasts and oocytes. A smaller version (2-248 AAs) of Abp120 also labeled F-actin in *Dictyostelium discoideum* (Bretschneider et al., 2004).

The prototype of F-Tractin was applied in HeLa cells in 2001 (Schell et al., 2001). Rat inositol 1,4,5-triphosphate 3-kinase (http://www.ncbi.nlm.nih.gov/nuccore/X56917.1) binds to F-actin with its N-terminus 66 AAs (also called N66). In 2009, a shorter version (9-52 AAs) of N66 was found to bind F-actin sufficiently and it was named F-Tractin (Johnson and Schell, 2009). An even shorter form was identified later (9-40 AAs) and is almost equivalent to F-Tractin in terms of their interactions with F-actin (personal communication).

In 2002, Abp140 protein (628 AAs) was used in budding yeast (Asakura et al., 1998). Abp140 was from budding yeast. By fusing the C-terminal of Abp140 with GFP (Abp140p-GFP) and expressing under *abp140* native promoter, F-actin patches and F-actin cables were visualized.

Fimbrin actin binding domain 2 (363 AAs) and LimE (full length, 199 AAs; C-terminal Coil-coil domain deletion construct, 145 AAs) were used as well in

2004 (Bretschneider et al., 2004; Sheahan et al., 2004). GFP-Fimbrin actin binding domain 2 was used in *Arabidopsis thaliana* and *Nicotiana tabacum*. GFP-LimE or LimE-GFP was used again in *Dictyostelium*.

In 2005, CHD (calponin homology domain, the N-terminal 1-189 AAs of fission yeast Rng2p) was utilized in fission yeast to monitor actin patch movement (Karagiannis et al., 2005). CHD was fused with GFP at the N-terminal (GFP-CHD) and expressed under fission yeast inducible *nmt41* promoter. Later, CHD was also used to track F-actin cable dynamics and actomyosin ring assembly (Coffman et al., 2009; Martin and Chang, 2006; Vavylonis et al., 2008). This CHD construct contains extra amino acids at the N and C-terminals.

In 2007, calponin homology domain of human Utrophin (Utr-CH, 261 AAs) was used to show actin dynamics in *Xenopus* oocytes in 2007 (Burkel et al., 2007). Utr-CH contains two putative calponin homology domains. Utr-CH-GFP also labels actin in mammalian cells (Quintero et al., 2009; Wang and Richards, 2011).

Then lifeact, the most recent F-actin monitoring probe, was developed in 2008 (Riedl et al., 2008). Lifeact has been successfully applied in many organisms (Berepiki et al., 2010; Delgado-Alvarez et al., 2010; Riedl et al., 2008; Riedl et al., 2010; Smertenko et al., 2010; Vidali et al., 2009). It is derived from the N-terminal 17 AAs of budding yeast Abp140 protein. It binds to both G-actin and F-actin with almost the same affinity probably by forming α-helical structure. Furthermore, lifeact has no homologous sequence in higher eukaryotes (only has orthologues from close relatives of budding yeast), which reduces the possible interaction with endogenous proteins. It is the smallest peptide identified so far to bind actin both *in vivo* and *in vitro*. However, despite all the advantages, lifeact was also reported to stabilize actin cytoskeleton when it was overexpressed (van der Honing et al., 2011).

Taken together, many F-actin monitoring probes are available but caution should be used when choosing a proper probe in the organism of interest.

## 1.8 MYOSINS IN FISSION YEAST CYTOKINESIS

### 1.8.1 Type II myosin Myo2p

Myo2p is one of the two type II myosins (the other one is named Myp2p which accumulates in the ring much later) in fission yeast. Myo2p, like most other myosins, move along F-actin filaments towards the barbed (+) end. It is the first identified and sole essential myosin in fission yeast (East and Mulvihill, 2011). Myo2p and its light chains (Cdc4p and Rlc1p) localize to the medial nodes before cells enter mitosis (Laporte et al., 2011; Motegi et al., 2000; Wu et al., 2006). Myo2p node localization depends on IQGAP protein Rng2p but not F-actin (Laporte et al., 2011; Motegi et al., 2000; Naqvi et al., 1999; Padmanabhan et al., 2011). Truncation analysis showed that the C-terminal 77 AAs of the Myo2p tail are essential for its recruitment to the actomyosin ring (Mulvihill et al., 2001). Actomyosin ring dynamics relies on an optimal cellular level of Myo2p; either deletion or overexpression of Myo2p is lethal (Kitayama et al., 1997; May et al., 1997; Stark et al., 2010). However, fission yeast cells could survive and divide with < 5% of Myo2p activity (Pollard, 2008). Tropomyosin-Cdc8p could enhance the ATPase activity of Myo2p and its binding affinity to actin (Stark et al., 2010). It was shown that budding yeast type II myosin could interact with She4p/Dim1p (UCS family protein) and the actin filament gliding activity of fission yeast Myo2p could be activated by the fission yeast UCS protein Rng3p (Lord and Pollard, 2004; Toi et al., 2003). A mature actomyosin ring contains ~2,900 molecules of Myo2p, and as ring constricts, Myo2p concentration increases (Wu and Pollard, 2005). Fission yeast Myo2p is considered the only myosin required for actomyosin ring assembly and contraction *in vivo* (Coffman et al., 2009; East and Mulvihill, 2011; Vavylonis et al., 2008). However, vertebrate nonmuscle type II myosin impaired in its motor activity was found to be sufficient for cytokinesis (Ma et al., 2012).

### 1.8.2 Type V myosin Myo51p

Two type V myosin genes were identified in fission yeast (Motegi et al., 2001; Win et al., 2001). One is *myo51* (also named *myo5*), the other one is *myo52* (also named *myo4*). Myo51p is the only fission yeast type V myosin localized to the contractile actomyosin ring (Win et al., 2001). However, *myo51* null

mutant is non-essential and displays no discernable cell growth defect or morphology defect (Hayles et al., 2013; Kim et al., 2010; Motegi et al., 2001; Win et al., 2001). Overexpression of Myo51p from pREP41 plasmid caused cytokinesis failure (Win et al., 2001). Actomyosin ring localization of Myo51p depends on an intact actin cytoskeleton but not microtubules network (Win et al., 2001). It is unclear how Myo51p localized to the actomyosin ring and whether it plays any role during ring assembly or constriction. However, both budding yeast type V myosins are found to interact with UCS domain containing protein She4p/Dim1p, which is homologous to fission yeast actomyosin ring protein Rng3p (Toi et al., 2003). In addition, like Myo2p, tropomyosin-Cdc8p increases the actin affinity and ATPase activity of Myo51p (Clayton et al., 2010). Recent work suggests that Myo51p together with Myo52p contributes to the organization and retrograde flow of interphase F-actin cables (Lo Presti et al., 2012). Interphase F-actin cables are curled and more bundled near the cell tip in *myo51*Δ *myo52*Δ cells. Also retrograde flows of the interphase F-actin cables are reduced, indicating formin-For3p mediated F-actin assembly may be impaired in *myo51*Δ *myo52*Δ cells. It is also found that the cargo binding tail of Myo51p is not required for interphase F-actin cable organization (Lo Presti et al., 2012). Furthermore, Myo51p may have an important role during meiosis. Although *myo51* gene transcriptional level does not display discernable change during vegetative cell growth, its increases dramatically upon entry into meiosis (Doyle et al., 2009). GFP tagged Myo51p was found to localize to the shmoo tip of the conjugating cell. This localization depends on F-actin cytoskeleton but not microtubule or Myo52p. Furthermore, overexpression of the cargo binding domain of Myo51p leads to the inhibition of cell-cell fusion. Suprisingly, Myo51p signal disperses and has no discrete localization after cell-cell fusion until meiotic prophase. During meiotic prophase and the rest of the cell cycle, Myo51p localized to the SPB in a microtubule cytoskeleton dependent, actin or septation initiation network (SIN) independent manner. In summary, the function of Myo51p during mitosis remains unclear while its role in meiosis is much clearer.

## 1.9 AIMS AND SIGNIFICANCE OF THIS THESIS

In view of the previous sections, it is worthwhile to point out again that how the actomyosin ring assembles in fission yeast *Schizosaccharomyces pombe* is still unclear. A lot has yet to be done. Below listed a few gaps currently present in this field:

1. Actin is intolerant to any ectopic tagging in fission yeast. The lack of a proper probe to monitor F-actin dynamics *in vivo* hampers the understanding of actin function;
2. Controversies exist between the actomyosin ring assembly models in fission yeast, especially how F-actin accumulates in the contractile ring;
3. Except Myo2p (type II myosin), it is still unclear whether the other 4 myosins play a role in fission yeast actomyosin ring assembly;
4. Studies of fission yeast actin suffered from a lack of sufficient actin mutants to dissect the function of actin in different cellular processes.

In order to solve these problems and gain more knowledge about actin function during cytokinesis, new methods to track F-actin dynamics *in vivo*, reexamine myosin mutants during actomyosin ring assembly and isolation of novel actin mutants are necessary and would be beneficial. Hence, the objectives of this study were to:

1. monitor F-actin dynamics *in vivo* in fission yeast cells. In order to monitor F-actin dynamics *in vivo*, lifeact, a remarkable small peptide that binds F-actin efficiently in many other organisms, will be applied in fission yeast cells. By ectopically tagging lifeact with a fluorescent protein such as GFP and expressing the fusion protein in wild-type or mutant fission yeast cells, F-actin dynamics can be studied by fluorescence microscopy and actomyosin ring assembly mechanisms could be inferred;
2. investigate the origin of F-actin in the actomyosin ring. Time-lapse confocal microscopy imaging of F-actin dynamics in live fission yeast cells should be helpful to solve this problem;
3. understand the roles of myosins during cytokinesis. Studying F-actin dynamics/localizations in different combinations of myosin mutants may

increase our knowledge of the functions of myosins;

4. screen and characterize novel actin mutants defective in cytokinesis. A new and efficient reverse genetic method called marker reconstitution mutagenesis should be fruitful for this purpose.

This study could be important and significant for the field of cytokinesis. It may provide new insights into mechanisms of actomyosin ring assembly and actin function during cytokinesis.

# CHAPTER II MATERIALS AND METHODS

## 2.1 YEAST STRAINS, MEDIUM AND REAGENTS

### 2.1.1 Yeast strains

Fission yeast strains used in this thesis are listed in Table I.

**Table I. *S. pombe* strains used in this thesis**

| Strain | Genotype | Source |
|---|---|---|
| MBY50 | *cdc3*-124 *ade6*-216 *ura4*-D18 *leu1*-32 $h^+$ | Lab collection |
| MBY102 | *ade6*-210 *ura4*-D18 *leu1*-32 $h^+$ | Lab collection |
| MBY103 | *ade6*-210 *ura4*-D18 *leu1*-32 $h^-$ | Lab collection |
| MBY104 | *ade6*-210 *ura4*-D18 *leu1*-32 $h^+$ | Lab collection |
| MBY112 | *cdc8*-110 *ade6*-210 *ura4*-D18 *leu1*-32 *his3*Δ $h^+$ | Lab collection |
| MBY144 | *cdc12*-112 *ura4*-D18 *leu1*-32 $h^-$ | Lab collection |
| MBY151 | *myo2*-E1 *ura4*-D18 *leu1*-32 $h^-$ | Lab collection |
| MBY169 | *wee1*-50 *leu1*-32 $h^-$ | Lab collection |
| MBY192 | *ura4*-D18 *leu1*-32 $h^-$ | Lab collection |
| MBY341 | *rng3-65 ade6*-210 *ura4*-D18 *leu1*-32 $h^-$ | Lab collection |
| MBY1241 | *cdc25*-22 *ura4*-D18 *leu1*-32 *his7*-366 $h^-$ | Lab collection |
| MBY2309 | P*nmt41*-GFP-CHD::*leu1*$^+$ *ade6*-216 *ura4*-D18 *leu1*-32 $h^-$ | Lab collection |
| MBY4678 | *adf1*-1::*ura4*$^+$ *ade6*-210 *ura4*-D18 *leu1*-32 $h^-$ | From K. Nakano[a] |
| MBY5856 | mCherry-*atb2*::*hph ura4*-D18 *leu1*-32 $h^-$ | Lab collection |
| MBY6247 | *cdc12*-3Venus::*kanMX6 ura4*-D18 *leu1*-32 $h^+$ | From I. Mabuchi[b] |
| MBY6248 | *cdc12*-3Venus::*kanMX6 ura4*-D18 *leu1*-32 $h^-$ | From I. Mabuchi |

| | | |
|---|---|---|
| MBY6501 | *act1::his5c*Δ*::ura4*$^+$ *leu1*-32 *his5*Δ *ura4*-D18 *ade5*Δ *ade7*Δ*::ade5*$^+$ h$^-$ | Lab collection |
| MBY6656 | P*act1*-Lifeact-GFP::*leu1*$^+$ *ura4*-D18 *leu1*-32 h$^-$ | This study |
| MBY6658 | P*act1*-Lifeact-GFP::*leu1*$^+$ *pcp1*-mCherry::*ura4*$^+$ *leu1*-32 h$^-$ | This study |
| MBY6659 | P*act1*-Lifeact-GFP::*leu1*$^+$ mCherry-*atb2*::*hph ura4*-D18 *leu1*-32 h$^-$ | This study |
| MBY6787 | *kanMX6*-P*nmt1-wee1*-50 *ura4*-D18 *leu1*-32 h$^-$ | This study |
| MBY6843 | P*act1*-Lifeact-mCherry::*leu1*$^+$ *ade6*-216 *ura4*-D18 *leu1*-32 h$^+$ | This study |
| MBY6844 | P*act1*-Lifeact-mCherry::*leu1*$^+$ *ade6*-216 *ura4*-D18 *leu1*-32 h$^-$ | This study |
| MBY6866 | *adf1*-1::*ura4*$^+$ *kanMX6*-P*nmt1-wee1*-50 P*act1*-Lifeact-GFP::*leu1*$^+$ h$^-$ | This study |
| MBY6914 | P*act1*-Lifeact-mCherry::*leu1*$^+$ *cdc12*-3Venus::*kanMX6* h$^+$ | This study |
| MBY6916 | *cdc25*-22 P*act1*-Lifeact-GFP::*leu1*$^+$ mCherry-*atb2*::*hph leu1*-32 h$^+$ | This study |
| MBY6955 | *cdc25*-22 P*act1*-Lifeact-mCherry::*leu1*$^+$ *rlc1*-3GFP::*kanMX6* h$^-$ | This study |
| MBY6988 | *cdc25*-22 P*act1*-Lifeact-mCherry::*leu1*$^+$ *cdc12*-3Venus::*kanMX6* | This study |
| MBY6996 | *cdc8*-110 P*act1*-Lifeact-GFP::*leu1*$^+$ | This study |
| MBY7004 | *for3*Δ::*kanMX6* P*act1*-Lifeact-GFP::*leu1*$^+$ mCherry-*atb2*::*hph leu1*-32 h$^+$ | This study |
| MBY7006 | *for3*Δ::*kanMX6 cdc25*-22 P*act1*-Lifeact-GFP::*leu1*$^+$ mCherry-*atb2*::*hph leu1*-32 | This study |
| MBY7103 | *mid1*Δ::*ura4*$^+$ P*act1*-Lifeact-GFP::*leu1*$^+$ mCherry-*atb2*::*hph leu1*-32 | This study |
| MBY7114 | P*act1*-Lifeact-GFP::*leu1*$^+$ | This study |

| | | |
|---|---|---|
| | mCherry-*atb2*::*hph ura4*-D18 *leu1*-32 $h^+$ | |
| MBY7132 | P*nmt41*-GFP-CHD::$leu1^+$ mCherry-*atb2*::*hph leu1*-32 $h^-$ | This study |
| MBY7133 | *cdc15*-140 P*act1*-Lifeact-GFP::$leu1^+$ mCherry-*atb2*::*hph leu1*-32 | This study |
| MBY7154 | *myo51*Δ::$ura4^+$ *ade6*-210 *ura4*-D18 *leu1*-32 $h^+$ | From D. P. Mulvihill[c] |
| MBY7160 | *mid1*-18 *cdc15*-140 P*act1*-Lifeact-GFP::$leu1^+$ mCherry-*atb2*::*hph leu1*-32 | This study |
| MBY7161 | *mid1*-18 P*act1*-Lifeact-GFP::$leu1^+$ mCherry-*atb2*::*hph leu1*-32 | This study |
| MBY7166 | *cdc15*Δ::$ura4^+$/$cdc15^+$ P*act1*-Lifeact-GFP::$leu1^+$ mCherry-*atb2*::*hph ura4*-D18/*ura4*-D18 *leu1*-32/*leu1*-32 $h^+/h^-$ | This study |
| MBY7167 | *cdc8*Δ::$ura4^+$/$cdc8^+$ P*act1*-Lifeact-GFP::$leu1^+$ mCherry-*atb2*::*hph ura4*-D18/*ura4*-D18 *leu1*-32/*leu1*-32 $h^+/h^-$ | This study |
| MBY 7176 | *cdc12*Δ::$ura4^+$/$cdc12^+$ P*act1*-Lifeact-GFP::$leu1^+$ mCherry-*atb2*::*hph ura4*-D18/*ura4*-D18 *leu1*-32/*leu1*-32 $h^+/h^-$ | This study |
| MBY7179 | *cdc7*-24 P*act1*-Lifeact-GFP::$leu1^+$ mCherry-*atb2*::*hph* | This study |
| MBY7200 | P*act1*-Lifeact-GFP::$leu1^+$ *ade6*-216 *ura4*-D18 *leu1*-32 $h^-$ | This study |
| MBY7228 | P*act1*-Lifeact-GFP::$leu1^+$ mCherry-*atb2*::*hph* (MBY6659) + *pREP42-cdc12*Δ*C*-GFP (pAY25, $ura4^+$) | This study (plasmid from F. Chang[d]) |
| MBY7244 | P*act1*-Lifeact-mCherry::$leu1^+$ *cdc12*-3GFP::*kanMX6* $h^-$ | This study |

| | | |
|---|---|---|
| MBY7277 | *cdc3*Δ::*ura4*$^+$/*cdc3*$^+$ P*act1*-Lifeact-GFP::*leu1*$^+$ mCherry-*atb2*::*hph ura4*-D18/*ura4*-D18 *leu1*-32/*leu1*-32 h$^+$/h$^-$ | This study |
| MBY7385 | *myo2*-E1 *myo51*Δ::*ura4*$^+$ *leu1*-32 | This study |
| MBY7465 | *cdc12*Δ::*ura4*$^+$/*cdc12*$^+$ *for3*Δ::*kanMX6*/*for3*$^+$ P*act1*-Lifeact-GFP::*leu1*$^+$ mCherry-*atb2*::*hph ura4*-D18/*ura4*-D18 *leu1*-32/*leu1*-32 h$^+$/h$^-$ | This study |
| MBY7519 | P*act1*-Lifeact-mGFP::*leu1*$^+$ *ade6*-210 *ura4*-D18 *leu1*-32 h$^+$ | This study |
| MBY7521 | *cdc25*-22 *for3*Δ::*kanMX6 ura4*-D18 | This study |
| MBY7629 | *cdc16*-116 P*act1*-Lifeact-GFP::*leu1*$^+$ *leu1*-32 | This study |
| MBY7639 | *his1*$^+$::P*act1*-Lifeact-GFP *ura4*-D18 *leu1*-32 *his5*$^-$ h$^-$ | This study |
| MBY7763 | *pREP41*-RFP-CHD (pCDL1548) in *his1*$^+$::Lifeact-GFP *his5*$^-$ *leu1*-32 | This study (plasmid from S. Martin[e]) |
| MBY7771 | *pREP42*-GFP-CHD in P*act1*-Lifeact-mCherry::*leu1*$^+$ | This study |
| MBY7840 | *for3*Δ::*kanMX6* P*nmt41*-GFP-*CHD* mCherry-*atb2*::*hph* | This study |
| MBY7862 | P*act1*-act1-GFP:: *leu1*$^+$ mCherry-*atb2*::*hph* | This study |
| MBY7867 | P*act1*-Utrophin-CH-GFP::*leu1*$^+$ mCherry-*atb2*::*hph* | This study |
| MBY7992 | *cdc3*-124 P*act1*-Lifeact-GFP::*leu1*$^+$ | This study |
| MBY7993 | *cdc25*-22 P*act1*-Lifeact-GFP::*leu1*$^+$ *rlc1*-mCherry::*ura4*$^+$ | This study |
| MBY7996 | *cdc16*-116 *cdc12*-112 | This study |

| | | |
|---|---|---|
| | P*act1*-Lifeat-GFP::*leu1*$^+$ *leu1*-32 | |
| MBY7998 | *cdc12*-3Venus::*kanMX6* mCherry-*atb2*::*hph* *ura4*-D18 *leu1*-32 h$^+$ | This study |
| MBY8025 | P*act1*-GFP::*leu1*$^+$ *ade6*-216 *ura4*-D18 *leu1*-32 h$^-$ | This study |
| MBY8029 | *myo51*Δ::*ura4*$^+$ *cdc12*-3Venus::*kanMX6* mCherry-*atb2*::*hph* | This study |
| MBY8031 | *myo2*-E1 *cdc12*-3Venus::*kanMX6* mCherry-*atb2*::*hph* | This study |
| MBY8033 | *myo2*-E1 *myo51*Δ::*ura4*$^+$ *cdc12*-3Venus::*kanMX6* mCherry-*atb2*::*hph* | This study |
| MBY8043 | P*act1*-GFP-CHD (1-189AAs)::*leu1*$^+$ *ade6*-216 *ura4*-D18 *leu1*-32 h$^-$ | This study |
| MBY8082 | P*act1*-GFP-F-Tractin (9-40AAs)::*leu1*$^+$ | This study |
| MBY8149 | *cdc25*-22 P*act1*-GFP-CHD (1-189AAs)::*leu1*$^+$ mCherry-*atb2*::*hph* | This study |
| MBY8246 | *act1*-j28::*his5*$^+$::*ura4*$^+$ *leu1*-32 *ade5*Δ *his5*Δ *ura4*-D18 *ade7*Δ::*ade5*$^+$ h- | This study |
| MBY8323 | P*act1*-GFP-GSTSG-*act1*::*leu1*$^+$ | This study |
| MBY8325 | P*act1*-GFP-GSTSGGSTSG-*act1*::*leu1*$^+$ | This study |
| MBY8437 | *aap1*-GFP::*ura4*$^+$ *ade6*-210 *ura4*-D18 *leu1*-32 h$^+$ | This study |
| MBY8458 | *aap1*-GFP::*ura4*$^+$ mCherry-*atb2*::*hph* | This study |
| MBY8460 | *aap1*-GFP::*ura4*$^+$ P*act1*-Lifeact-mCherry::*leu1*$^+$ | This study |
| MBY8462 | *aap1*-GFP::*ura4*$^+$ *rlc1*-tdTomato::*natMX6* | This study |
| MBY8558 | wt with pCDL1000 (pALKS) | This study |
| MBY8559 | wt with suppressor plasmid 2-2 (*act1*$^+$) | This study |
| MBY8560 | wt with suppressor plasmid 2-10 (*aap1*$^+$) | This study |

| | | |
|---|---|---|
| MBY8561 | *act1*-J28 with pCDL1000 (pALKS) | This study |
| MBY8562 | *act1*-J28 with suppressor plasmid 2-2 (*act1*$^{+}$) | This study |
| MBY8563 | *act1*-J28 with suppressor plasmid 2-10 (*aap1*$^{+}$) | This study |

[a]University of Tsukuba, Tsukuba, Japan.

[b]Gakushuin University, Tokyo, Japan.

[c]University of Kent, Kent, England, UK.

[d]Columbia University, New York, NY.

[e]University of Lausanne, Switzerland

### 2.1.2 Medium, culturing and saving conditions

Fission yeast cells are grown on Yeast Extract with Supplements (YES) or Edinburgh Minimal Medium (EMM) with supplements added as required (Moreno et al., 1991).

For physiological experiments, cells from either YES or selection plates were inoculated into liquid YES or selection medium overnight at 24°C. Only when O.D reaches 0.2 ~ 0.6, cells were used for further experiments. For temperature shift experiments, midlog phase cells were shifted to 36°C water bath incubator.

For strain saving, all strains were saved in YES + 30% glycerol and were freezed in -80°C.

### 2.1.3 Drugs used

To disrupt F-actin cytoskeleton, Latrunculin A (LatA, from Enzo Life Sciences) was used at a final concentration of 50 μM in all experiments. In Figure 6, after adding LatA, cells were shaken manually every minute to make sure all the cells were evenly treated with LatA.

To arrest cells in S phase, Hydroxyurea (HU, from Sigma-Aldrich) was used at a stock concentration of 1.2 M in all the experiments. In Figure 16 A and B,

cells were cultured in YES medium at 24°C overnight to midlog phase. 1 ml cells were treated with 10 µl HU at 24°C for 4 h. After adding another 10 µl HU, cells were shifted to 36°C for an additional 2.5 h. Then, HU was washed out (with 36°C YES medium), and cells were grown at 36°C for another 2 h (cells were at 36°C for 4.5 h before fixation). Then, cells were fixed with formaldehyde (final concentration of 3.7%) and stained with Alexa Fluor 488 phalloidin and antitubulin (TAT1, anti-α-tubulin mouse monoclonal antibody; a gift from K. Gull, University of Oxford, Oxford, England, UK) antibody to visualize F-actin and tubulin, respectively. In Figure 15 B, *cdc16*-116 LAGFP cells were cultured in YES medium at 24°C overnight to midlog phase. 1 ml cells were treated with 10 µl HU at 24°C for 4 h. After adding another 10 µl HU, cells were cultured at 24°C for an additional 1 h. Then, cells were shifted up to 36°C for 25 min and imaged on a YES agarose pad (cells were still immersed in HU) at 36°C.

To suppress *nmt* promoter expression, thiamine was used at a final concentration of 15 µM. For expressing CHD fusion protein in pREP41 or pREP42 plasmid, cells were first cultured in thiamine supplemented EMM without leucine (leu-) or EMM without uracil (ura-) overnight to midlog phase, respectively. Then cells were washed with leu- or ura- medium three times and resuspended in leu- or ura- medium for 18-24 h. For the expression of GFP-CHD under the *nmt41* promoter at *leu1* locus, *nmt41*-GFP-CHD-containing cells (MBY2309 and MBY7132) were first grown in YES at 24°C overnight to midlog phase and washed with complete minimal medium three times. Then, cells were resuspended in complete minimal medium for 18-24 h to induce the expression of GFP-CHD. For overexpression of Wee1-50p under the *nmt1* promoter to arrest cells in G2 phase, *nmt1*-*wee1*-50 *adf1*-1 LAGFP cells (MBY6866) were first grown in leu- medium with thiamine at 24°C overnight to midlog phase. After washing with leu- medium without thiamine three times, cells were resuspended in leu- medium without thiamine and cultured at 24°C for 16-20 h for the induction of Wee1-50p. After being shifted up to 36°C in a water bath shaker for 20 min, cells were put on a YES agarose pad and imaged in 36°C spinning-disk chamber. Cells would enter into mitosis after around 30 min from the time

they were shifted up in water bath shaker.

Phloxin B (final concentration: 5 mg/l) was used with YES medium to assist identification of temperature sensitive mutants or suppressors in 36°C.

## 2.2 MOLECULAR CLONING

### 2.2.1 PCR

All PCR were performed on a PTC-100$^{TM}$ Programmable Thermal Controller.

For a standard PCR, components were listed as follow: Template (0.4 µl), Buffer (10x Expand high fidelity buffer 2 from Rhoche), dNTP (2 mM, used as 10x), Forward primer (100 µM, used as 200x), Reverse primer (100 µM, used as 200x), Polymerase (Homemade taq from Temasek Life Sciences Laboratory or Expand high fidelity taq from Rhoche), dd$H_2O$ (add up to the total volume). Standard PCR program was as follow: 94°C 3 min, 94°C 15 s, 50°C 20 s, 72°C l min (per kb of DNA), 30 cycles from step 2 to step 4, 72°C 5 min, 16°C hold.

For inserting a fragment into a plasmid by Inverse PCR, two long primers (each primer around 50 bp, should have 25-30 bp overlap with the plasmid used later, PAGE purified) were used to clone the gene of interest. After purifying the PCR fragment, a 50 µl Inverse PCR was performed as follow: Plasmid template (30 ng), Purified PCR fragment (500 ng), Pfu Buffer (10x), dNTP (2 mM, used as 10x), Pfu Turbo (1 µl, Agilent), dd$H_2O$ (add up to the total volume). PCR program was as follow: 94°C 3 min, 94°C 15 s, 50°C 20 s, 68°C 2 min (per kb of DNA), 20 cycles from step 2 to step 4, 68°C 5 min, 16°C hold.

For sequencing PCR, 20 µl was used for one PCR: 8 µl Big Dye (from Temasek Life Sciences Laboratory), 4 µl Sequencing primer (1 pmol/µl), DNA (volume depends on concentration), dd$H_2O$ (add up to the total volume). For sequencing DNA fragment, total amount of DNA should be 30-50 ng. For plasmid sequencing, total amount of DNA should be 150-200 ng.

For random mutagenesis PCR by marker reconstitution mutagenesis method, most steps were the same as standard PCR except higher magnesium (final magnesium concentration: 4.0 mM~6.5 mM) and homemade taq (easier to incorporate mutation) were used in the reaction.

### 2.2.2 Restriction digestion and ligation

All restriction digestion and ligation were done using enzymes from NEB and protocols as NEB suggested.

### 2.2.3 Purification of PCR product

PCR products were purified by using QIAquick® spin columns 50 (QIAGEN). For 50 µl PCR, 250 µl Buffer PB was added and mixed by pipetting. Then the mixture was added into the QIAquick spin column and spun at 13,000 rpm for 30 s. After discarding flow-through and adding 750 µl Buffer PE, the column was spun for another 30 s. Fow-through was discarded and column was centrifuged for 1 min at maximum speed. 50 µl warm dd$H_2O$ was used to dissolve DNA.

### 2.2.4 Transformation of *E. coli*

*E. coli* XL1-Blue strain was used. Chemically competent cells (calcium chloride treated) were used to transform plasmids into *E. coli.* An appropriate amount of plasmids or ligation products were mixed with 100 µl competent cells on ice for 30 min. Cells were then heat shock at 42 °C for 2 min. For ampicillin resistant gene containing plasmids, cells were directly plated on LB ampicillin plates after heat shock and grew at 37 °C overnight.

### 2.2.5 Plasmid extraction

To extract plasmids from *E. coli*, PD column (Geneaid) was used. *E. coli* cells containing the plasmid of interest were overnight cultured in 4 µl LB ampicillin medium in 37°C shaker. After centrifugation, supernatant was discarded and 200 µl Buffer PD1 was added. Cells were mix by vortex. Then 200 µl Buffer PD2 and 300 µl Buffer PD3 were added sequentially to release DNA and precipitate proteins. Mixture was spun down at maximum speed (16,000 g) for 10 min. The recovered supernatant was passed through the PD

column. 400 µl Buffer W1 was added into the column and followed by 30 s centrifugation. 600 µl Wash Buffer was added and the column was spun for 30 s. Microcentrifuge again for 3 min to dry the column. 60 µl warm dd$H_2O$ was used to dissolve plasmids.

### 2.2.6 Plasmids constructed

Plasmids constructed in this thesis are listed in Table II.

To construct the pJK148-P*act1*-LAGFP plasmid (pCDL1484), oligonucleotides MOH4378 (with restriction site for EcoRI underlined in the following sequence: 5'-CCGGAATTCCAAAACCTTCTCTGCC-3') and MOH4379 (this primer contains the N-terminal sequence of lifeact: 5'-TTCTTGATAAGGTCAGCGACACCCATGGTCTTGTCTTTTGAGGGT T-3') were used in a PCR to obtain the 1 kb actin promoter from yeast genomic DNA. The purified fragment was then used as a template, together with MOH4380 (this primer contains the C-terminal sequence of lifeact with restriction site BamHI underlined in the following sequence: 5'-CGCGGATCCTTCCTTAGAAATAGACTCGAACTTCTTGATAAGGTC AGCGAC-3') and MOH4378, in a PCR to generate an actin promoter-LA fragment with EcoRI and BamHI sites at two ends. This actin promoter-LA fragment and pJK148-linker-GFP plasmid (pCDL1485; a gift from S. Oliferenko, Temasek Life Sciences Laboratory, Singapore; EGFP sequence was inserted between NdeI and NotI) were double digested by EcoRI and BamHI. The digested actin promoter-LA fragment was ligated into the pJK148-linker-GFP plasmid by T4 DNA ligase and transformed into *E. coli*. The plasmid was confirmed by sequencing (a point mutation was found at -408 in the actin promoter region; T was changed to A). The final codon-optimized lifeact sequence in fission yeast *S. pombe* is 5'-ATG-GGTGTCGCTGACCTTATCAAGAAGTTCGAGTCTATTTCTAAGGAA-3' (this sequence only encodes the first 16 amino acids of the original lifeact peptide).

To construct the pJK148-P*act1*-LAmCh plasmid (pCDL1564), the EGFP sequence of pCDL1484 was replaced by the mCh sequence by restriction

digestion and ligation method (NdeI and NotI restriction sites were used).

To construct the pJK148-P*act1*-Utr-CH-GFP plasmid (pCDL1561), the LA sequence of pCDL1484 was replaced by the first 783 base pairs (cloned from the pCDL1560 mCherry-Utrophin plasmid; a gift from A. Bershadsky, Mechanobiology Institute, Singapore; (Burkel et al., 2007)) of the human Utr gene by Inverse PCR (van den Ent and Lowe, 2006) using high fidelity Pfu DNA polymerase. Oligonucleotides used are as follows: MOH5182, 5'-CGAACCAAAAAACCCTCAAAAGACAAGACCATGGCCAAGTATG GAGAAC-3', and MOH5183, 5'-CATATGACCACCGGGACCACCGGAT-CCGTCTATGGTGACTTGCTGAGGT-3'. Two point mutations were found within the Utr gene, a silent mutation T339C and a missense mutation A707G (Gln236Arg).

To construct the pJK148-P*act1*-GFP-CHD plasmid (pCDL1581), LA sequence in the pJK148-P*act1*-LAGFP plasmid (pCDL1484) was first deleted by Inverse PCR to generate the pJK148-P*act1*-GFP plasmid (pCDL1577). Oligonucleotides used are as follows: MOH5262, 5'-AACCCTCAAAAGA-CAAGACCATGAGTAAAGGAGAAGAACTTTTCACTG-3', and MOH-5263, 5'-AGTTCTTCTCCTTTACTCATGGTCTTGTCTTTTGAGGGTTTT-TTGGTTCG-3'. Then, the linker sequence and the sequence encoding the first 189 amino acids of fission yeast protein Rng2p (these are exactly the same linker-CHD sequences used in the previous *nmt41*-GFP-CHD strain) were cloned from pCDL270 (pREP42-GFP-CHD plasmid) by PCR. The oligonucleotides used are as follows: MOH5264, 5'-CACATGGCATGG-ATGAACTATACAAAGGGCATATGTCGACAATGGACGT-3', and MOH-5265, 5'-GAGCTCCACCGCGGTGGCGGCCGCTTAAGCTTTGAAGTTA-GGAAGGAT-3'. This PCR fragment was used as a primer for Inverse PCR to insert the linker-CHD sequence into pJK148-P*act1*-GFP plasmid (pCDL1577), generating the pJK148-P*act1*-GFP-CHD plasmid (pCDL1581).

To construct the pJK148-P*act1*-GFP-F-Tractin plasmid, primers containing the codon-optimized F-Tractin (Johnson and Schell, 2009) sequence (GG-TATGGCTCGTCCTCGTGGTGCTGGTCCTTGTAGTCCTGGTTTAGAAC

GTGCTCCTCGTCGTAGTGTTGGTGAACTTCGTCTTCTTTTTGAAGCT) were used in an Inverse PCR to insert the linker (GGTAGTGGTGGTAGTG-GT)-F-Tractin sequence into pJK148-P*act1*-GFP plasmid (pCDL1577), generating the pJK148-P*act1*-GFP-F-Tractin plasmid (pCDL1584).

To construct the pJK148-P*act1*-GFP-GSTSG-*act1* (pCDL1608) or pJK148-P*act1*-GFP-GSTSGGSTSG-*act1* (pCDL1610) plasmids, primers containing either linker were used to clone *act1* gene first, then the purified DNA fragment was used in an an Inverse PCR to insert either GSTSG-*act1* or GSTSGGSTSG-*act1* into pJK148-P*act1*-GFP plasmid (pCDL1577).

To construct the pJK148-P*act1-act1*-GFP (pCDL1562), lifeact sequence in pJK148-P*act1*-LAGFP plasmid (pCDL1484) was replaced by *act1* gene by Inverse PCR.

**Table II. *S. pombe* plasmids constructed in this thesis**

| Plasmid No. | Description |
|---|---|
| pCDL1484 | pJK148-P*act1*-LAGFP |
| pCDL1561 | pJK148-P*act1*-Utr-CH-GFP |
| pCDL1562 | pJK148-P*act1-act1*-GFP |
| pCDL1564 | pJK148-P*act1*-LAmCh |
| pCDL1577 | pJK148-P*act1*-GFP |
| pCDL1581 | pJK148-P*act1*-GFP-CHD |
| pCDL1584 | pJK148-P*act1*-GFP-F-Tractin |
| pCDL1608 | pJK148-P*act1*-GFP-GSTSG-*act1* |
| pCDL1610 | pJK148-P*act1*-GFP-GSTSGGSTSG-*act1* |

## 2.3 YEAST CLASSIC GENETICS

### 2.3.1 Genetic crosses

To cross two haploid strains, equal amount of h+ and h- cells were mixed evenly with 1 µl $ddH_2O$ on YPD plates and kept in 24°C for two to three days. To cross a diploid strain with a haploid strain, the diploid cells were first patched on EMM without adenine (ade-) plate and were sporulated for 4 days. This process was repeated for 4 times to gain diploid cells which could not sporulate. Mating type was checked for these non-sporulating diploid cells. Equal amount of opposite mating type haploid cells were then mixed with these non-sporulating diploid cells with 1 µl $ddH_2O$ on YPD evenly and kept in 24°C for two to three days.

### 2.3.2 Tetrad analysis

To perform tetrad analysis, sporulated cells from YPD plates were first patched into a line on the side of an even YES plate by a loop. A new loop was used again to patched cells out of the line to a certain extent. The YES plate was then placed in the Biohazard Safty Cabinet for 30 min before the asci were dissected by a Singer Micromanipulator (MSM-Series 300, SINGER INSTRUMENT CO. LTD).

### 2.3.3 Random spore analysis

To perform random spore analysis, sporulated cells from YPD plates were suspended in 600 µl $ddH_2O$, mixed with 3µl Glusulase (from PerkinElmer Life Sciences, Inc), and incubated in 36°C shaker overnight. After spun down, spores were resuspended with 500 µl $ddH_2O$. Then 250 µl ethanol (70%) was added to eliminate the vegetative cells and the tube was gently inverted twice. Spores were immediately washed with $ddH_2O$ three times and resuspended in 1000 µl $ddH_2O$. Generally, 0.3 µl of spores were then resuspended in 75 µl $ddH_2O$ and plated onto YES or selection plate.

## 2.4 YEAST MOLECULAR GENETICS

### 2.4.1 Yeast transformation

For yeast transformation, midlog phase cells (O.D multiplied by the volume of cells should equal to 10) were spun down and washed with equal volume of

water. After washing with 1 ml LiAc (1 M, pH 7.5, used as 10x)/TE ( 0.1 M Tris-HCl, 0.01 M EDTA, pH 7.5, used as 10x) buffer, cells were resuspended in 100 µl LiAc /TE (concentrations same as above) and incubated with 2 µl sonicated salmon sperm DNA (10 mg/ml, boiled, from STRATAGENE) and plasmid (or DNA fragment) at room temperature for 15 min. 240 µl polyethylene glycol/LiAc/TE solution (LiAc and TE concentrations same as above; 8 g of polyethylene glycol 4000 in 2 ml 10x LiAc and 2 ml 10x TE and 9.75 ml dd$H_2O$, filter sterilize) was added, and cells were incubated at 24°C or 30°C (depend on whether the cells were temperature sensitive) for 45 min. Then, 43 µl DMSO (from Sigma-Aldrich) was added, and cells were given a heat shock at 42°C for 5 min. Cells were spun down, resuspended in 75 µl dd$H_2O$, and spread onto appropriate plate.

### 2.4.2 Yeast genomic DNA purification

To purify genomic DNA from fission yeast, fresh cells from appropriate plates were suspended in 0.5 ml 1x TE. After spun down, cells were resuspended in 0.5 ml 1.2 M Sorbital/0.1 M EDTA/2 mg per ml Zymolyase (USBiological)/ 5 mg per ml Lysine Enzyme (SIGMA)/1% 2-Mercaptoethanol (SIGMA) at 37°C for 30 min. Spheroplasts were then spun down, resuspended in 450 µl 100 mM NaCl/50 mM EDTA/50 mM Tris, 50 µl 10% SDS, and 10 µl 20 mg/ml Proteinase K (Finnzymes) at 65°C for 45 min. Cells were kept on ice for 10 min, added 200 µl 5 M potassium acetate, mixed, and kept on ice for another 30 min. Cells were spun down at 4°C for 30 min to remove proteins. Supernatant was recovered and equal volume of isopropanol was added to precipitate DNA. DNA pellet was spun down and washed with 70% ethanol. DNA pellet was recovered by centrifuge. After air dried, DNA was resuspended in 50 µl dd$H_2O$.

### 2.4.3 Yeast colony PCR

To perform yeast colony PCR, yeast cells were suspended in a PCR tube containing 25 µl dd$H_2O$. Cells were boiled in 99°C PRC machine for 10 min to release DNA. After spun down, 5 µl of the supernatant was used in a 20 µl PCR. PCR program was the same as normal PCR.

### 2.4.4 Yeast marker reconstitution mutagenesis

For generating fission yeast actin mutants (including *act1*-j28), a reverse genetic method called marker reconstitution mutagenesis was used as described (Subramanian et al., 2013; Tang et al., 2011). Briefly, an *act1*::his5C (*act1* gene followed by the C-terminal region of *his5* gene) DNA fragment was amplified under high magnesium concentration (final magnesium concentration: 4.0 mM~6.5 mM) by PCR to randomly mutate the *act1*::his5C DNA fragment. Then the randomly mutated fragments were transformed into MBY6501 (*act1::his5c*Δ*::ura4*$^{+}$ *leu1*-32 *his5*Δ *ura4*-D18 *ade5*Δ *ade7*Δ*::ade5*$^{+}$ h$^{-}$) and cells were grew on EMM without histidine and uracil (his- ura-) plates. Cells grew up from his- ura- plates had a high chance to replace the *act1*+ gene and reconstruct the *his5* gene. Colonies were then replicated toYES + Phloxin B and cultured at 36$^{o}$C overnight. Dark red or pink red colonies were sequenced to confirm the mutation at the *act1* locus. Actin mutants were back crossed to confirm the unique insertion.

### 2.4.5 Yeast high copy suppressor screen

To identify genes that could rescue *act1*-j28 mutant lethality at restrictive temperature, a high copy suppressor screen was performed as described (Forsburg, 2001; Nakamura et al., 2001; Tanaka et al., 2000). Fission yeast genomic DNA library (pTN-L1) was first transformed into *act1*-j28 cells (overnight YES cultured midlog phase cells) on leu- plates and put in 24$^{o}$C. After colonies grew up, cells were replicated to fresh YES + Phloxin B plates and grew in 36$^{o}$C overnight. Then colonies showing white color or light pink color were checked under microscopy to confirm rescue. Plasmids in these potential suppressor colonies were recovered by genomic DNA purification process, *E.coli* transformation and plasmid purification. Sequencing PCR was used to examine the genes in the suppressor plasmids. 11 individual transformations were carried out.

### 2.4.6 Yeast GFP tagging

To tag the potential *act1*-j28 suppressor Aap1p with GFP at the C-terminal, a forward primer (MOH5646) containing 80 bp of *aap1* ORF at the 3' end (no stop codon, followed by a linker sequence: GGTAGCGGCAGCGGTAGC)

with homologous sequence upstream of GFP::*ura4*$^{+}$ cassette and a downstream primer (MOH5647) containing the first 88 bp of *aap1* 3' UTR with homologous sequence downstream of GFP::*ura4*$^{+}$ cassette were used in a PCR to amplify a fragment from pCDL778 plasmid. Then this DNA fragment was transformed into wt fission yeast cells on ura- plates. Fluorescence was confirmed under widefield microscopy.

### 2.4.7 Yeast strain construction

To construction yeast strains carrying the pJK148 constructs, the integrative pJK148 plasmids (pJK148-P*act1*-LAGFP, pJK148-P*act1*-LAmCh, pJK148-P*act1*-GFP, pJK148-P*act1*-Utr-CH-GFP, pJK148-P*act1*-GFP-CHD, pJK148-P*act1*-GFP-F-Tractin, pJK148-P*act1-act1*-GFP, pJK148-P*act1*-GFP-GSTSG-*act1* and pJK148-P*act1*-GFP-GSTSGGSTSG-*act1*) were digested by NruI within the *leu1*+ gene. The digested products were purified and transformed into the yeast cells. The transformants were selected on leu- medium, and the colonies were further screened visually for fluorescence. The pJK148 constructs carrying strains were then used to cross with the other strains of interest. Diploid strains were transformed by NruI-digested pJK148-P*act1*-LAGFP plasmid. Positive strains were grown on ade- leu- ura- or ade- leu- his- (depending on the marker used to delete the essential gene in the diploid). The diploids carrying LAGFP were patched out every 4 d until nonsporulating strains were obtained. The LAGFP-expressing nonsporulating strains were then used to cross with cells expressing both LAGFP and mCh-Atb2p (MBY6659 or MBY7114) to get the sporulating diploid strains carrying both LAGFP and mCh-Atb2p.

To construction the P*nmt1-wee1*-50 strain (with *KanMX6* marker), a DNA fragment containing the *KanMX6* cassette and *nmt1* promoter was cloned from plasmid pFA6a-KanMX6-P3*nmt1*-3HA (pCDL953; a gift from Jian-qiu Wu, Ohio State University, Columbus, OH) and then transformed into the *wee1*-50 strain (MBY169). The oligonucleotides used are as follows: MOH5304, 5'-GCATTCCAATTCAATTTAATTAAATCAAAAATTTCATATCTATTT TTTTGTTAAATTGCCACATTTTCCATACAGAAAACGAATTCGAGCTC GTTTAAAC-3', and MOH5305, 5'-GTAGCACGATTTAGATTCATGGAG-

CGTTGGGACCGCCGTAAGCCATAAGATCTATGACTGCTGGTATTAG AAGAAGAGCTCATCATGATTTAACAAAGCGACTATA-3'. The transformants were selected on G418 plates and replicate to complete minimal medium for screening the positive clones, which showed a G2-arrested phenotype.

## 2.5 YEAST CELL BIOLOGY METHODS

### 2.5.1 Cell fixation

Cells were either fixed by either formaldehyde solution (stock concentration: 37%, from MERCK) or freshly prepared paraformaldehyde solution (powder from Sigma-Aldrich).

For formaldehyde fixation, after adding 100 µl formaldehyde into 900 µl cells, cells were fixed on a shaker for 10 min at appropriate temperature. Then cells were washed with 1 ml 1x PBS for twice.

As white precipitates (paraformaldehyde) may develop during storage, the concentration of the ready-made formaldehyde solution may differ. Therefore freshly prepared paraformaldehyde solution was also used. For paraformaldehyde fixation, 0.2 g paraformaldehyde power was first dissolved in 1x PBS (total final volume: 1 ml) at 90°C for around 15 min. After cooling down, 200 µl paraformaldehyde solution was added into 800 µl cells and fixed on a shaker for 10 min at appropriate temperature. Cells were washed with 1 ml 1x PBS for twice.

### 2.5.2 F-actin staining

To stain F-actin structures in fission yeast, fixed cells were first permeablized with 1 ml 1% Triton X-100 (SIGMA, diluted by 1x PBS) for 1 min and washed with 1 ml 1x PBS for twice. After concentration, 9.8 µl fixed cells were mixed with 0.2 µl Alexa Fluor 488 phalloidin (Invitrogen) and incubated in dark for 7 min.

### 2.5.3 Nucleus and cell wall staining

After paraformaldehyde fixation, fission yeast nucleus was stained by DAPI

(4', 6-diamidino-2-phenylindole) and cell wall was stained by Aniline Blue.

### 2.5.4 Immunofluorescence staining

Fixed cells were treated with 1 ml 1% Triton X-100 for 1 to 2 min, washed twice with 1x PBS and once with PBS containing 1. 2 M sorbitol. Then cells were resuspended in 140 µl PBS solution containing 1. 2 M sorbitol and 60 µl protoplasting enzyme mixture containing 5 mg/ml lysing enzyme and 3 mg/ml zymolyase (made in PBS containing 1.2 M sorbitol). Cells were kept in 36°C to protoplast for around 1 h. The protoplast process was then monitored under light microscopy every 5 to 10 min by mixing small amount of cell suspension with SDS on glass slides. Protoplasted cells were spun down and washed 3 times with 1x PBS and once with PBAL blocking solution (PBS + 10% BSA, 100 mM lysine hydrochloride, 50 µg/ml carbenicillin and 1 mM sodium azide). Cells were blocked in PBAL solution for 1 h at room temperature. Then cell suspension was incubated with primary antibodies for 3 h at room temperature or overnight at 4°C. After 3 times washed with PBAL, cells were incubated in dark with flurochrome-conjugated secondary antibodies for 1 h at room temperature. Cells were washed 3 times with PBS before image acquisition. Anti-TAT1 antibodies were used at a dilution of 1:100 to visualize microtubules. Anti-Cdc4p antibodies were used at a dilution of 1:200 to visualize fission yeast Cdc4p. Flurochrome-conjugated secondary antibodies were used at a dilution of 1:200.

### 2.5.5 FM4-64 staining

To stain the cell membrane, 1000 µl cells were fist spun down at 2,600 rpm for 1 min. After getting rid of 800 µl supernatant, 2 µl FM4-64 (Life technologies) was added and cells were incubated on a shaker for 30 min.

### 2.5.6 Yeast cell cycle synchronization

Cells for synchronization were cultured in YES medium at 24°C overnight to midlog phase. 1 ml cells were treated with 10 µl HU (1.2 M, Sigma-Aldrich) at 24°C for 4 h. After adding another 10 µl HU, cells were cultured for one more hour. Synchronization was checked under microscopy before imaging.

## 2.6 MICROSCOPY IMAGE ACQUISITION AND DATA ANALYSIS

### 2.6.1 Epifluorescent microscopy

Bright field and epifluorescent images were captured using an Olympus IX71 microscopy (PlanApo 100x/1.45 Oil objective lens) equipped with a Photometrics CoolSNAP HQ CCD camera and Metamorph (v6.2r6) software (Molecular Devices).

### 2.6.2 Spinning disk microscopy

Spinning disk images were captured either by spinning disk using a Zeiss Axiovert 200M microscopy or Microlambda spinning disk (manufacturer: *micro*LAMBDA). Spinning disk using a Zeiss Axiovert 200M microscopy (Plan-APOCHROMAT 100x/1.4 Oil objective lens) was equipped with a Yokogawa CSU-21 spinning disk system, Hamamatsu ORCA-ER camera and MetaMorph (v7.6.5.0) software. Cobolt Calypso™ 491 nm solid-state laser and Cobolt Jive™ 561 nm solid-state laser were used for excitation. Microlambda spinning disk using a Nikon ECLIPSE Ti microscopy (Plan Apo *Vc* 100x/1.40 Oil objective lens) was equipped with a Yokogawa CSUX1FW spinning disk system, Photometrics CoolSNAP $HQ^2$ camera and MetaMorph (v7.7.7.0) software. Cobolt Calypso™ 491 nm DPSS laser, Cobolt Fandango™ 515 nm DPSS laser and Cobolt Jive™ 561 nm DPSS laser were used for excitation.

### 2.6.3 TIRF microscopy

TIRFM images were acquired on a custom setup from TILL Photonics based on an automated iMic-stand and an Olympus 1.45 NA 100x objective. Lasers at 488 nm (Coherent Sapphire 75 mW) and 561 nm (Cobolt Jive 75mW) were coupled through an AOTF and a galvanometer-driven scan head to adjust TIRF angles.

### 2.6.4 Time-lapse movie slide preparation

For all spinning disk time-lapse movies, cells were concentrated by centrifugation at 4,200 rpm for 10 s to 1 min. 1 µl of cells were placed on a single concave glass slide (Sail brand) with either YES + 2% agarose pad or selection medium + 2% agarose pad (on the concave side), then sealed under a

coverslip using VALAP and imaged at the respective temperature.

### 2.6.5 Image acquisition

All time-lapse movies were taken either by spinning disks or TIRFM.

3D Spinning disk images were collected with a step size of 0.2-0.5 μm. Time-lapse images were acquired with an interval time of 5 s, 10 s, 15 s, 25 s or 30 s. Unless specified otherwise, all these 3D images were shown by 2D maximum-intensity projection. Double color single plane spinning disk images were collected with an interval time of 1.3 s. For time-lapse movies at 36°C, temperature was controlled and maintained by a full enclosure incubation chamber. If not specified, the fluorescent images were taken at 24°C.

All TIRF images were taken by Dr. Haochen Yu or Dr. Roland Wedlich-Soldner (Max Planck Institute of Biochemistry, Germany). TIRF images were collected with an Andor iXON DU-897 EMCCD camera at maximum gain after a 2x magnifying lens (Andor). Acquisition was controlled by the Live Acquisition (LA) software package. Cable extension rates were quantified from TIRFM series with 200 ms frame rate. Cable ends were tracked for at least 4 frames. Rates are given as mean ± SD. Unpaired t-tests with Welch correction were performed to test significance of variations. For TIRFM double color time-lapse images, the interval time were 5 s. Switching between two filters took about 1 s. TIRF images were notified in the figure legends. If not specified, the fluorescent images were taken by spinning disk.

### 2.6.6 FRAP

FRAP (fluorescence recovery after photobleaching) experiments were done with Microlambda spinning disk equipped with i*Las*$^2$ system (Roper Scientific).

### 2.6.7 Image analysis and data processing

Images were analyzed using ImageJ (http://rsb.info.nih.gov/ij/) or Metamorph. All maximum-intensity projected spinning disk images were background subtracted using “Process/Subtract Background” function in ImageJ. After

background subtraction, some time-lapse movies were bleach corrected using "Plugins/Stacks-T-functions/Bleach Correction" plugin in ImageJ. For making kymographs, a line was first drawn from one pole to another along the cell long axis of the cell of interest, then "Image/Stacks/Reslice" function in ImageJ was used to make the kymograph. Many lines were drawn in one cell but only one representative kymograph of each cell was shown. For measuring the average intensity along the cell long axis, a square was first drawn outside each cell, then "Analyze/Plot Profile" function in ImageJ was used to measure the average intensities along the cell long axis. In some images, different channels of the same cell taken at the same time point were combined together using "Plugins/Stacks-Building/Stack Combiner" plugin or "Plugins/Stacks-Building/Stack Inserter" in ImageJ. All time-lapse movies were edited by ImageJ or MetaMorph software. Graphs in this thesis were made by Excel or Adobe Illustrator. Pseudocolors were used to facilitate visualization in some images. Some widefield images were deconvoluted by AutoQuant (Media Cybernetics, Inc.). Imaris (Bitplane) was used for 3D visualization.

## 2.7 BIOINFORMATICS

For muti-sequence alignment, CluterX (1.81) and BLAST (Basic Local Alignment Search Tool, http://blast.ncbi.nlm.nih.gov/) were used. For transmembrane prediction, TMHMM Server v.2.0 was used.

# CHAPTER III NON-MEDIAL ACTIN CABLES MIGRATE TOWARDS THE MIDDLE OF THE CELL DURING ACTOMYOSIN RING ASSEMBLY

## 3.1 INTRODUCTION

Fission yeast utilizes an actomyosin based contractile ring for cell division (Mishra and Oliferenko, 2008; Pollard and Wu, 2010). Despite decades of analysis, the mechanism of actomyosin ring assembly is still not completely understood. However, previous work established two main ring assembly models in fission yeast, both agree that F-actin is *de novo* nucleated in the cell medial region (Chang et al., 1997; Coffman et al., 2009; Pollard and Wu, 2010; Vavylonis et al., 2008; Wu et al., 2003; Yonetani et al., 2008).

In this chapter, we used lifeact as an F-actin monitoring probe to study F-actin dynamics during cytokinesis in fission yeast. Our results suggest that a significant fraction of F-actin in the actomyosin ring was recruited from the non-medial region (see Section 3.2.4, 3.2.5 & 3.2.7). The nucleation of non-medial F-actin depended on formin-Cdc12p but was independent on the ring assembly pathways (Mid1p-dependent pathway and SIN-dependent pathway) (see Section 3.2.11-3.2.13). Further experiments also showed that these non-medially assembled F-actin cables migrated towards the medial region of the cell in a Myo2p (type II myosin) and Myo51p (type V myosin) dependent manner (see Section 3.2.16 & 3.2.18).

## 3.2 RESULTS

### 3.2.1 F-actin cables are connected to the actomyosin ring during cytokinesis in fixed wild-type cells

F-actin cables are one of the three F-actin structures in fission yeast and are composed of bundles of short F-actin filaments (Kamasaki et al., 2005; Kanbe et al., 1994). Although these F-actin cables are known to be important for cell polarity and cargo transport (Kovar et al., 2011; Lo Presti et al., 2012; Nakano et al., 2002), they are considered dispensable for actomyosin ring assembly (Feierbach and Chang, 2001). Previous work showed that actomyosin ring was intact but F-actin cables were missing in *for3*Δ cells (Feierbach and Chang,

2001). However, this result is debatable because work from another group found that, although F-actin cables were reduced in number, short F-actin cables were still present in mitotic *for3*Δ cells (Arai and Mabuchi, 2002; Nakano et al., 2002). It is unknown whether these longitudinal F-actin cables contribute to actomyosin ring assembly in fission yeast. In order to address this, we checked the spatial relationship between F-actin cables and the actomyosin ring by phalloidin staining of the paraformaldehyde fixed wild-type (wt) cells and cells expressing the cell cycle stage indicator mCherry-Atb2p (mCh-Atb2p) (Figure 1 A and B) (Ding et al., 1998). Interestingly, long F-actin cables were found in all stages of cell cycle (Figure 1 A and B). In some cases, short F-actin cables were found located near the cell tips without any obvious link to the medial region of the cell (Figure 1 A, yellow asterisk). Meanwhile, some other long F-actin cables were often found to extend from regions near the tip directly into the assembling actomyosin ring (Figure 1 B, red asterisks). Since F-actin cables were seen in mitotic cells, we next investigated the role of actin cables in actomyosin ring assembly.

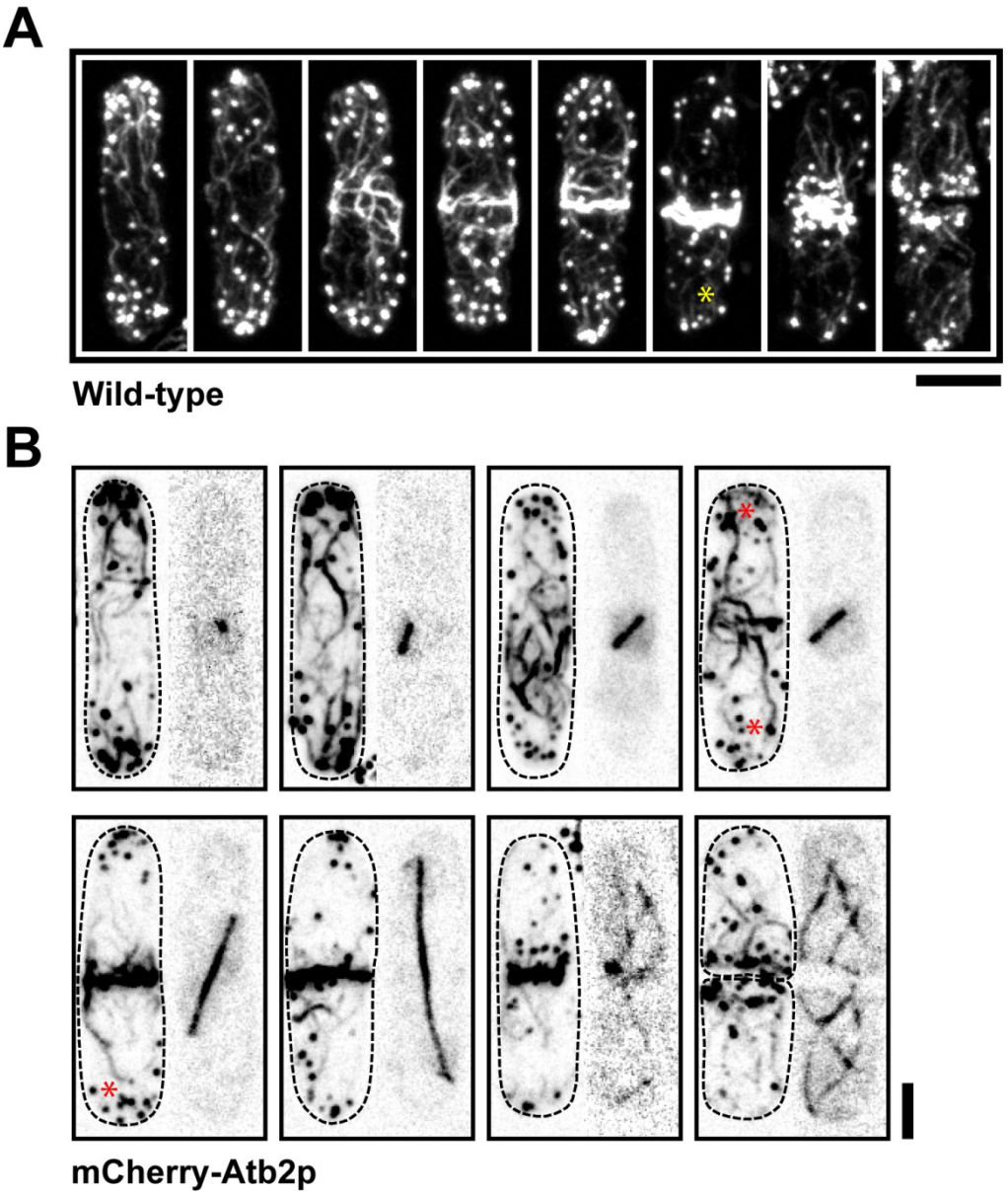


**Figure 1.** F-actin cables were observed in all stages of cell cycle in fission yeast.

(A) Wt cells were fixed with paraformaldehyde and stained with Alexa-488 phalloidin. Yellow asterisk shows a short F-actin cable located near the tip of a mitotic cell. (B) Cells expressing mCherry-Atb2p as cell cycle marker were fixed with paraformaldehyde and stained with Alexa-488 phalloidin. Red asterisks show long F-actin cables connecting to the actomyosin ring from the ends. Dashed line indicates the cell boundary. Bars, 5 μm.

### 3.2.2 Direct tagging of actin hampered its function

To test whether F-actin cables participate in actomyosin ring assembly, a reliable probe for monitoring F-actin dynamics in live fission yeast cells is necessary. F-actin dynamics in higher eukaryotes were monitored for decades by direct fluorophore tagging (Ballestrem et al., 1998; Vishwasrao et al., 2012). But unfortunately, even though actin is highly conserved among eukaryotes, both fission yeast and budding yeast actin do not tolerate direct fluorophore tagging (Chen et al., 2012; Doyle and Botstein, 1996; Pollard and Wu, 2010; Wu and Pollard, 2005). Even tetracysteine (a 12 AAs long modified version) tagged actin could not be incorporated into fission yeast F-actin cables or rings (Chen et al., 2012; Martin et al., 2005a). It was suggested that this intolerance to tagging could be because the tagged G-actin monomer could not pass through the formin homodimeric FH2 ring (Chen et al., 2012; Xu et al., 2004). However, the reason is still unclear and need further investigation. To test whether the intolerance was due to low expression level or expression nonuniformity by the commonly used inducible *nmt* promoters, a second copy of fission yeast actin was tagged with GFP at the C-terminal and expressed under the high expression *actin* promoter in *leu1* locus. However, actin-GFP still failed to be incorporated into F-actin cables or rings (Figure 2 A). Similar to previous work (Chen and Pollard, 2013; Wu and Pollard, 2005), actin-GFP did incorporate into some actin patch-like structures. And similar to untagged actin patches, these actin-GFP patch-like structures could also accumulate in the division site during mitosis (Figure 2 A, arrows). Furthermore, three other possible methods to solve the tagging intolerance are to use different tagging sites, different linker sequence and different linker length. As N-terminal tagging of mammalian actin was successful (Ballestrem et al., 1998), the same linker sequence (GSTSG) was used for the N-terminal tagging of fission yeast actin under actin promoter (Figure 2 B). Same as the C-terminal tagging, GFP-GSTSG-actin patch-like structures were found and no incorporation into F-actin cables were observed (Figure 2 B, left). Interestingly, we realized that GFP-GSTSG-actin cable-like structures present in some cells (Figure 2 B, right, asterisks; cells were from plate), suggesting it might still be possible to tag actin successfully if conditions are further modified. In order to check whether a longer linker would aid the incorporation (Figure 2 C), a linker with

double the length (GSTSGGSTSG) was used. GFP-GSTSGGSTSG-actin was expressed as a second copy of actin under actin promoter. As in the previous case, only actin patch-like structures were observed while fluorescent F-actin cables were still absent (Figure 2 C, left). But once again, cable-like structures were also found in some of the GFP-GSTSGGSTSG-actin cells (Figure 2 C, right, asterisks; cells were from plate). Taken together, this data suggests that direct tagging of actin with GFP either at the C- or N-terminus hampers the incorporation of actin monomers into F-actin cables.

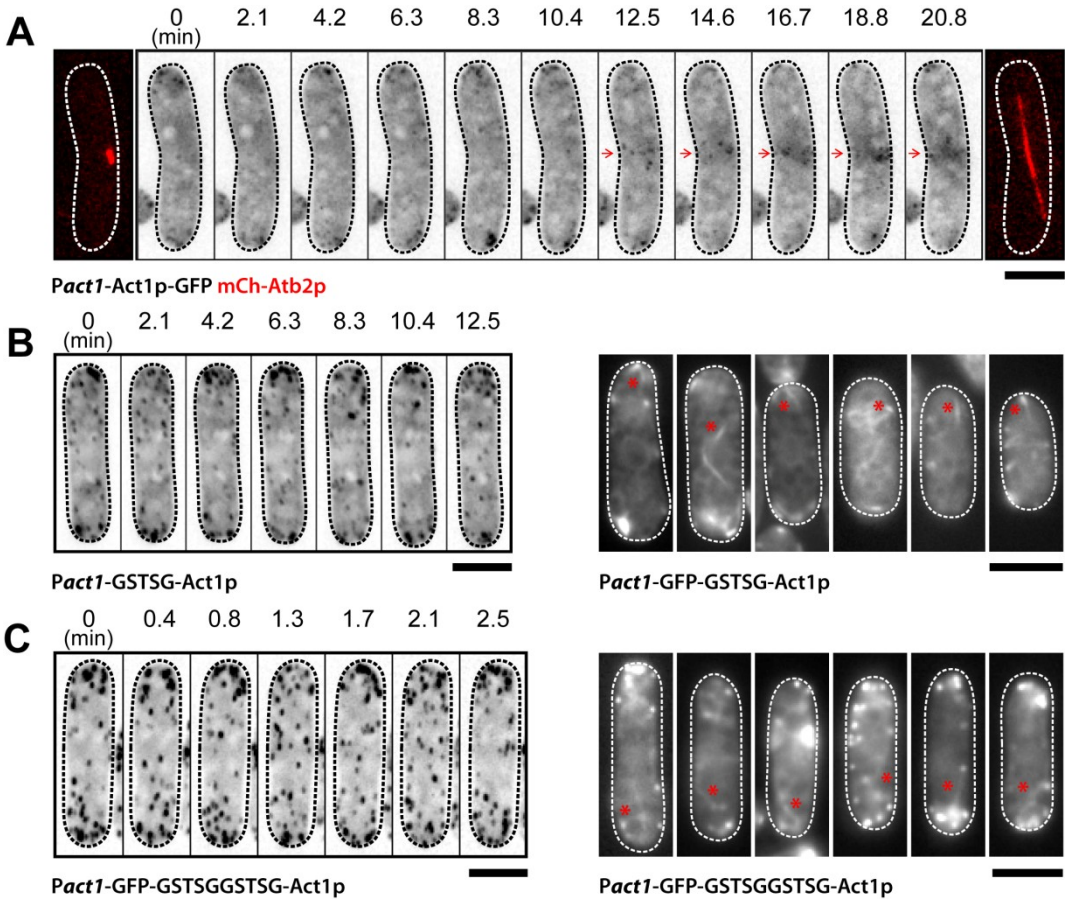


**Figure 2.** Direct tagging of actin hampered its function.

(A) Time-lapse images of a P*act1*-Act1p-GFP mCh-Atb2p cell. The pseudo-color red mCh-Atb2p micrographs on the left and right were taken at 0 and 20.8 min, respectively. Arrows show medial accumulation of patches-like structures during mitosis. All the GFP tagged actin constructs in Figure 2 were expressed under fission yeast *actin* promoter and integrated into the genome at the *leu1* locus as a second copy of actin. pJK148 plasmid was used for the integration and expression. (B) Time-lapse images on the left show a P*act1*-GFP-GSTSG-Act1p cell from liquid YES culture. Micrographs on the right show cells directly taken from plate. Red asterisks indicate the cable-like structures. (C) Time-lapse images on the left show a P*act1*-GFP-GSTSGGSTSG-Act1p cell from liquid YES culture. Micrographs on the right show cells directly taken from plate. Red asterisks indicate the cable-like structures. Dashed line indicates the cell boundary. Bars, 5 μm.

### 3.2.3 Lifeact is a reliable probe to visualize F-actin in living fission yeast cells

As shown earlier, direct tagging of actin with GFP could not accomplish the goal of monitoring F-actin cable dynamics in fission yeast. Moreover, direct fluorophore tagging of actin may affect its dynamics (Aizawa et al., 1997; Deibler et al., 2011; Feng et al., 2005; Westphal et al., 1997). Alternatively, another protein that binds F-actin cables uniformly may be monitored as an indirect approach to study actin dynamics. This strategy has been widely adopted in many organisms (Berepiki et al., 2010; Edwards et al., 1997; Riedl et al., 2008; Riedl et al., 2010; Schell et al., 2001; Vidali et al., 2009). Among the many actin binding proteins available, only one peptide called Calponin Homology Domain (CHD, 1-189 AAs from fission yeast Rng2p) was used for visualizing F-actin in live fission yeast before this thesis (Martin and Chang, 2006; Wachtler et al., 2003; Wu and Pollard, 2005). Fluorophore tagged CHD was capable of labeling F-actin patches clearly in fission yeast (Wachtler et al., 2003). However, comparing to phalloidin labeled F-actin cables, F-actin cables labeled by fluorophore tagged CHD were not clear enough in time-lapse imaging (Wu and Pollard, 2005). Hence, a new marker was necessary for monitoring F-actin cable dynamics in fission yeast.

Lifeact appeared to be a good candidate for this purpose (Riedl et al., 2008). Lifeact is the N-terminal 17 AAs short peptide from budding yeast Abp140 protein that has been successfully applied to label F-actin in many organisms, such as mammalian cells, plant cells and fungi (Berepiki et al., 2010; Delgado-Alvarez et al., 2010; Riedl et al., 2008; Riedl et al., 2010; Vidali et al., 2009). Lifeact is considered to have little deleterious effect on actin functions, due to a number of reasons: small size, rapid exchange rate and the lack of homologous sequence in many cell types. BLAST result shows that lifeact has no homologous sequence in the fission yeast proteome as well (data not shown). This decreases the possible interaction between lifeact and other endogenous proteins. We fused lifeact with various fluorophores at the C-terminus, expressed under fission yeast *actin* promoter and integrated into the genome at the *leu1* locus.

Cells expressing lifeact-GFP (LAGFP) or lifeact-mCherry (LAmCh) fusion proteins had no obvious morphology defects (Figure 3 A and D) and grew at the same rate as the untagged wt cells (Figure 3 B). Lifeact decorated all the three F-actin structures clearly in fission yeast (Figure 3 C, asterisks show F-actin cables) and colocalized with the phalloidin (a conventional F-actin binding dye) staining pattern (Figure 3 D), suggesting that the lifeact labeled structures represent the real fission yeast F-actin structures. F-actin cables depend on profilin-Cdc3p for their assembly and tropomyosin-Cdc8p for their stability (Balasubramanian et al., 1992; Balasubramanian et al., 1994). Therefore, *cdc3*Δ and *cdc8*Δ cells were tested by lifeact (Figure 3 E). In these cells, lifeact-labeled F-actin cables were absent or significantly reduced, matching the description in previous studies. To examine the turnover of lifeact molecules on the F-actin structure, FRAP experiments were carried out (Figure 3 F). Results show that lifeact has a fast turnover rate. In conclusion, our study suggests that lifeact is a reliable probe to visualize F-actin structures in living fission yeast cells.

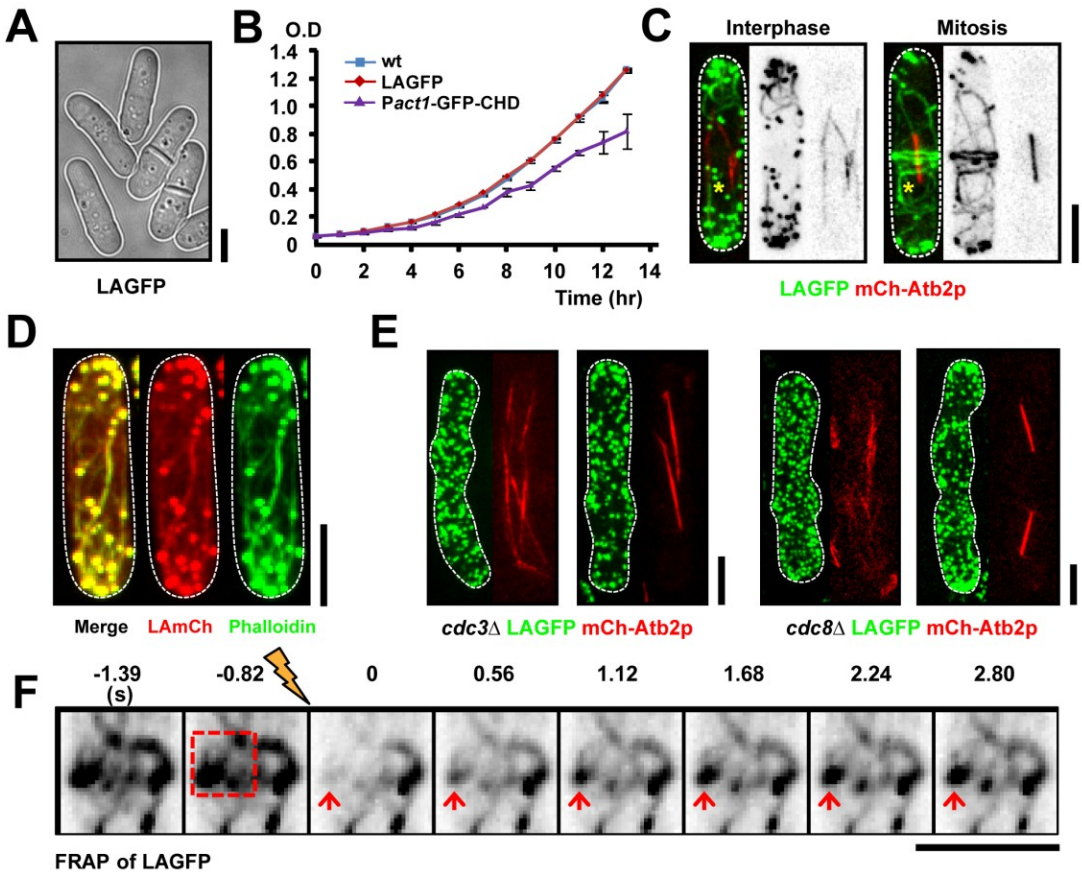


**Figure 3.** Lifeact is a reliable probe to visualize F-actin in living fission yeast cells.

(A) Bright field image of LAGFP cells. (B) Growth curves of wt, LAGFP and P*act1*-GFP-CHD cells grown in YES at 30°C. O.D = Optical Density. Error bars show means ± SD of three independent experiments. (C) LAGFP mCh-Atb2p cells in interphase and mitosis. Asterisks indicate actin cables. (D) LAmCh cells were were fixed with paraformaldehyde and stained with Alexa-488 phalloidin. Images are maximum-intensity projected. (E) Images of interphase and mitotic cells of *cdc3Δ* LAGFP mCh-Atb2p and *cdc8*Δ LAGFP mCh-Atb2p germinated from spores. (F) Representative FRAP experiment of a single layer of LAGFP cells. The broken box illustrates the medial bleached area. Red arrows show the recovery of a bleached structure. Dashed line indicates the cell boundary. Bars, 5 μm.

### 3.2.4 Non-medially assembled F-actin cables incorporate into the actomyosin ring

To address the mechanisms responsible for F-actin accumulation in the medial region during cytokinesis, time-lapse double color imaging was performed in live fission yeast cells coexpressing LAGFP and mCh-Atb2p. Interestingly, after cells entered mitosis (shown by a short mitotic spindle marked by mCh-Atb2p in Figure 4 A time 0), plenty of F-actin cables arose from non-medial regions and appeared to incorporate into the assembling actomyosin ring (Figure 4 A, after time 0). Similar mitotic actin dynamics were found in LAmGFP or LAmCh cells (data not shown).

To observe the actomyosin ring assembly more carefully, *cdc25*-22 LAGFP mCh-Atb2p cells were checked (Russell and Nurse, 1986). Cells containing the *cdc25*-22 allele arrested in $G_2$/M transition at 36$^{o}$C for 3-4 h are twice as long as wild-type. Previous studies using electron microscopy showed that after heat arrest in 36°C and release to 24°C, *cdc25*-22 cells possessed longer and thicker F-actin cables than wt cells (Kamasaki et al., 2005). Consistent with Kamasaki et al, our data showed that F-actin cables in the elongated *cdc25*-22 LAGFP mCh-Atb2p cells were longer and brighter than those in the wt cells (Figure 4 B and D). Furthermore, the non-medial assembly and migration of F-actin cables towards the division site was more apparent (Figure 4 B, asterisks marked the end of the cable; Figure 4 D, lower part of the cell, actin cable labeled by asterisks). To assist the analysis of actin cable movement, a longitudinal line connecting the cell poles was drawn within the *cdc25*-22 cell and then kymographs were derived by reslicing the same line from consecutive time points. These kymographs also suggest F-actin cables flowed from the non-medial region towards the middle (Figure 4 C, arrow). However, this does not exclude the possibility of medial F-actin nucleation/assembly. The same kymographs also indicate the existence of such medially assembled F-actin (Figure 4 C, broken box). Interestingly, in some cases, the F-actin cables disassembled before they associated with the actomyosin ring (Figure 4 D). This is not surprising, as the F-actin severing protein cofilin-Adf1p localizes to the division site during cytokinesis (Nakano and Mabuchi, 2006b; Okada et al., 2006).

As colocalization analysis showed FM4-64 stained cell membrane was in close proximity to LAGFP decorated F-actin cables (Figure 4 E, white arrows point out F-actin cables nearby the membrane), to gain higher temporal resolution and better signal to noise ratio, total internal reflection fluorescence (TIRF) microscopy was used to checked F-actin dynamics (Tokunaga et al., 2008; Yu et al., 2011). This part of the work was in collaboration with Dr. Haochen Yu and Dr. Roland Wedlich-Soldner (Max Planck Institute of Biochemistry, Germany). With this method, we managed to acquire with 0.2 s interval time in time-lapse series. To better quantify F-actin dynamics during mitosis, we categorized F-actin cables according to their orientations (Figure 4 F, G and H). Our data suggests that the majority (47.2%) of the F-actin cables extended towards the cell equator while the remaining F-actin cables either moved towards the poles or in random orientations (Figure 4 F, polar and random orientations: each 26.4%). We also measured the velocities of F-actin cable extension by tracking the leading actin cable ends over time along their moving path (Figure 4 G and H). On average, F-actin cables labeled by LAGFP extended at a rate of 0.75 ± 0.08 μm/s (mean ± SEM, $n$ = 53). Interestingly, equatorial cables grew at significantly faster rates than polar or randomly oriented cables (Figure 4 G and H, equatorial: 0.99 ± 0.13 μm/s, mean ± SEM, $n$ = 25, and rest: 0.54 ± 0.08 μm/s, mean ± SEM, $n$ = 28; $P < 0.01$, unpaired $t$ test with Welch correction). In some cases, extensions of the non-medially assembled F-actin cables near the cell tips were observed (Figure 4 I, asterisks mark the end of the extending cable). Kymographs from these TIRF time-lapse series again showed the medial migration of actin cables as well as possible medial nucleation events (Figure 4 I, asterisks show the non-medial movement and broken box indicates the possible medial nucleation events). Thus, these experiments showed that non-medially assembled actin cables incorporated into the cytokinetic ring in fission yeast.

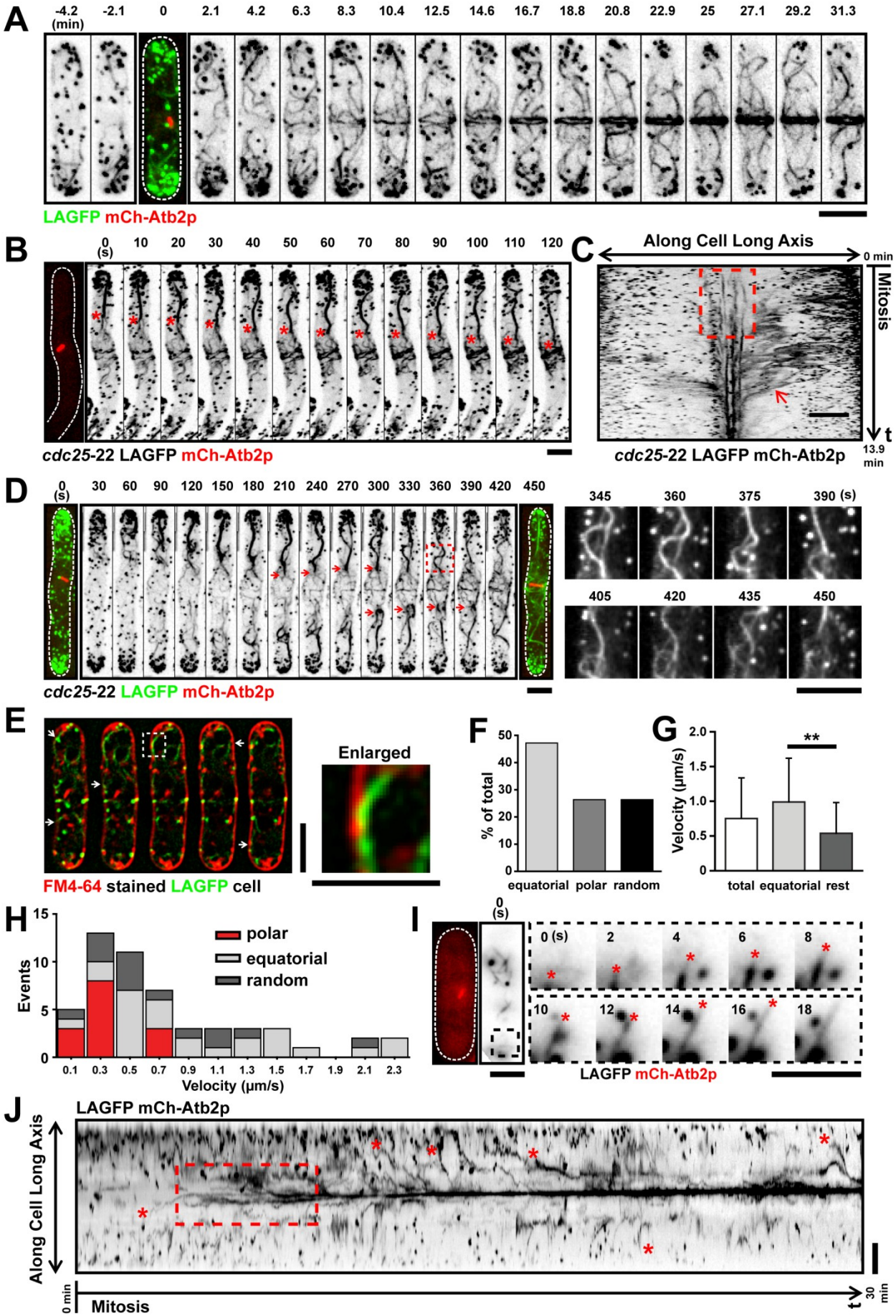
A
-4.2 (min)
-2.1
0
2.1
4.2
6.3
8.3
10.4
12.5
14.6
16.7
18.8
20.8
22.9
25
27.1
29.2
31.3
LAGFP mCh-Atb2p
B
0 (s)
10
20
30
40
50
60
70
80
90
100
110
120
cdc25-22 LAGFP mCh-Atb2p
C
Along Cell Long Axis
0 min
Mitosis
t
13.9 min
cdc25-22 LAGFP mCh-Atb2p
D
0 (s)
30
60
90
120
150
180
210
240
270
300
330
360
390
420
450
345
360
375
390 (s)
405
420
435
450
cdc25-22 LAGFP mCh-Atb2p
E
Enlarged
FM4-64 stained LAGFP cell
F
% of total
equatorial
polar
random
G
Velocity (μm/s)
**
total
equatorial
rest
H
Events
polar
equatorial
random
Velocity (μm/s)
I
0 (s)
2
4
6
8
10
12
14
16
18
LAGFP mCh-Atb2p
J
LAGFP mCh-Atb2p
Along Cell Long Axis
0 min
Mitosis
t
30 min

**Figure 4.** Non-medially assembled F-actin cables incorporate into the actomyosin ring.

(A) Time-lapse images of a LAGFP mCh-Atb2p cell. The third panel (time 0 min) is shown as a merged image to indicate the cell cycle stage. (B) Time-lapse images of a *cdc25*-22 LAGFP mCh-Atb2p cell after released from 36°C to 24°C. The first micrograph on the left was taken before the movie was started. Red asterisks show a non-medially assembled F-actin cable migrating towards the medial region during actomyosin ring assembly. Time interval of this movie was 5 s. (C) Kymograph of ring assembly in a *cdc25*-22 LAGFP mCh-Atb2p cell revealing a flow of F-actin fluorescence signal to the cell middle. The red broken box indicates *de novo* nucleation of F-actin filaments at the division site. Numbers on the right indicate the duration of the movie. (D) Time-lapse images of another representative *cdc25*-22 LAGFP mCh-Atb2p cell after released from 36°C to 24°C. The merged micrographs on the left or the right were taken at time 0 s or 450s, repectively. Red arrows show medial disassembling events of migrating non-medial F-actin cables. Time-lapse images of the red broken box were enlarged on the right. Time interval of this movie was 15 s. (E) Montage showing the medial sections of a FM4-64 staining of a LAGFP cell. Step size: 0.3 μm. White arrows point out the F-actin cables nearby the cell membrane. White broken box was enlarged on the right. These images were processed by deconvolution. (F) Graph showing the fraction of cables extending towards the cell middle (equatorial), cell poles (polar) or in other directions (random), in mitotic cells expressing LAGFP and mCh-Atb2p. 59 cables were counted. Data were counted from TIRFM movies in F, G, and H. (G) Graph showing extension rates of cables grouped by their orientations. Error bars show means ± SD. Left to right, n = 59, 28, and 31 cables; **P<0.01. (H) Stacked histogram showing distributions of cable-extension velocities for polar (red), equatorial (light grey) and randomly oriented (dark grey) F-actin cables in mitotic LAGFP mCh-Atb2p cells. 59 cables were counted. (I) TIRFM images showing typical extension of an F-actin cable in a mitotic LAGFP mCh-Atb2p cell. The images on the left indicate the mitotic spindle and cable at the start of the movie. The montage shows an extending equatorial cable (end marked with asterisks) from the black dashed box. (J) Kymograph of LAGFP signal in a wt cell passing

through mitosis. Asterisks illustrate non-medial F-actin cables that migrate to the middle during actomyosin ring assembly. The broken box indicates *de novo* nucleation of F-actin at the division site. Numbers indicate the duration of the movie. Time interval of this kymograph was 2 s. Dashed line indicates the cell boundary. Bars, 5 μm.

### 3.2.5 Non-medial F-actin cable movement is more obvious in some cytokinetic mutants, including *adf1*-1

To better understand the migration events of the non-medial F-actin cables, some temperature sensitive cytokinetic mutants were analyzed by LAGFP dynamics. As mentioned in the previous section, in some F-actin cable migration events, the non-medially assembled F-actin cables appeared to be severed upon reaching the medial region of the cell (Figure 4 D). Previous work has shown that cofilin-Adf1p localizes to the division site, severs F-actin and contributes to the actomyosin ring assembly in fission yeast (Chen and Pollard, 2011; Nakano and Mabuchi, 2006b). Therefore, we first analyzed F-actin dynamics in the temperature sensitive mutant *adf1*-1 (Nakano and Mabuchi, 2006b). Interestingly, although the direct incorporation of individual F-actin cables into the actomyosin ring was hard to distinguish, F-actin rings in some *adf1*-1 cells underwent rapid remodeling at restrictive temperature (Figure 5 A). In order to observe the non-medial F-actin cable migration more carefully in the *adf1*-1 mutant, *adf1*-1 cells were arrested in $G_2$ stage of the cell cycle by overexpression of Wee1-50 mutant protein under *nmt1* promoter (Figure 5 B). Overexpression of Wee1-50p at 24$^{o}$C inhibits the Cdc2p dependent mitotic entry and inactivation of Wee1-50p at 36$^{o}$C allows cells enter mitosis. In these elongated cells, the mitotic F-actin cables were found to be fewer in number but were more bundled (Figure 5 B). Migration of the non-medial F-actin cables and fusion with the assembling actomyosin ring was also observed (Figure 5 B, asterisks show the medially migrating F-actin cables). Intriguingly, the disassembly of the non-medial F-actin cables near the division site was not observed in these elongated *adf1*-1 cells (Figure 5 B), suggesting a possible role of cofilin-Adf1p in re-organizing the F-actin cables into the forming actomyosin ring. Additional experiments using the *act1*-138 (Subramanian et al., 2013) and *cdc4*-8 (McCollum et al., 1995) mutants also showed the non-medial F-actin cable migration events (Figure 5 C and D). In summary, the migration of non-medially assembled F-actin cables could be better observed in *adf1*-1 temperature sensitive mutants and cofilin-Adf1p may play a role in the reorganization of the non-medially assembled F-actin cables into the actomyosin ring.

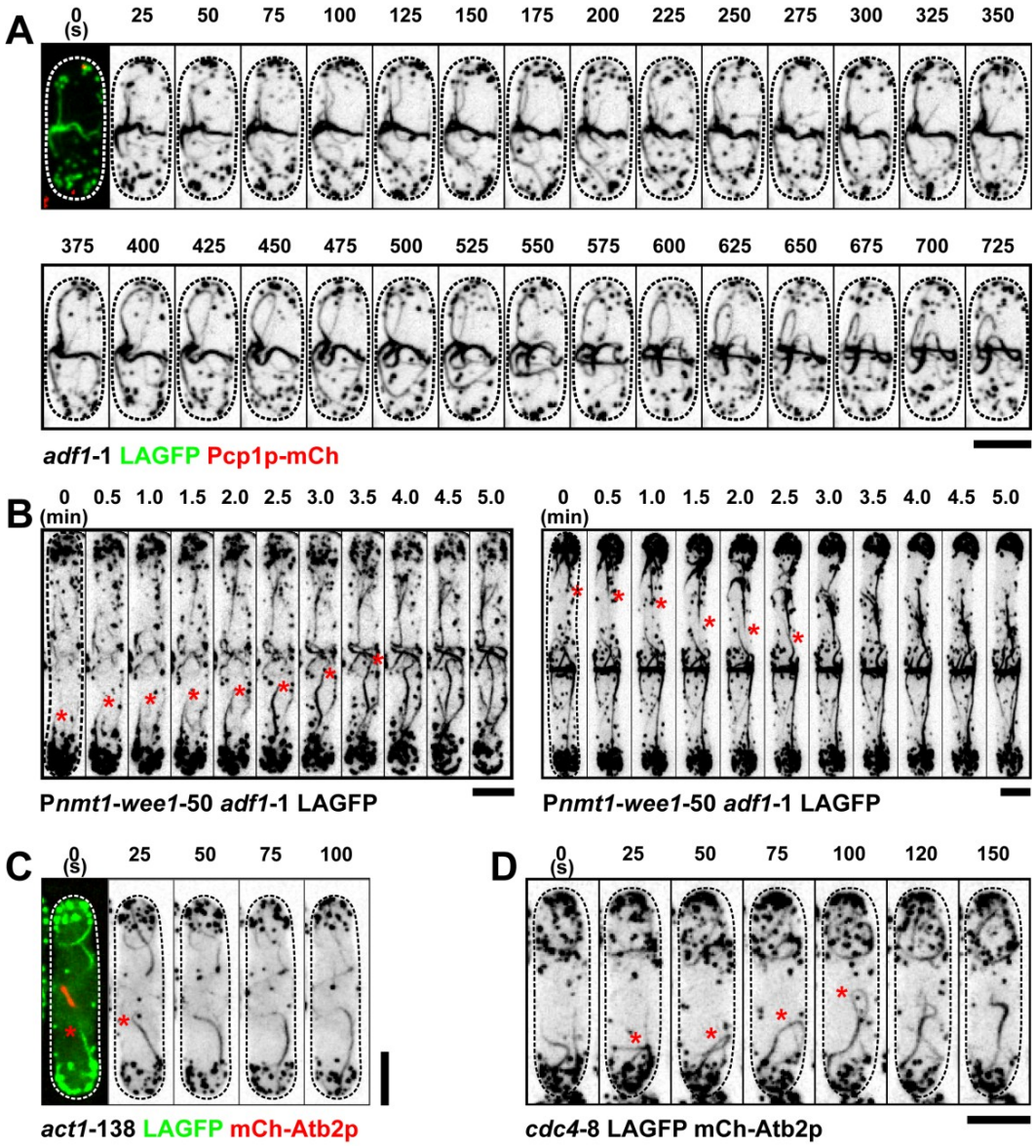


**Figure 5.** Non-medial F-actin cable movement is more obvious in some cytokinetic mutants, including *adf1*-1.

(A) Time-lapse images of a mitotic *adf1*-1 LAGFP Pcp1p-mCh cell at 36°C. Time zero (cell with two just fully separated SPB) is shown as a merged image to indicate the cell cycle stage. (B) Time-lapse images of two mitotic P*nmt1-wee1*-50 *adf1*-1 LAGFP cells at 36°C. Asterisks show F-actin cables migrating from the non-medial region to the cell middle. (C and D) Time-lapse images of an *act1*-138 LAGFP mCh-Atb2p cell and a *cdc4*-8 LAGFP mCh-Atb2p cell at 36°C, respectively. Red asterisks show F-actin cable migrating from the non-medial region to the cell middle. Dashed line indicates the cell boundary. Bars, 5 μm.

### 3.2.6 Comparison of the stabilization effects upon F-actin between lifeact and CHD

Using lifeact-GFP as a probe, we have found that non-medially assembled F-actin cables may contribute to actomyosin ring assembly. However, our results are at odds with previous work using P*nmt41*-GFP-CHD (Coffman et al., 2009; Laporte et al., 2012; Wu and Pollard, 2005), which suggested that F-actin in the actomyosin ring was *de novo* nucleated in the medial region. In light of this disagreement and to compare LAGFP with P*nmt41*-GFP-CHD, Latrunculin A (LatA) treatments were carried out to test if there was any stabilization of F-actin structures upon expression of LA or CHD. We used 50 uM LatA (final concentration) in all the experiments (Figure 6). Unexpectedly, we found that CHD had a significant stabilizing effect on fission yeast F-actin structures (Figure 6). A significant amount of CHD labeled F-actin structures (F-actin cables and/or F-actin patches) remained after LatA treatment (Figure 6 A, B and D). By contrast, most of the LAGFP labeled F-actin structures were absent after LatA treatment (Figure 6 A, B and D). To confirm whether these "aberrant" CHD labeled structures were bona fide F-actin structures, LatA treated CHD expressing cells were stained with Alexa Fluor 488 phalloidin (Figure 6 C). Interestingly, our results showed that the remaining CHD labeled structures were bona fide F-actin containing structures (Figure 6 C). To compare GFP-CHD with LAGFP exactly under the same condition, we also generated a P*act1*-GFP-CHD strain, in which GFP-CHD was expressed under fission yeast actin promoter as LAGFP and integrated at *leu1* locus. The F-actin stabilization defects of P*nmt41*-GFP-CHD, P*act1*-GFP-CHD and LAGFP over time were studied (Figure 6 D). Our results showed that, although LAGFP had a low F-actin stabilization defect compared to wt cells (Figure 6 D, 4 min), LAGFP was a better probe than GFP-CHD (P*act1*-GFP-CHD was worse than P*nmt41*-GFP-CHD) for visualizing F-actin *in vivo*. In summary, we find that lifeact is a more reliable probe than GFP-CHD to study actin dynamics.

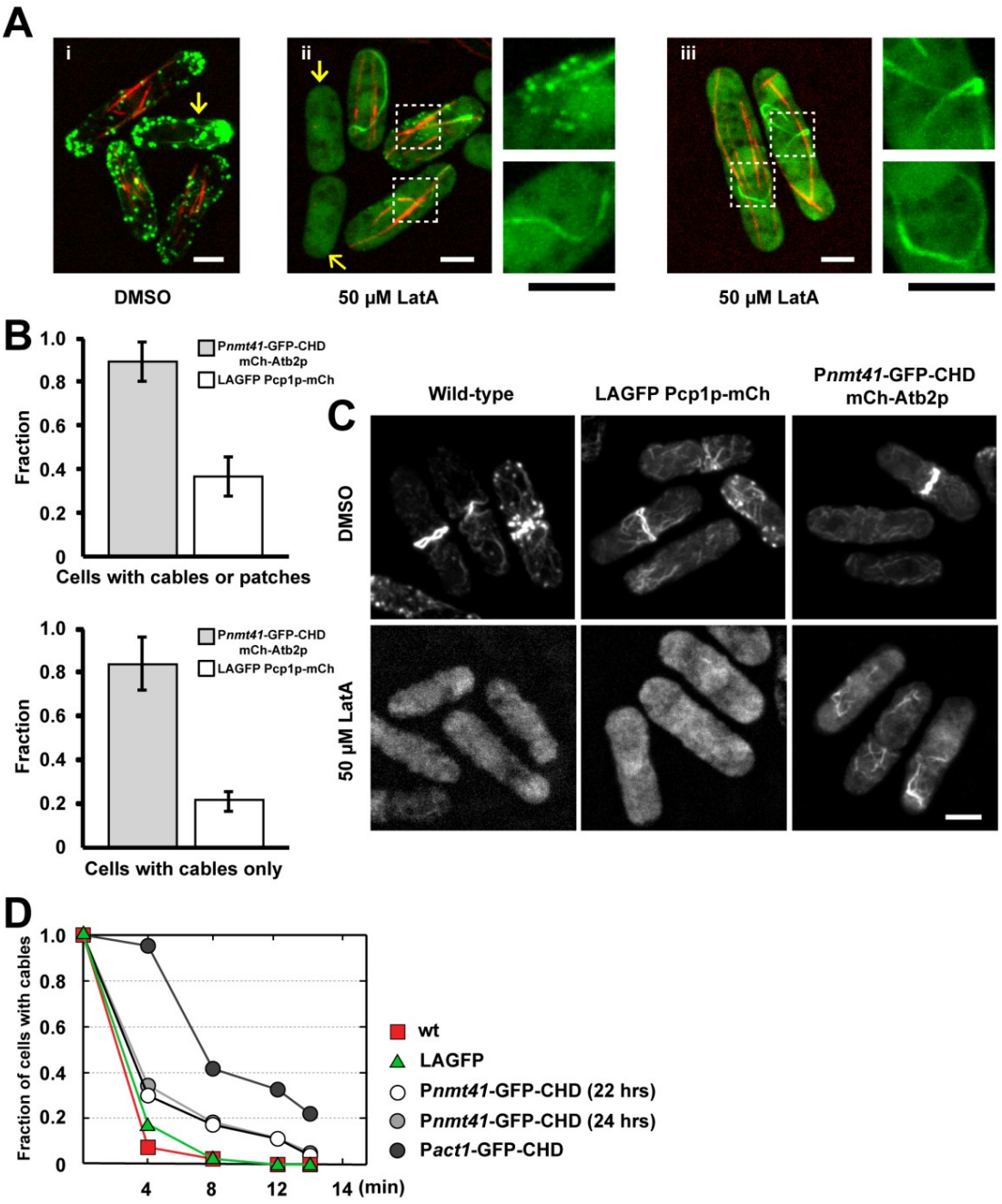


**Figure 6.** The previously used marker, GFP-CHD, generates stabilized F-actin structures.

(A) Mixture of LAGFP Pcp1p-mCh cells and P*nmt41*-GFP-CHD mCh-Atb2p cells treated with DMSO or LatA. P*nmt41*-GFP-CHD mCh-Atb2p cells were induced in complete minimal medium for 22 to 24 hrs and mixed with equal amount of LAGFP Pcp1p-mCh cells just before LatA treatment. The mixing ensured that the LatA treatment regime was identical in both strains. Live cell images were taken immediately after LatA treatment for 12-30 min. DMSO was used as control and as solution to dissolve LatA. White dashed boxes are

enlarged on the right. Yellow arrows show the LAGFP Pcp1p-mCh cells, in which F-actin is more completely lost upon LatA treatment, compared to the GFP-CHD strain in which F-actin persists. (B) Graphs showing percentages of the indicated cells with aberrant F-actin structures after LatA treatment. LAGFP Pcp1p-mCh cells and 24 hrs induced P*nmt41*-GFP-CHD mCh-Atb2p cells were mixed equally and treated with LatA for 12 min. All cells counted in this figure were live cells. Error bars show means ± SD of three independent experiments. In each experiment, more than 100 cells were counted for each strain. Upper graph shows percentage of cells with either stabilized aberrant cables or patches. Lower graph shows percentage of cells with only aberrant cables. (C) Images of DMSO or LatA treated, formaldehyde fixed and Alexa Fluor 488 phalloidin stained wt, LAGFP Pcp1p-mCh and P*nmt41*-GFP-CHD mCh-Atb2p cells, showing that the GFP-CHD labeled aberrant structures in (A) were *bona fide* actin structures. All these LatA treated and formaldehyde fixed cells did not show any fluorescent structures before the staining by Alexa Fluor 488 phalloidin (data not shown). (D) Graphs showing percentage of the indicated cells with aberrant actin cables after LatA treatment. The results are the means of two independent experiments. In each experiment, 100 cells were counted for each data point. P*nmt41*-GFP-CHD cells were induced in complete minimal medium for 22 or 24 hrs. Wt, LAGFP and P*act1*-GFP-CHD cells were cultured in YES at 24°C overnight to midlog phase. After LatA was added, cells were collected at 0 min, 4 min, 8 min, 12 min and 14 min. Cells were then immediately fixed by paraformaldehyde and stained by Alexa Fluor 488 phalloidin for counting. For detailed description of LatA treatment and induction of P*nmt41*-GFP-CHD containing cells, see Materials and methods. Bars, 5 μm.

### 3.2.7 Incorporation of F-actin cables into the actomyosin ring can also be observed using other actin monitoring probes

The data described in sections 3.2.4 and 3.2.5 suggests that non-medially assembled F-actin cables incorporate into the actomyosin ring during cytokinesis. However, it was still possible that lifeact was altering F-actin dynamics in fission yeast. We therefore used other F-actin monitoring probes to further investigate actin dynamics.

Work in other organisms has shown that F-Tractin (32 AAs) is a useful probe in monitoring F-actin dynamics (Johnson and Schell, 2009; Schell et al., 2001; Yi et al., 2012). We therefore generated a strain expressing the GFP-F-Tractin under fission yeast actin promoter. However, although F-Tractin might be a good probe to study F-actin patches, it only showed a dim ring and some indistinct short cable-like structures (Figure 7 A, short cable like structures indicated by asterisks). Thus, we turned to another widely used probe called Utrophin Calponin Homology Domains (Utr-CH) (Andersen et al., 2011; Burkel et al., 2007). Interestingly, time-lapse imaging of P*act1*-Utr-CH-GFP cells showed similar F-actin dynamics as lifeact labeled cells (Figure 7 B). Therefore, to better understand the reason why GFP-CHD showed different results, a careful analysis on the P*nmt41*-GFP-CHD cells was carried out (Figure 7 C). Using longer exposures, we were surprised to find that long F-actin cables could also be observed connecting the assembling actomyosin ring from locations near the tips in P*nmt41*-GFP-CHD cells (Figure 7 C, asterisk shows the long F-actin cable). This result indicated that the contradictory results (between us and other labs) could be due to the photobleaching effect, the low exposure time or the low laser power applied in the previous time-lapse imaging studies. This could also explain why blurry non-medial GFP-CHD F-actin cables were visible in the previous time-lapse movies (Vavylonis et al., 2008; Wu and Pollard, 2005). To support this idea, P*nmt41*-GFP-CHD mCh-Atb2p cells were carefully quantified according to mitotic spindle length (Figure 7 D). This experiment showed clearly that long F-actin cables were also present throughout mitosis in P*nmt41*-GFP-CHD cells. And interestingly, lower percentage of cells possessed F-actin cables in late mitosis (Figure 7 D). To enable unambiguous evaluation of the CHD probe,

F-actin dynamics were also checked in P*act1*-GFP-CHD cells (Figure 7 F). Although P*act1*-GFP-CHD cells exhibited slower growth (Figure 3 B) and a weak cytokinesis defect (Figure 7 E, ~ 12.2% abnormal cells), P*act1*-GFP-CHD again showed similar F-actin dynamics as LAGFP (Figure 7 F) and provided evidence for migration and incorporation of non-medial F-actin cables into the assembling actomyosin ring (Figure 7 G, end of F-actin cables marked by asterisks). As GFP-CHD showed similar results as lifeact in this thesis, to further test whether lifeact and CHD marked the same F-actin structures, CHD were coexpressed with lifeact in living fission yeast cells (Figure 7 H and I). Our results showed that there was no difference between the lifeact labeled structures and CHD labeled structures. Taken together, these data suggest that non-medial F-actin cables do exist and incorporate into the fission yeast actomyosin ring.

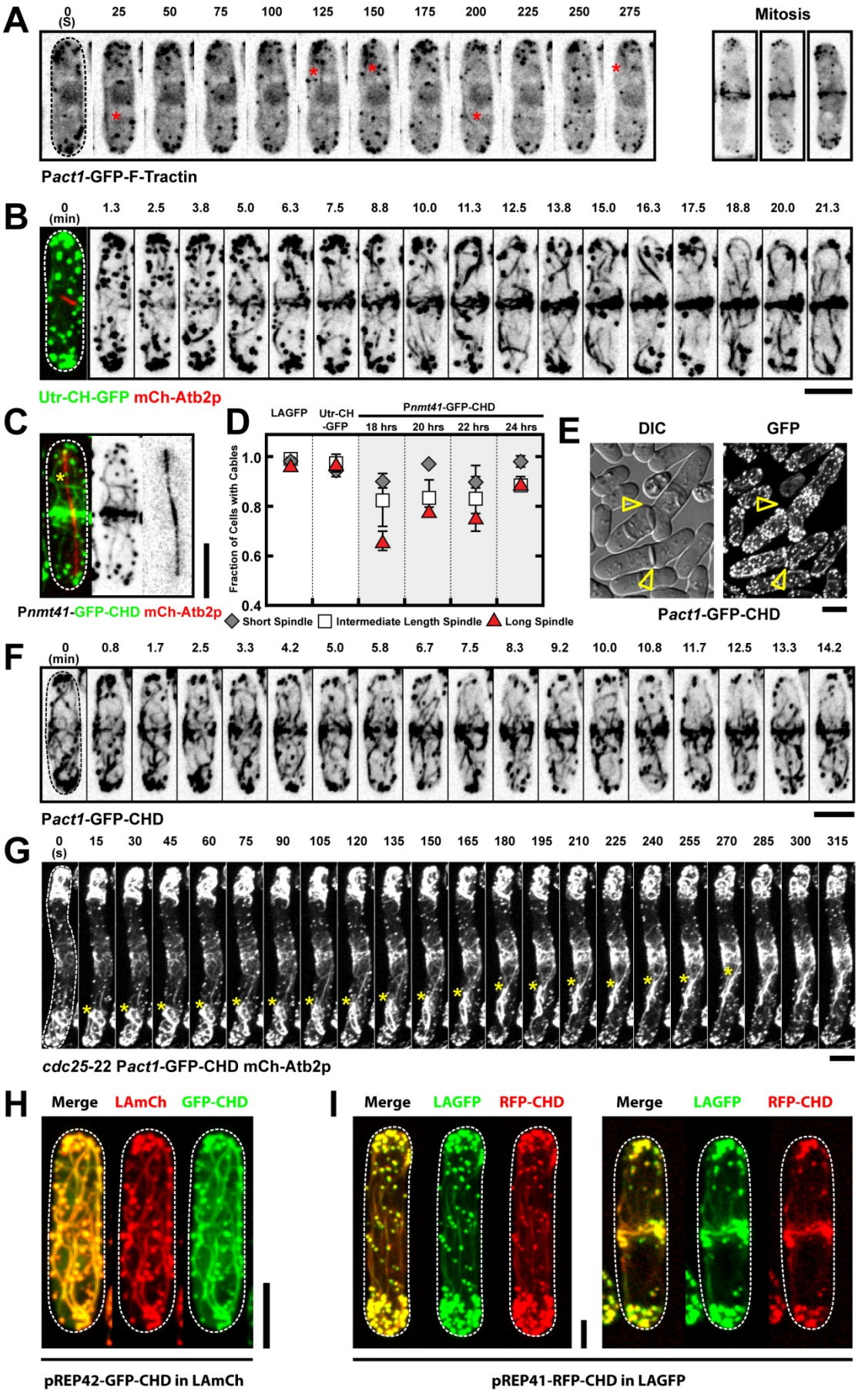
A
0 (S)
25
50
75
100
125
150
175
200
225
250
275
Mitosis
Pact1-GFP-F-Tractin
B
0 (min)
1.3
2.5
3.8
5.0
6.3
7.5
8.8
10.0
11.3
12.5
13.8
15.0
16.3
17.5
18.8
20.0
21.3
Utr-CH-GFP mCh-Atb2p
C
Pnmt41-GFP-CHD mCh-Atb2p
D
LAGFP
Utr-CH -GFP
Pnmt41-GFP-CHD
18 hrs
20 hrs
22 hrs
24 hrs
Fraction of Cells with Cables
1.0
0.8
0.6
0.4
Short Spindle
Intermediate Length Spindle
Long Spindle
E
DIC
GFP
Pact1-GFP-CHD
F
0 (min)
0.8
1.7
2.5
3.3
4.2
5.0
5.8
6.7
7.5
8.3
9.2
10.0
10.8
11.7
12.5
13.3
14.2
Pact1-GFP-CHD
G
0 (s)
15
30
45
60
75
90
105
120
135
150
165
180
195
210
225
240
255
270
285
300
315
cdc25-22 Pact1-GFP-CHD mCh-Atb2p
H
Merge
LAmCh
GFP-CHD
pREP42-GFP-CHD in LAmCh
I
Merge
LAGFP
RFP-CHD
Merge
LAGFP
RFP-CHD
pREP41-RFP-CHD in LAGFP

**Figure 7.** Incorporation of F-actin cables into the actomyosin ring can also be observed using other actin monitoring probes.

(A) Left, time-lapse images of a P*act1*-GFP-F-Tractin cell at 24°C. Red asterisks indicate the short cable-like structures shown by GFP-F-Tractin; Right, images of three mitotic P*act1*-GFP-F-Tractin cells. All the actin monitoring constructs in Figure 7 were expressed under *actin* promoter and integrated into the genome at the *leu1* locus as a second copy of actin. pJK148 plasmid was used for the integration and expression. (B) Time-lapse images of a Utr-CH-GFP mCh-Atb2p cell. Time zero (cell with short spindle) is shown as a merged image to indicate the cell cycle stage. (C) Images of a P*nmt41*-GFP-CHD mCh-Atb2p after 20 h induction. Asterisks show long cables in the non-medial region. (D) Graph showing percentage of cells with cables in LAGFP, Utr-CH-GFP, P*nmt41*-GFP-CHD (18, 20, 22 and 24 h induction), respectively. mCh-Atb2p was used in all these cells to measure spindle length. Cells with spindles were grouped into three categories: short, intermediate and long spindles. Error bars show means ± SD of two independent experiments (N > 30 cells / experiment). (E) Images of P*act1*-GFP-CHD cells cultured in YES. Arrowheads identify cells with septation defects. (F) Time-lapse images of a P*act1*-GFP-CHD cell. (G) Time-lapse images of a *cdc25*-22 P*act1*-GFP-CHD mCh-Atb2p cell after released from 36°C to 24°C. Yellow asterisks show cables migrating towards the cell middle. (H) Images showing a LAmCh (red) cell coexpressing GFP-CHD (green) from a pREP42 plasmid. Merged signal is shown in yellow. (I) Images showing an interphase (left) and a mitotic (right) *his1*$^{+}$::LAGFP (green) cell coexpressing RFP-CHD (red) from a pREP41 plasmid. Merged signal is shown in yellow. Dashed line indicates the cell boundary. Bars, 5 μm.

### 3.2.8 Medially assembled F-actin cables could also be observed by TIRFM

As shown by kymographs in Figure 4 C and J, in early mitosis, actin fluorescence was present at the division site as well. This result indicated medial F-actin nucleation events may also exist, consistent with some previous work (Noguchi and Mabuchi, 2001; Vavylonis et al., 2008). To further confirm this result, TIRF microscopy was used again to verify the medial nucleation events in *for3*Δ LAGFP mCh-Atb2p cells (Figure 8 A). Interestingly, in some cases, we found that non-medial and medial F-actin assembly could be detected concurrently during fission yeast actomyosin ring assembly (Figure 8 A, red and blue broken boxes). In conclusion, we found that medially assembled F-actin cables could also be observed by TIRFM.

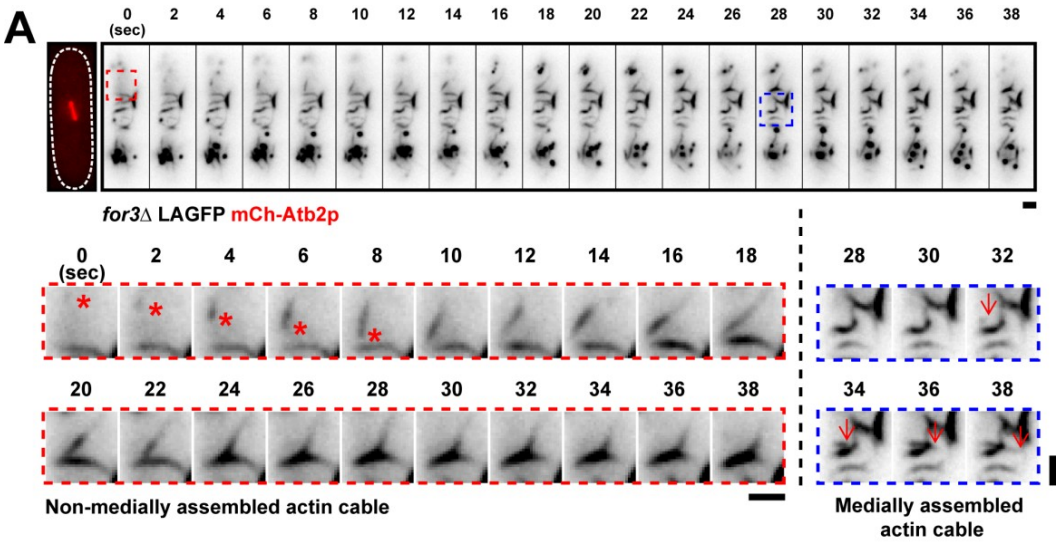


**Figure 8.** Mitotic actin cable assembly could be observed in both medial region and non-medial region in *for3*Δ LAGFP mCh-Atb2p cell.

(A) Time-lapse TIRF microscopy images of a representative *for3*Δ LAGFP mCh-Atb2p cell at 24°C. The first image of the upper panel shows the appearance of the mitotic spindle before the movie was started. Lower red panels on the left show the magnified time-lapse images of the red dashed box, starting from time zero. The red asterisks trace the movement of a single non-medially assembled F-actin cable. Lower blue panels on the right show the magnified time-lapse images of the blue dashed box. The red arrows trace the movement of a single medially assembled F-actin cable. In some images, the cell boundary is marked with dashed lines. Bars, 2 μm.

### 3.2.9 Spatial relationship between non-medial F-actin cables and nodes

Although some of the non-medially assembled F-actin cables were assembled far away from the cell middle, it was necessary to address the spatial relationship between the non-medial F-actin cables and the medially localized nodes. To examine this, we performed fast spinning disk single plane time-lapse imaging (1.3 s/frame) in the synchronized *cdc25*-22 LAmCh Rlc1p-3GFP cells. Our results showed that, although dynamics of Rlc1p-3GFP nodes were same as previously described (Vavylonis et al., 2008), non-medial F-actin cables were again found to be assembled far away from the medial Rlc1p-3GFP nodes (Figure 9 A, asterisks mark the end of a non-medial actin cable). Interestingly, TIRFM double color time-lapse imaging with a similar strain showed that F-actin cables could be captured by the medially located Rlc1p-mCherry containing nodes (Figure 9 B). Taken together, our data indicates that non-medial F-actin cables were assembled away from the medially located nodes and these non-medial F-actin cables could associate with nodes once they reached the cell middle.

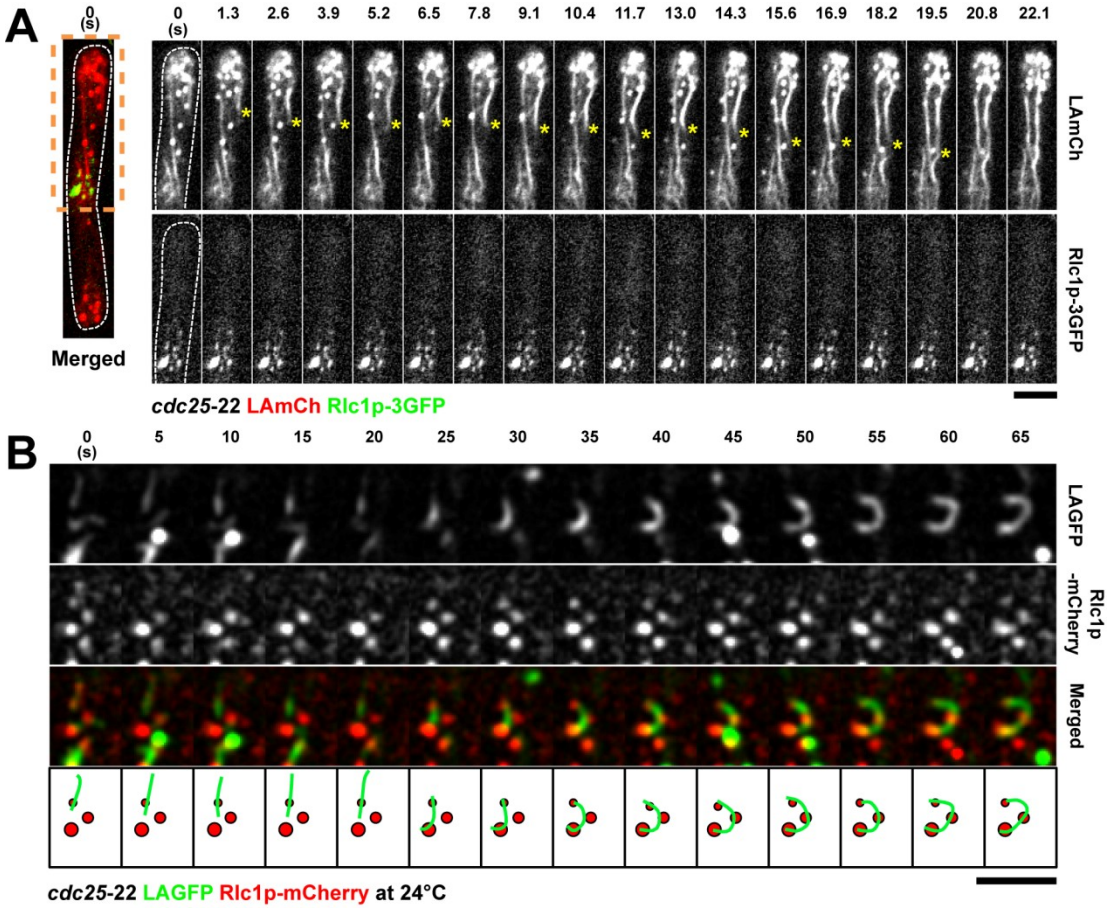


**Figure 9.** Double color imaging of nodes and lifeact labeled F-actin cables. (A) Spinning disk single plane images of a *cdc25*-22 LAmCh Rlc1p-3GFP cell after released from 36°C to 24°C. Image on the left is shown as a merged image (red, LAmCh; green, Rlc1p-3GFP) to indicate the spatial relationship between nodes and non-medial actin cables. Time-lapse images of the region of the cell within the orange dashed box are shown on the right. Time interval is 1.3 s. Asterisks show the migration of a non-medial cable towards the middle. (B) TIRFM time-lapse double color images of a *cdc25*-22 LAGFP Rlc1p-mCherry cell at 24°C, showing an actin cable that was captured and bent by 3 static Rlc1p nodes. The lowest panel is a schematic representation of the merged montage. Green, F-actin cable; Red, cortical nodes. Dashed line indicates the cell boundary. Bars, 5 μm.

### 3.2.10 Dynamics of F-actin cables

We then studied mitotic F-actin cable dynamics with greater temporal resolution by TIRFM. Interestingly, we observed various behaviors of these F-actin cables (Figure 10). Our data showed that some F-actin cables could move without an apparent change in length (Figure 10 A, cable translocation; end of cable marked by asterisks and the path of cable movement indicated by a blue dashed line). This was reminiscent of F-actin cable translocation by myosins in budding yeast (Yu et al., 2011). We also observed extensive buckling of individual F-actin cables (Figure 10 B, cables buckling) or cable bundles (Figure 10 C, cable whip). In some other cases, breakage or fragmentation of long F-actin cables was observed (Figure 10 D, cable break). This could be due to the function of cofilin-Adf1 as mentioned previously (Nakano and Mabuchi, 2006b). Finally, we also observed F-actin cables being directly pulled and incorporated into the assembling actomyosin ring (Figure 10 E, cable compaction). Interestingly, this compaction often occurred perpendicular to the F-actin cable axis and was coupled to transient bundling and zipping up of neighboring cables (Figure 10 E, asterisk). In summary, F-actin cables showed various dynamic behaviors during cytokinesis, undergo extensive lateral reorganization and ultimately compact into the assembling actomyosin ring.

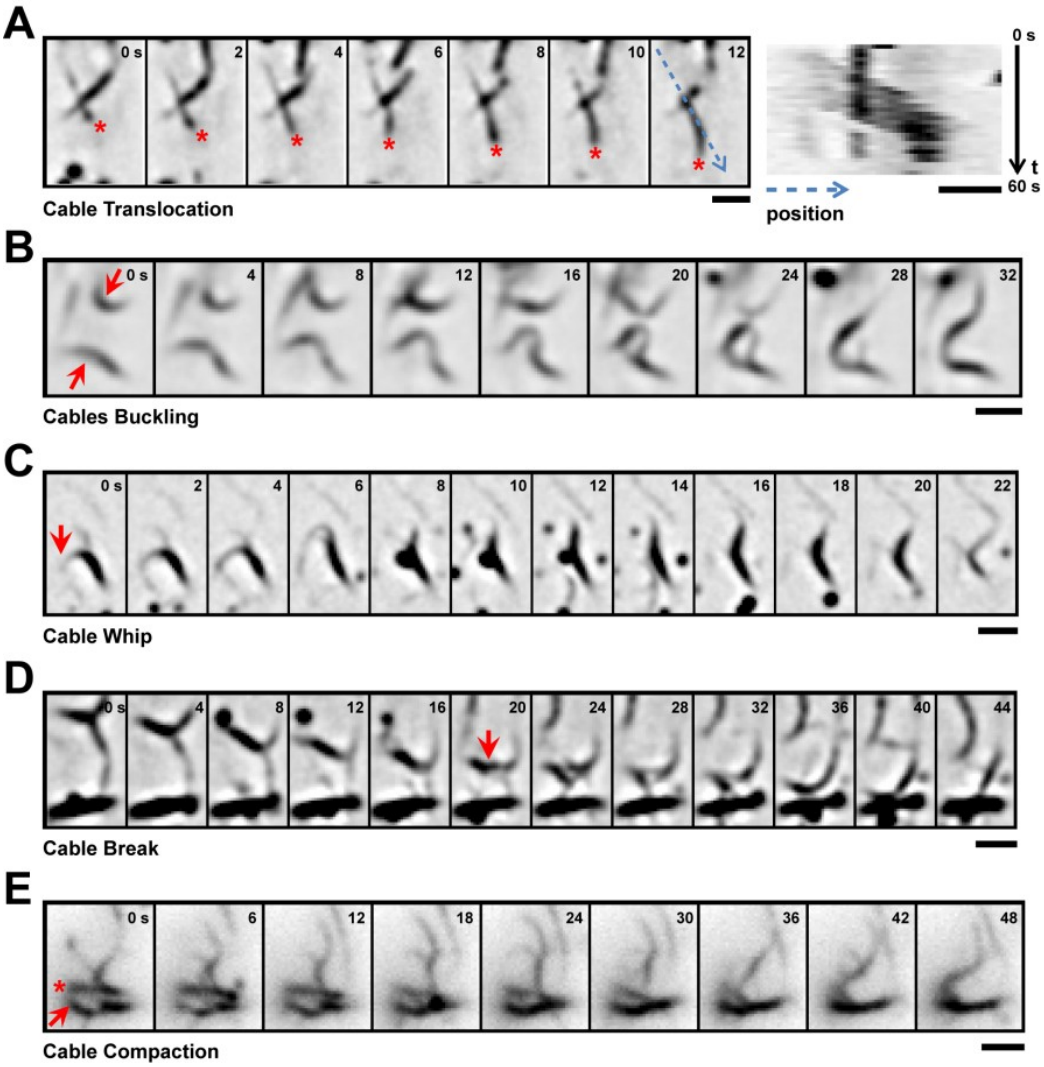


**Figure 10.** Various dynamics of F-actin cables.

(A) Translocation of a single F-actin cable. Leading end is marked by an asterisk. Kymograph on the right was made by reslicing a one-pixel-wide line along the path (indicated by the blue dotted line in the 12 s time point) of the moving cable. Numbers on the right corners of the kymograph indicate the start time and end time. (B) Buckling of F-actin cables (marked by arrows). The two cables fused at the end of the sequence. (C) Whip-like bending of a F-actin cable bundle. Note the rotation of the marked (arrow) cable by nearly 180°. (D) Break in an apparently continuous F-actin cable (break position indicated by arrow). (E) Lateral translation of an F-actin cable bundle (asterisk) and incorporation into the medial ring (arrow). All images in this figure were from TIRFM movies. Time points are given in s. Bars, 2 µm.

### 3.2.11 Non-medially assembled F-actin cables are nucleated by formin-Cdc12p, not For3p

Previous studies have suggested that the formin-For3p plays an important role in the nucleation of F-actin cables in interphase, the formin-Cdc12p is responsible for nucleating F-actin filaments at the division site and the formin-Fus1p participates in cell fusion upon nutrient starvation (Chang et al., 1997; Feierbach and Chang, 2001; Petersen et al., 1998; Vavylonis et al., 2008; Yonetani et al., 2008). Thus, we tested whether formin-For3p was also responsible for the assembly of the non-medial F-actin cables we observed in the former sections. F-actin dynamics was checked in *for3*Δ cells expressing LAGFP and mCh-Atb2p (Figure 11 A). To our surprise, although F-actin cables were mostly missing in interphase *for3*Δ cells (Figure 11 A, before time 0), non-medial F-actin cables were readily observed in mitosis and again incorporated into the assembling actomyosin ring (Figure 11 A, after time 0). A similar result was also obtained in *for3*Δ cells expressing the previously used P*nmt41*-GFP-CHD probe (Figure 11 B). To check this nucleation process more carefully, F-actin dynamics was examined in synchronized *for3*Δ *cdc25*-22 LAGFP mCh-Atb2p cells (Figure 11 C). This experiment provided further evidence that formin-For3p was dispensable for the nucleation of non-medial actin cables (Figure 11 C, end of cable indicated by arrow heads). Kymographs again supported the idea that non-medial F-actin cables co-exist with medially assembled F-actin (Figure 11 D).

As previous work showed that F-actin cables were absent in the *for3*Δ cells (Feierbach and Chang, 2001), to establish that the non-medial F-actin cables detected in these *for3*Δ cells were not an artifact of the presence of LA or CHD, phalloidin was used to stain the untagged *cdc25*-22 and *for3*Δ *cdc25*-22 cells (Figure 11 E). This experiment clearly demonstrated the presence of non-medial F-actin cables in mitotic *for3*Δ cells.

Since formin-For3p was not responsible for the nucleation of the non-medial F-actin cables and formin-Cdc12p was essential for the actomyosin ring assembly (Chang et al., 1997; Kovar et al., 2011), we tested whether Cdc12p played a role in the non-medial F-actin cable nucleation. This was possible, as

formin-Cdc12p has recently been shown to localize to speckles throughout the cell in addition to its localization at the division site (Coffman et al., 2009). Towards this goal, germinated *cdc12*Δ spores expressing LAGFP and mCh-Atb2p were imaged by spinning disk microscopy (Figure 11 F and G). Surprisingly, F-actin cables were not perturbed in the interphase *cdc12*Δ cells (Figure 11 F, asterisks) but were mostly absent in the mitotic *cdc12*Δ cells (Figure 11 G). This experiment indicated that formin-Cdc12p was essential for the non-medial F-actin cable nucleation during mitosis. Because a low amount of F-actin cables could still be observed and accumulated near the division sites in mitotic *cdc12*Δ cells (Figure 11 G, accumulated F-actin cables indicated by arrow heads), *for3*Δ *cdc12*Δ double mutant was examined to identify the source of these remaining F-actin cables (Figure 11 H and I). Strikingly, F-actin cables were totally abolished in the double mutant (Figure 11 H and I). Cumulatively, our data suggest that the majority of the mitotic non-medially assembled F-actin cables were nucleated by formin-Cdc12p, but not For3p.

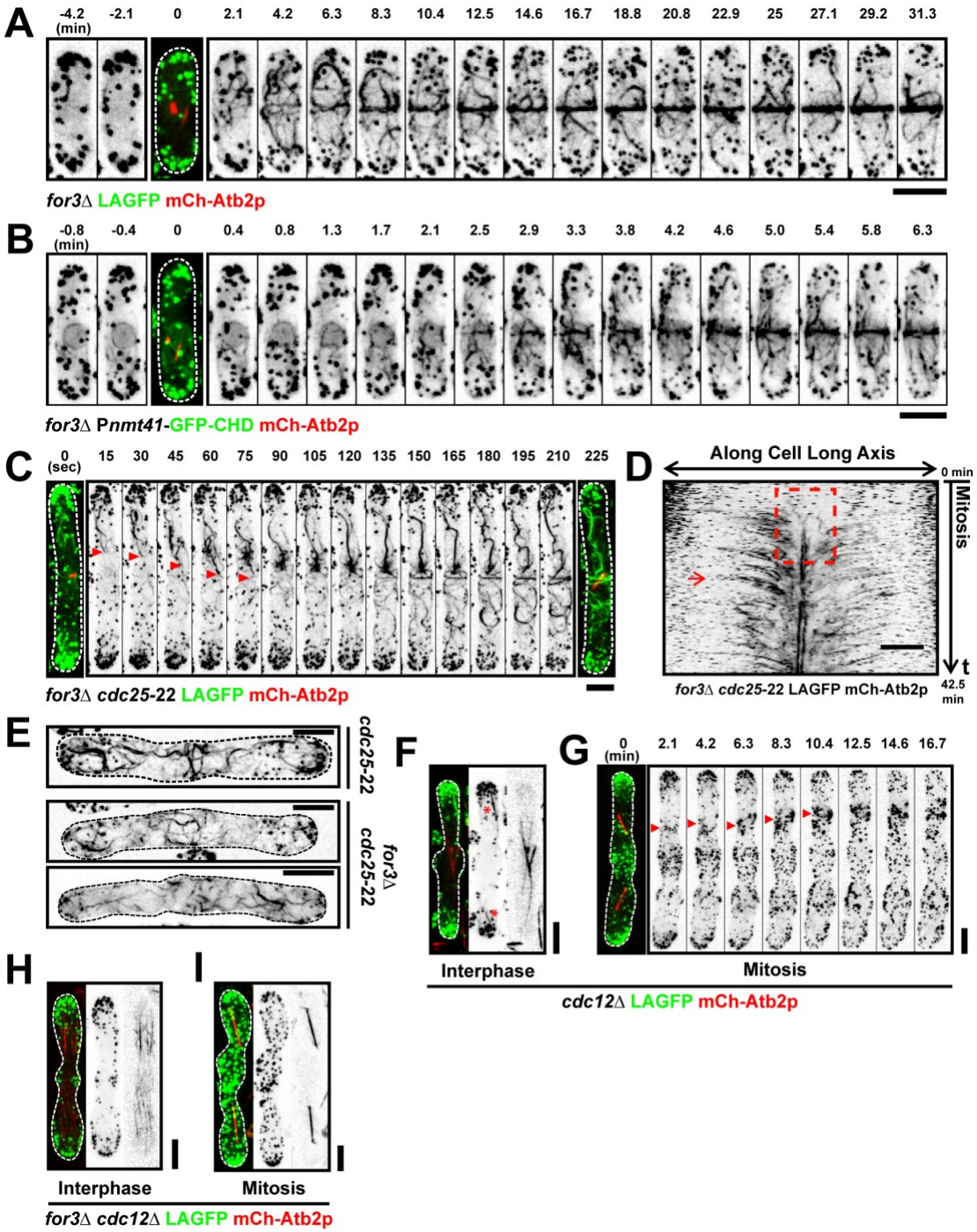
A
-4.2 (min)
-2.1
0
2.1
4.2
6.3
8.3
10.4
12.5
14.6
16.7
18.8
20.8
22.9
25
27.1
29.2
31.3
for3Δ LAGFP mCh-Atb2p
B
-0.8 (min)
-0.4
0
0.4
0.8
1.3
1.7
2.1
2.5
2.9
3.3
3.8
4.2
4.6
5.0
5.4
5.8
6.3
for3Δ Pnmt41-GFP-CHD mCh-Atb2p
C
0 (sec)
15
30
45
60
75
90
105
120
135
150
165
180
195
210
225
for3Δ cdc25-22 LAGFP mCh-Atb2p
D
Along Cell Long Axis
0 min
Mitosis
t
for3Δ cdc25-22 LAGFP mCh-Atb2p
42.5 min
E
cdc25-22
for3Δ cdc25-22
F
Interphase
G
0 (min)
2.1
4.2
6.3
8.3
10.4
12.5
14.6
16.7
Mitosis
cdc12Δ LAGFP mCh-Atb2p
H
Interphase
Mitosis
for3Δ cdc12Δ LAGFP mCh-Atb2p

**Figure 11.** Non-medially assembled F-actin cables are nucleated by formin-Cdc12p, not For3p.

(A) Time-lapse images of a *for3*Δ LAGFP mCh-Atb2p cell. The third panel (time 0 with short spindle) is shown as a merged image to indicate the cell cycle stage. (B) Time-lapse images of a *for3*Δ P*nmt41*-GFP-CHD mCh-Atb2p cell. The third panel (time 0 with short spindle) is shown as a merged image to indicate the cell cycle stage. (C) Time-lapse images of a *for3*Δ *cdc25*-22 LAGFP mCh-Atb2p cell after released from 36°C to 24°C. Arrowheads point to an F-actin cable migrating to the cell middle during ring assembly. (D) Kymograph of a *for3*Δ *cdc25*-22 LAGFP mCh-Atb2p cell after released from 36°C to 24°C, revealing a flow of F-actin signals from the non-medial region to the cell middle. The red broken box illustrates *de novo* nucleation of F-actin at the division site. Numbers indicate duration of the movie. Time interval, 15 s. (E) *cdc25*-22 and *for3*Δ *cdc25*-22 cells were fixed with paraformaldehyde and stained with Alexa-488 phalloidin. (F) Image of an interphase *cdc12*Δ LAGFP mCh-Atb2p cell germinated from spore. Red asterisks show the interphase F-actin cables. (G) Time-lapse images of a mitotic *cdc12*Δ LAGFP mCh-Atb2p cell germinated from spore. Red arrow heads indicate the remaining accumulated F-actin cables. (H and I) Images of an interphase and a mitotic *for3*Δ *cdc12*Δ LAGFP mCh-Atb2p cell germinated from spore, respectively. Dashed line indicates the cell boundary. Bars, 5 μm.

### 3.2.12 Formin-Cdc12p also localizes in speckles in the non-medial region during mitosis and colocalizes with non-medial F-actin cables

In the previous section, we have genetically established that non-medially assembled actin cables were nucleated by formin-Cdc12p. However, except one recent paper showing that formin-Cdc12p localized to speckles scattered throughout the cell in interphase (Coffman et al., 2009), all other studies concluded that Cdc12p only localizes in the cell middle during mitosis (Chang et al., 1997; Laporte et al., 2011; Lee et al., 2012; Vavylonis et al., 2008; Wu et al., 2006). Formin-Cdc12p is one of the least abundant proteins in fission yeast cytokinetic machinery and hence it is hard to study its localization (Wu and Pollard, 2005). Therefore, we first confirmed the localization of formin-Cdc12p in mitosis more carefully. As previous work (Coffman et al., 2009) using Cdc12p-3YFP showed a satisfactory signal to noise ratio, we checked the localization in a similar strain expressing Cdc12-3Venus (Figure 12 A). Our results showed that Cdc12p-3Venus was dispersed throughout the cell as speckles in interphase (Figure 12 A, left corner bottom cells) and localized to the cell middle as nodes in early mitosis (Figure 12 A, arrows show medially localized nodes; Figure 12 B, left cell). Moreover, Cdc12p-3Venus signal also presented in the non-medial region during mitosis (Figure 12 A, top cell; Figure 12 B), consistent with the previous finding that Cdc12p nodes or Cdc12p rings only contribute ~24% or ~62% of total Cdc12p intensity, respectively (Coffman et al., 2009). To test whether these formin-Cdc12p speckles colocalized with the non-medial F-actin cables, TIRF microscopy and spinning disk microscopy were utilized. TIRFM time-lapse imaging performed in cells coexpressing LAmCh and Cdc12p-3GFP showed that the Cdc12p-3GFP speckles could move rapidly along the actin cables (Figure 12 C, arrows mark the moving Cdc12p speckle). Furthermore, double color spinning disk imaging of the synchronized *cdc25*-22 LAmCh Cdc12-3Venus cells showed that mitotic Cdc12p-3Venus speckles in the non-medial region clearly colocalized with the non-medially assembled actin cables during cytokinesis (Figure 12 D, single plane images of the broken boxes were enlarged on the right). In summary, our data shows that Cdc12p also present in the non-medial region as speckles during mitosis and these Cdc12p speckles colocalized with mitotic non-medial actin cables.

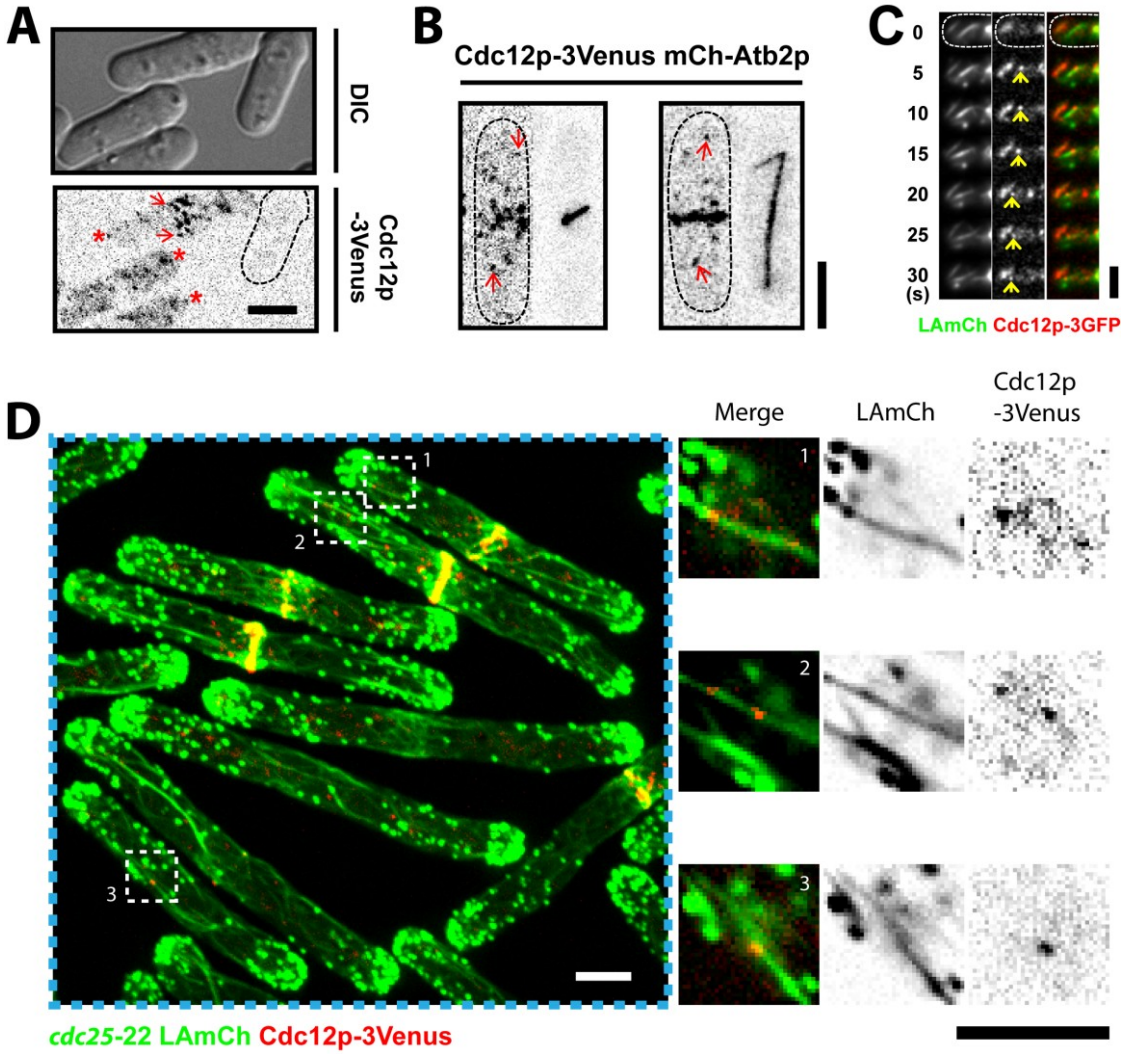
A
DIC
Cdc12p
-3Venus
B
Cdc12p-3Venus mCh-Atb2p
C
0
5
10
15
20
25
30
(s)
LAmCh Cdc12p-3GFP
D
Merge
LAmCh
Cdc12p
-3Venus
1
2
3
cdc25-22 LAmCh Cdc12p-3Venus

**Figure 12.** Formin-Cdc12p also localizes in speckles in the non-medial region during mitosis and colocalizes with non-medial F-actin cables.

(A) Cdc12p-3Venus nodes (red arrows) and speckles (red asterisks) could be clearly distinguished from the background at 515 nm. Cdc12p-3Venus LAmCh cells and wt cells were grown in YES at 24°C and mixed before imaging. Dashed line shows the boundary of a wt cell. (B) Images of two mitotic Cdc12p-3Venus mCh-Atb2p cells. Red arrows show non-medially located Cdc12p-3Venus speckles during mitosis. (C) TIRFM time-lapse double color images of a LAmCh Cdc12p-3GFP cell, showing a Cdc12p-3GFP speckle moving rapidly along a LAmCh labeled F-actin cable. Arrows point to the Cdc12p-3GFP speckle. Red, Cdc12p-3GFP; Green, LAmCh labeled F-actin cable. (D) Spinning disk images of *cdc25*-22 LAmCh Cdc12p-3Venus cells after released from 36°C to 24°C. Green, LAmCh labeled F-actin cable; Red, Cdc12p-3Venus speckles. The merged image on the left was maximum-intensity projected. White broken boxes point out the possible colocalization sites and are enlarged on the right (only one single plane image from the Z stack was enlarged). Dashed line indicates the cell boundary. Bars, 5 μm.

### 3.2.13 Mid1p-dependent and Cdc15p-dependent pathways are not essential for non-medial F-actin cable assembly

Previous studies have shown that fission yeast actomyosin ring assembly occurs through one of the two pathways: Mid1p-dependent pathway and Cdc15p-dependent pathway (Hachet and Simanis, 2008; Huang et al., 2008). The Mid1p-dependent pathway operates in early mitosis (Laporte et al., 2011; Vavylonis et al., 2008; Wu et al., 2006), whereas the Cdc15p-dependent (also called SIN-dependent) pathway operates in later stages of mitosis (Hachet and Simanis, 2008; Huang et al., 2008). However, it was unclear whether these pathways affect the assembly of the non-medially assembled F-actin cables in mitosis. Thus, non-medial F-actin cable assembly was checked in the mutants defective in one or both of the pathways. The anillin-like protein Mid1p is one of the most upstream proteins in the Mid1p-dependent pathway (Coffman et al., 2009; Sohrmann et al., 1996); therefore non-medial F-actin cable assembly was first checked in the *mid1*-18 temperature sensitive mutant at 36°C. Results showed no obvious effect on non-medial F-actin cable assembly in *mid1*-18 cells (Figure 13 A and B). Cdc15p is one of the most downstream proteins in the Cdc15p-dependent pathway (Fankhauser et al., 1995; Laporte et al., 2011; Padmanabhan et al., 2011). Non-medial F-actin cable assembly was also checked in the *cdc15*-140 temperature sensitive mutant (Figure 13 A-C) at 36°C and *cdc15* null mutant at 24°C (Figure 13 D). Interestingly, F-actin rings were clearly visualized in *cdc15*-140 or *cdc15* null (Figure 13 A-D), and non-medial F-actin cable assembly was not compromised in the *cdc15* mutants. To further confirm this result, we also checked non-medial F-actin cable assembly in *cdc7*-24 mutant (Figure 13 E), as Cdc7p is one of the most upstream proteins in the regulatory network in the Cdc15p-dependent pathway (Cerutti and Simanis, 1999; Singh et al., 2011). Again, our results suggested that Cdc15p-dependent pathway did not affect the non-medial F-actin cable assembly. Since a single mutation in either of the pathways did not affect the non-medial F-actin cable assembly, we tested if loss of both pathways would have effects on non-medial actin cables. Surprisingly, even cells defective in both pathways were not compromised for non-medial F-actin cable assembly (Figure 13 F). Moreover, when both pathways were disrupted in the *mid1*-18 *cdc15*-140 double mutant, non-medially assembled F-actin cables from

opposite ends moved to the cell middle and subsequently moved towards one of the poles (Figure 13 F). Taken together, the Mid1p-dependent and Cdc15p-dependent pathways are dispensable for non-medial F-actin filament assembly and cells defective in both pathways could not anchor the non-medial F-actin cables in the division site.

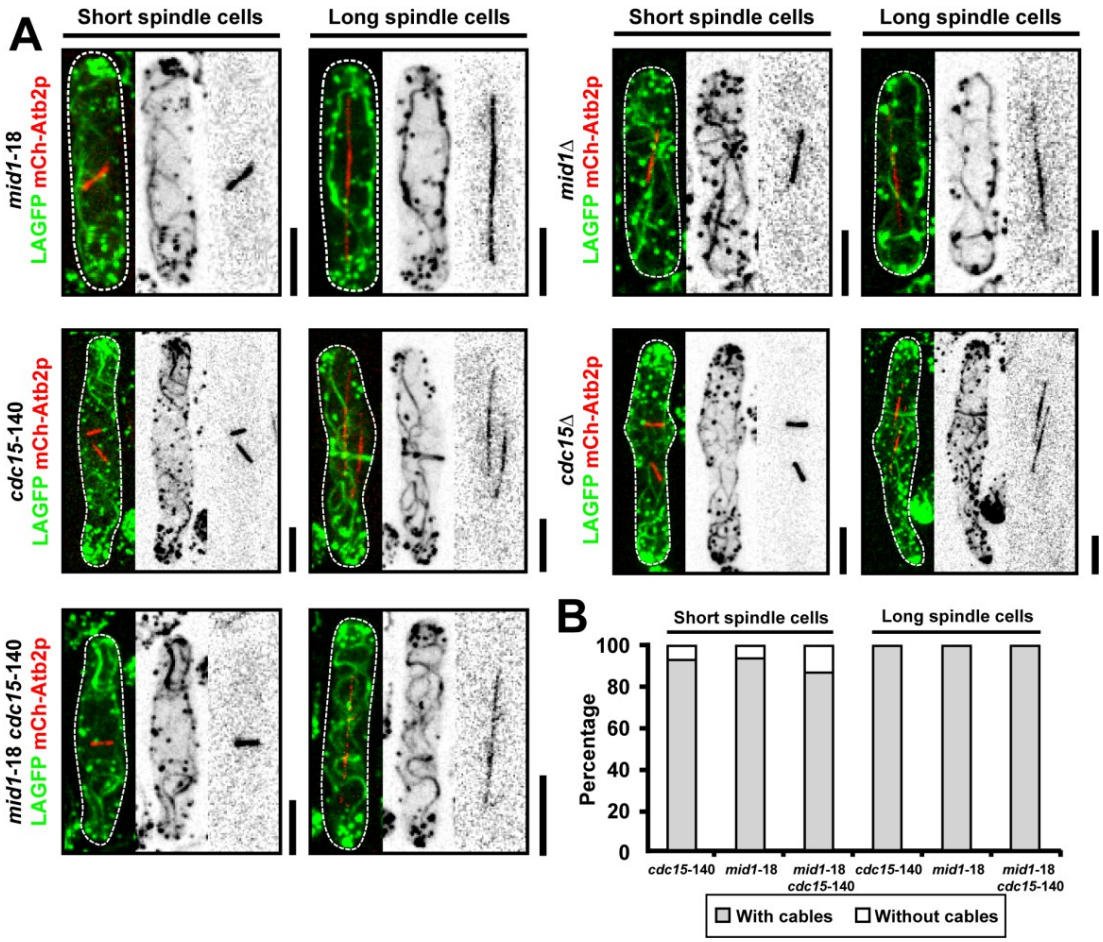

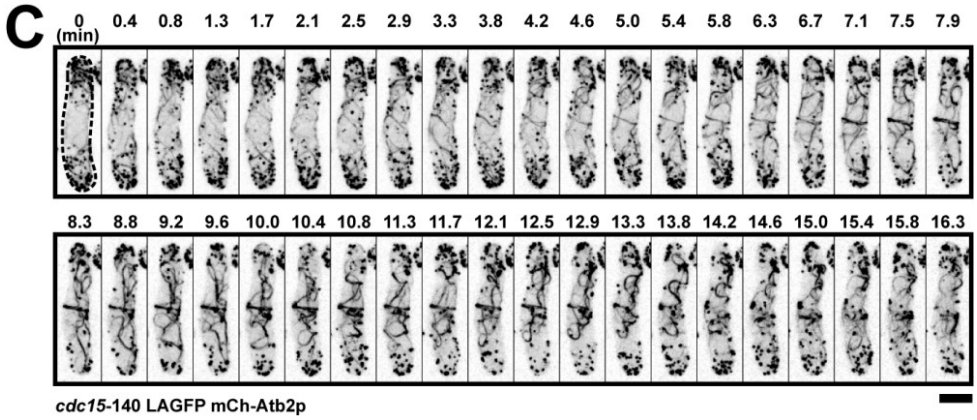
C
0 (min) 0.4 0.8 1.3 1.7 2.1 2.5 2.9 3.3 3.8 4.2 4.6 5.0 5.4 5.8 6.3 6.7 7.1 7.5 7.9
8.3 8.8 9.2 9.6 10.0 10.4 10.8 11.3 11.7 12.1 12.5 12.9 13.3 13.8 14.2 14.6 15.0 15.4 15.8 16.3
cdc15-140 LAGFP mCh-Atb2p

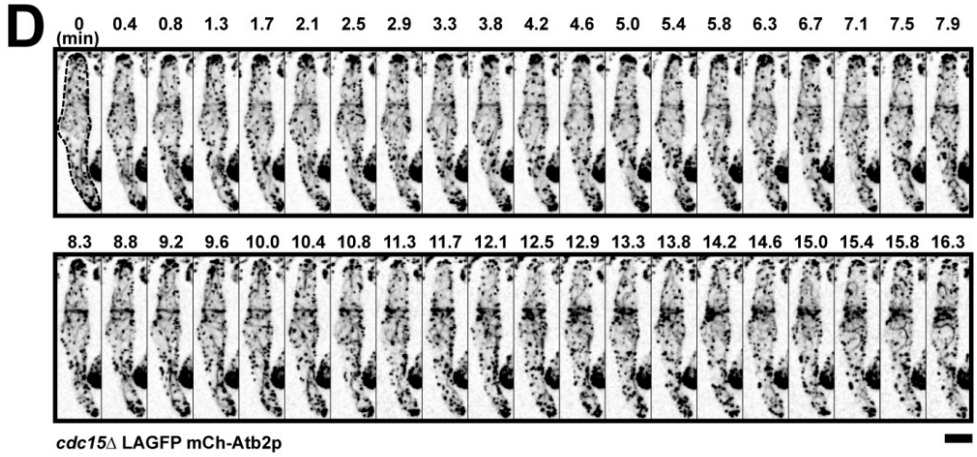
D
0 (min) 0.4 0.8 1.3 1.7 2.1 2.5 2.9 3.3 3.8 4.2 4.6 5.0 5.4 5.8 6.3 6.7 7.1 7.5 7.9
8.3 8.8 9.2 9.6 10.0 10.4 10.8 11.3 11.7 12.1 12.5 12.9 13.3 13.8 14.2 14.6 15.0 15.4 15.8 16.3
cdc15Δ LAGFP mCh-Atb2p

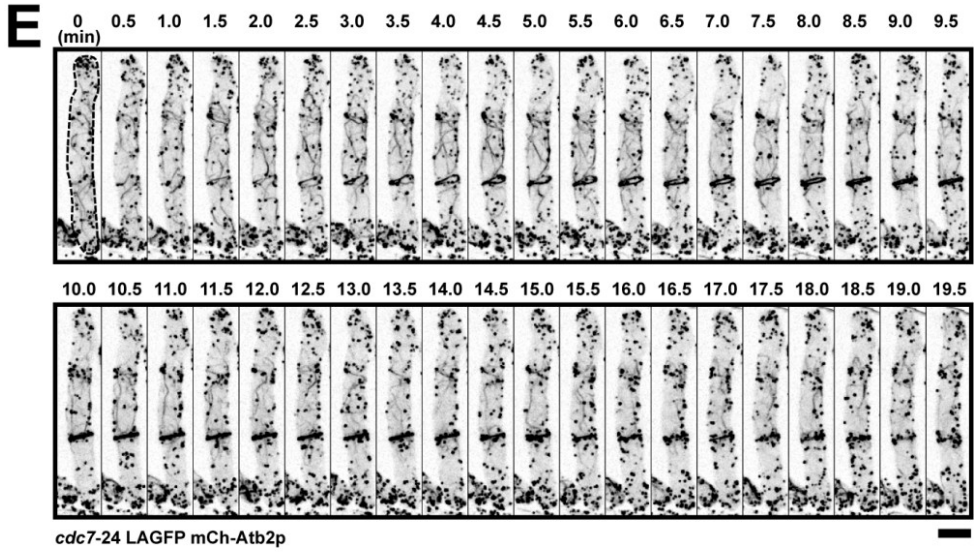
E
0 (min) 0.5 1.0 1.5 2.0 2.5 3.0 3.5 4.0 4.5 5.0 5.5 6.0 6.5 7.0 7.5 8.0 8.5 9.0 9.5
10.0 10.5 11.0 11.5 12.0 12.5 13.0 13.5 14.0 14.5 15.0 15.5 16.0 16.5 17.0 17.5 18.0 18.5 19.0 19.5
cdc7-24 LAGFP mCh-Atb2p

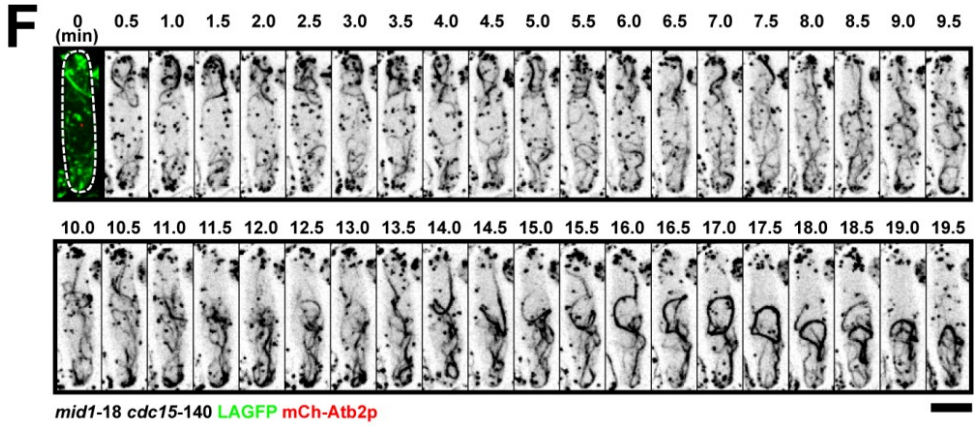
F
0 (min) 0.5 1.0 1.5 2.0 2.5 3.0 3.5 4.0 4.5 5.0 5.5 6.0 6.5 7.0 7.5 8.0 8.5 9.0 9.5
10.0 10.5 11.0 11.5 12.0 12.5 13.0 13.5 14.0 14.5 15.0 15.5 16.0 16.5 17.0 17.5 18.0 18.5 19.0 19.5
mid1-18 cdc15-140 LAGFP mCh-Atb2p

**Figure 13.** Mid1p-dependent and Cdc15p-dependent pathways are not essential for F-actin cable assembly.

(A) *mid1*-18, *cdc15*-140 and *mid1*-18 *cdc15*-140 cells expressing LAGFP and mCh-Atb2p were shifted to 36°C, imaged by spinning disk microscopy at 36°C. *mid1*Δ and *cdc15*Δ cells expressing LAGFP and mCh-Atb2p were grown at 24°C, imaged by spinning disk microscopy at 24°C. *cdc15*Δ LAGFP mCh-Atb2p cell was germinated from spores. (B) Quantification of the mutant cells in (A) with actin cables. Cells with spindles were grouped into two categories: short and long spindles. A single representative image from three independent experiments is shown. In each experiment, 100 cells were counted for each bar. (C) Time-lapse images of a representative mitotic *cdc15*-140 LAGFP mCh-Atb2p cell at 36°C. (D) Time-lapse images of a representative mitotic *cdc15*Δ LAGFP mCh-Atb2p cell at 24°C. Cell was germinated from spore. (E) Time-lapse images of a representative mitotic *cdc7*-24 LAGFP mCh-Atb2p cell at 36°C. (F) Time-lapse images of a representative mitotic *mid1*-18 *cdc15*-140 LAGFP mCh-Atb2p cell at 36°C. Dashed line indicates the cell boundary. Bars, 5 μm.

### 3.2.14 Non-medial F-actin cables might contribute to the early stages of actomyosin ring assembly

During the course of colocalization analysis between Cdc12p-3Venus nodes and the non-medial F-actin cables, we fortuitously discovered that Cdc12p-3Venus was not clearly detected (i.e., less than four nodes) in 23.8% of elongated *cdc25*-22 cells, in which small fraction of F-actin already accumulated at the division site (Figure 14 A and B, broken boxes in A show the cell middle). This result was consistent with some previous studies showing that formin-Cdc12p only localized to the medial nodes after mitosis onset (Wu et al., 2003; Wu and Pollard, 2005). Furthermore, in cells possessing strong medial accumulation of F-actin, more Cdc12p-3Venus nodes were present in the division site (data not shown). Collectively, our data suggests that non-medial F-actin cables might initiate ring assembly, and further accumulation of Cdc12p nodes might enhance F-actin assembly at the division site.

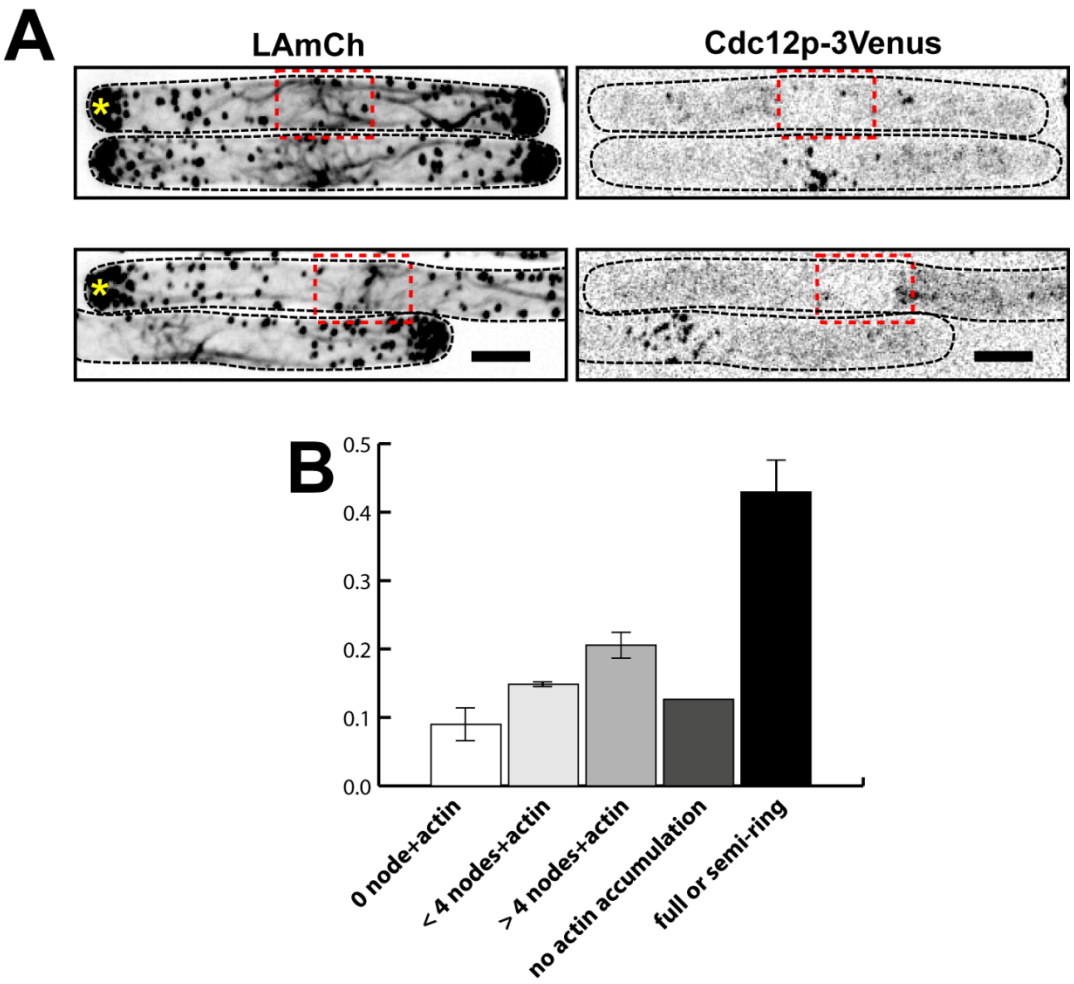


**Figure 14.** Non-medial F-actin cables might contribute to the early stages of actomyosin ring assembly.

(A) Maximum-intensity projected images of *cdc25*-22 LAmCh Cdc12p-3Venus cells after released from 36°C to 24°C. Yellow asterisks point out the cells with medial accumulation of F-actin cables but without obvious accumulation of Cdc12p-3Venus nodes. Red broken boxes show the medial region of the indicated cells. (B) Quantification of *cdc25*-22 LAmCh Cdc12p-3Venus cells. Cells were blocked in 36°C for 4 h. Counting started after released back to 24°C for 20 min and ended at 60 min. Cells were grouped into five categories: 0 node with medial accumulation of cables, less than 4 nodes with medial accumulation of cables, more than 4 nodes with medial accumulation of cables, no actin cable accumulation and cells already formed a ring or semi-ring. Error bars show means ± SD of two independent experiments (N ≥ 30 cells / bar). Dashed line indicates the cell boundary. Bars, 5 μm.

### 3.2.15 Movement of nuclei is not required for the migration of non-medial F-actin cables to the cell division site

Another important aspect of actomyosin ring assembly is the force involved in this process. Thus, it would be fruitful to study the force by which non-medial F-actin cables adopted for migration. Previous work in other organisms showed that cytoplasmic flow in a cell could help in positioning some cell fate determinants (Golden, 2000). We therefore considered the possibility that the migration of nuclei towards the cell ends might generate a counter flow of F-actin cables to the cell middle. Nevertheless, results from interphase LAGFP mCh-Atb2p cells over-expressing pREP42-*cdc12*ΔC-GFP (Yonetani and Chang, 2010) and hydroxyurea (HU)-arrested interphase *cdc16*-116 LAGFP cells (Hachet and Simanis, 2008) suggested that non-medial F-actin cables could still migrate to the cell middle and formed a compact actomyosin ring without nucleus division (Figure 15 A and B). To sum up, we found that the movement of nuclei is not required for the migration of the non-medial F-actin cables to the cell division site.

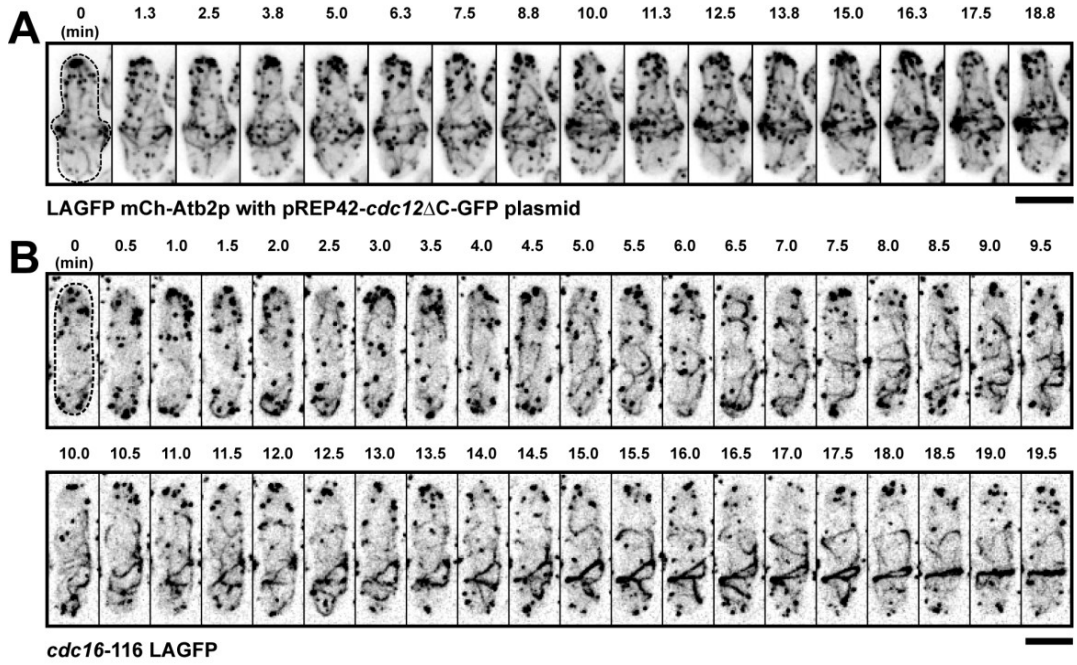


**Figure 15.** Movement of nuclei is not required for the migration of non-medial F-actin cables to the cell division site.

(A) Time-lapse images of a representative interphase LAGFP mCh-Atb2p cell over-expressing pREP42-*cdc12*ΔC-GFP plasmid. Cells were cultured in minimal medium lacking uracil (ura-) with thiamine to midlog phase. Then cells were induced in medium without thiamine for 25 h before imaging. (B) Time-lapse images of a representative hydroxyurea (HU)-arrested interphase *cdc16*-116 LAGFP cell at 36°C. For detailed description of HU treatment, please see Materials and methods. Dashed line indicates the cell boundary. Bars, 5 μm.

### 3.2.16 Myo51p functions together with Myo2p during actomyosin ring assembly

We then investigated the behavior of actin cables in various mutants defective in actomyosin ring assembly. Of all the mutants tested, *rng3*-65, a mutant defective in the UCS (UNC-45/CRO1/She4) domain–containing myosin assembly factor and activator (Lord and Pollard, 2004; Mishra et al., 2005; Wong et al., 2000), failed to compact actin cables to the cell division site (Figure 16, A and B). Notably, whereas fluorescence intensity plots over the cell length showed a sharp compaction of actin fluorescence in wt cells, such fluorescence was scattered throughout the entire cell length of rng3-65 cells (Figure 16 A and B). Because fission yeast Rng3p was a type II myosin activator, we tested the distribution of F-actin cables in the *myo2*-E1 mutant (Figure 16 A and B). Although F-actin cables were not properly compacted into a ring, F-actin signals concentrated at the medial region of the cell, consistent with previous studies (Coffman et al., 2009; Wong et al., 2000). This data suggested that an additional molecule also participated in F-actin cable reorganization. Budding yeast Rng3p homolog She4p/Dim1p has been shown to interact with type V myosins (Toi et al., 2003). Therefore, we considered the possibility that type V myosin may participate in F-actin cable reorganization. In fission yeast, two myosin Vs have been identified (Myo51p and Myo52p), of which only Myo51p localizes to the actomyosin ring (Motegi et al., 2001; Win et al., 2001). We noted that around 10% of *myo51*Δ cells failed to compact F-actin cables into a ring (Figure 16 A and B, see cell 2 in *myo51*Δ). This experiment suggested that Myo51p participated in, but was not essential for, F-actin cable reorganization to the division site. Given the phenotypes of *myo2*-E1 and *myo51*Δ mutants, we considered the possibility that these proteins might perform an overlapping role in this process. To this end, we tested the distribution of F-actin cables in *myo2*-E1 *myo51*Δ cells. Strikingly, in these cells, we found that F-actin cables, as in *rng3*-65 cells, were scattered throughout the cell (Figure 16 A and B). In summary, our data suggest that Myo51p functions together with Myo2p in F-actin cable reorganization during actomyosin ring assembly.

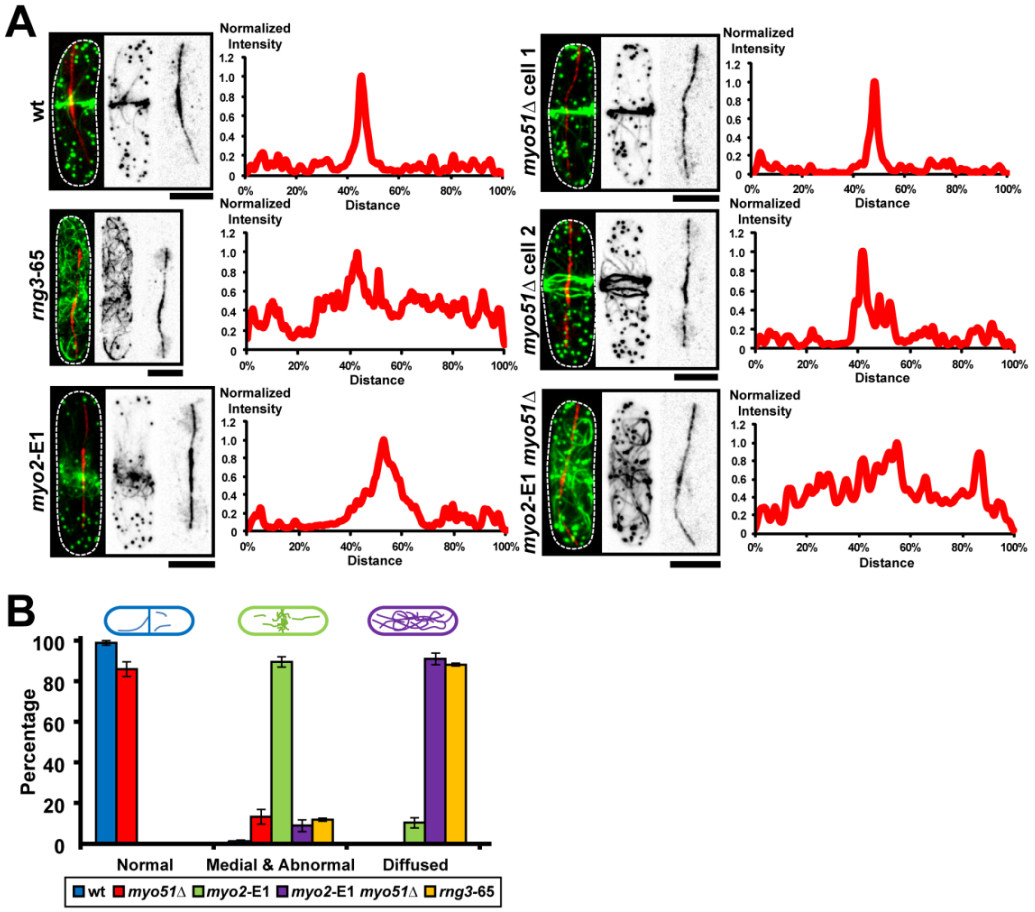


**Figure 16.** Myo51p functions together with Myo2p during actomyosin ring assembly.

(A) Cells of indicated genotype (without any fluorescent marker) were treated with hydroxyurea for 4 h at 24°C, and then shifted to 36°C for 2.5 h. Hydroxyurea was washed out and cells continued to grow at 36°C for 2 more hours. Cells were fixed, stained with Alexa-488 phalloidin and TAT1 antibody to visualize F-actin and tubulin, respectively. Fluorescence intensities of F-actin in various mutants were measured along the cell length. The data shown are from a single representative experiment out of more than three repeats. (B) Quantification of different F-actin localization patterns in various mutants. Error bars show means ± SD of three independent experiments (N = 100 cells / experiment). Cells were grouped into three categories based on the actin patterns. Normal: cells with normal sharp actin ring; Medial & Abnormal: cells with actin cables concentrated at the medial region of the cell but not properly compacted into a ring; Diffused: cells with actin cables scattered throughout the cell. Dashed line indicates the cell boundary. Bars, 5 μm.

### 3.2.17 Formin-Cdc12p localization is unaffected in *myo2*-E1 *myo51*Δ double mutant

We have found that Myo51p was functioning together with Myo2p during cytokinesis. Nevertheless, how these myosins functioned together during cytokinesis was unknown. To study the mechanisms, we first tested whether the dispersed F-actin organization pattern in *myo2*-E1 *myo51*Δ double mutant was due to the mislocalization of the F-actin cable nucleator formin-Cdc12p. Instead of forming the medially localized Cdc12p nodes, if mitotic formin-Cdc12p was dispersed in the *myo2*-E1 *myo51*Δ double mutant at 36°C, F-actin cables could be nucleated and assembled all over the cell. To test this hypothesis, Cdc12p-3Venus localizations were checked in wt, *myo51*Δ, *myo2*-E1 and *myo2*-E1 *myo51*Δ cells at 36°C, respectively. Our results showed that Cdc12p-3Venus localized to the medial region in all the cells checked (Figure 17 A). Thus, we found that formin-Cdc12p localization was unaffected in *myo2*-E1 *myo51*Δ double mutant, establishing that the mislocalization of actin cables is not related to formin-Cdc12p mislocalization but due to defective migration of actin cables in the double mutant.

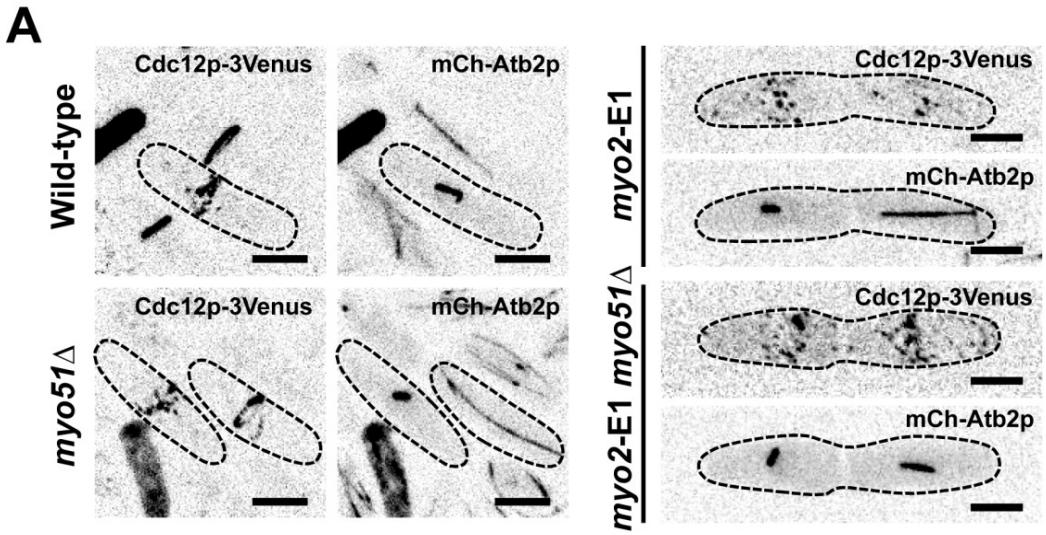


**Figure 17.** Formin-Cdc12p localization is unaffected in *myo2*-E1 *myo51*Δ double mutant.

(A) Spinning disk maximum-intensity projected images of wt, *myo2*-E1, *myo51*Δ and *myo2*-E1 *myo51*Δ cells expressing both Cdc12p-3Venus and mCh-Atb2p. All cells were shifted to 36°C for 4 h before imaging. Dashed line indicates the cell boundary. Bars, 5 μm.

### 3.2.18 F-actin cables move more slowly in *myo2*-E1 *myo51*Δ double mutants

To investigate more about the mechanism of migration of actin cables, single plane imaging was performed in wt, *myo2*-E1 and *myo2*-E1 *myo51*Δ cells at 36°C using spinning disk microscopy. Our results showed that F-actin cables in the *myo2*-E1 *myo51*Δ double mutant were much more stable than those in the wt or single mutants (Figure 18 A and B). Hence, Myo51p and Myo2p act in concert in F-actin cable movement.

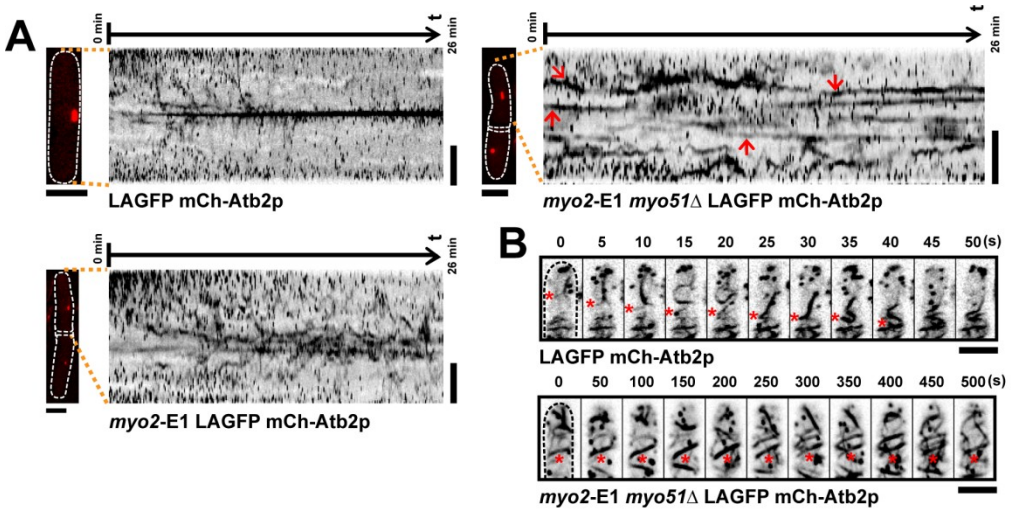


**Figure 18.** F-actin cables move more slowly in *myo2*-E1 *myo51*Δ double mutants.

(A) Kymographs of LAGFP mCh-Atb2p, *myo2*-E1 LAGFP mCh-Atb2p and *myo2*-E1 *myo51*Δ LAGFP mCh-Atb2p cells. Spinning disk single plane images were taken every 5 s. Maximum-intensity projected mCh-Atb2p images on the left of the kymographs were taken just before the start of the movies. Arrows in the kymograph of *myo2*-E1 *myo51*Δ LAGFP mCh-Atb2p cell indicate the stable actin structures observed in mitosis. Numbers on top of each kymograph indicate the start time and end time of the movie. (B) Stable actin structures were observed in *myo2*-E1 *myo51*Δ LAGFP mCh-Atb2p cells. Cell culturing and imaging conditions were the same as in (A). Asterisks in the upper montage show the migration of an actin cable to the middle in LAGFP mCh-Atb2p cell. Asterisks in the lower montage show the stable F-actin structures in *myo2*-E1 *myo51*Δ LAGFP mCh-Atb2p cell. Dashed line indicates the cell boundary. Bars, 5 μm.

## 3.3 DISCUSSION

### 3.3.1 Choosing a suitable probe to monitor F-actin dynamics

Previous research in fission yeast suggested that longitudinal F-actin cables did not contribute to actomyosin ring assembly (Feierbach and Chang, 2001; Kovar et al., 2011; Vavylonis et al., 2008). In this thesis, it is found that F-actin cables were present throughout the cell cycle in fission yeast. In mitotic cells, some cables located at the cell tips with no obvious connections to the cell middle while some others stretched from the cell tips to the cell center. These results all pointed to the possibility that longitudinal F-actin cables may contribute to actomyosin ring assembly.

To check this possibility, a proper probe for monitoring F-actin dynamics in fission yeast became necessary. Direct tagging of actin was undoubtedly the first choice. Previous studies in higher eukaryotic cells raised the possibility of directly tagging actin in live cells (Ballestrem et al., 1998; Vishwasrao et al., 2012). Unfortunately, in both budding yeast and fission yeast, fluorophore tagged G-actin did not incorporate into unbranched F-actin structures *in vivo* (Doyle and Botstein, 1996; Pollard and Wu, 2010; Wu et al., 2003; Wu and Pollard, 2005; Wu et al., 2006). Reason for this failure is still unclear. Hence, we reexamined the possibility of tagging fission yeast actin by changing the tagging or expression conditions. Our results show that neither GFP-actin nor actin-GFP incorporated into F-actin cables or rings *in vivo*. Changing the linker length between GFP and actin did not improve incorporation. Interestingly, some cable-like structures were observed in GFP-actin expressing cells, indicating that it might still be possible to tag actin if the tagging conditions are further modified.

In a recent study, a 12 AAs modified version (Martin et al., 2005a) of tetracysteine was utilized to tag fission yeast actin at 10 elaborately chosen sites (Chen et al., 2012). Surprisingly, even though tetracysteine is such a short peptide, the genetically modified G-actin still did not incorporate into F-actin cables or ring. Chen et al. suggested that the failure to incorporate tagged actin into cables or ring was possibly due to filtering by the homodimeric formin FH2 rings. This suggestion is reasonable. However, we could not rule out the

possibility that direct tagging of actin might lead to the folding defect of G-actin, as G-actin folding was a complex process (Hansen et al., 1999; Stirling et al., 2006). Future work should apply even smaller tags such as unnatural amino acids (Chin et al., 2003) to tag actin. Moreover, artificial engineering of formin-Cdc12p to enlarge the homodimeric FH2 ring may be helpful.

Alternative methods to monitor actin dynamics are to microinject phalloidin or rhodamine-actin into cells (Alsop et al., 2009; Cao and Wang, 1990b; Chen et al., 2008; Guha et al., 2005; Zhou and Wang, 2008) or monitoring the dynamics of actin binding proteins (Burkel et al., 2007; Edwards et al., 1997; Martin and Chang, 2006; Riedl et al., 2008; Riedl et al.; Schell et al., 2001; Vidali et al., 2009). The first method, microinjections of phalloidin or rhodamine-actin, was proved useful in some cell lines. However, cells in these experiments need to be big enough and micro-injectable, which is not convenient for small cells and cell wall-possessing organisms such as fission yeast. What is more, the amount of phalloidin or rhodamine-actin are hard to control. The second method is to utilize actin binding proteins. There is a plethora of actin binding proteins/peptides (dos Remedios et al., 2003; Winder and Ayscough, 2005) with different actin binding efficiency and therefore choosing a suitable probe is important for studying actin dynamics.

Lifeact is a good probe to study F-actin dynamics (Berepiki et al., 2010; Delgado-Alvarez et al., 2010; Riedl et al., 2008; Riedl et al., 2010; Vidali et al., 2009). It is a 17 AAs peptide from the N-terminus of budding yeast Abp140 protein (Asakura et al., 1998) and has been proved useful in many organisms. Previously, lifeact has been used to study F-actin dynamics in fission yeast (Coffman et al., 2009). However, lifeact did not label fission yeast F-actin cables clearly due to unknown reasons. In this thesis, by changing the promoter from *nmt1* to actin promoter, using a 16 AAs shorter version of lifeact, tagging lifeact at the C-terminus instead of N-terminus and increasing the linker length, we successfully apply lifeact in fission yeast.

### 3.3.2 Non-medial F-actin cables in actomyosin ring assembly

Lifeact labeled F-actin dynamics was studied by 3D Time-lapse spinning disk microscopy. We found non-medially assembled F-actin cables migrated towards and subsequently joint the assembling actomyosin ring during cytokinesis, which was at odds with previous studies (Coffman et al., 2009; Feierbach and Chang, 2001; Vavylonis et al., 2008). To examine the reliability of this result, additional experiments were conducted. First, migration and incorporation of non-medially assembled actin cables into the actomyosin ring were confirmed in other lifeact expressing cells, the synchronized *cdc25*-22 cells, P*nmt1*-*wee1*-50 *adf1*-1 mutant, *act1*-138 mutant and *cdc4*-8 mutant. Second, similar actin cable incorporation was observed by TIRF microscopy with shorter time interval. In some cases, F-actin cable assembly and elongation was observed near the cell tips. Third, kymographs derived from either spinning disk or TIRF microscopy showed similar non-medial actin cable incorporation events. Lastly, non-medial F-actin cable assembly and migration were also observed using other F-actin monitoring probes such as Utr-CH-GFP and P*act1*-GFP-CHD. Thus, based on these experiments, we conclude that non-medially assembled F-actin cables contribute to actomyosin ring assembly during cytokinesis in fission yeast. Future research should investigate how these non-medially assembled actin cables incorporate into the actomyosin ring at the division site and whether these non-medial actin cables stay in the actomyosin ring.

Previous researches using GFP-CHD as a probe to monitor F-actin dynamics in fission yeast concluded that F-actin was *de novo* nucleated by formin-Cdc12p in the cell middle (Coffman et al., 2009; Vavylonis et al., 2008). In the LatA sensitivity assays, we found that GFP-CHD stabilized F-actin structures much more than lifeact. This is not surprising, as the N-terminal fragments of Rng2p (contains CHD) were found to bundle actin filaments (Takaine et al., 2009). Moreover, CHD is derived from fission yeast Rng2p, an early mitotic node component (Laporte et al., 2011; Padmanabhan et al., 2011; Wu et al., 2003). Hence, it is possible that CHD could interact with node related proteins in the cell middle and lead to a more robust detection of F-actin in the medial region during actomyosin ring assembly.

During the quantitation of actin cable movement by TIRF microscopy, we found that most of the mitotic actin cables moved towards the cell middle but a small fraction of the cables moved towards the poles at lower speed. The function of these polar moving actin cables is unknown. There are two explanations for these polar moving cables. First, these "polar moving" actin cables are artifacts from TIRF imaging. Mitotic non-medially assembled F-actin cables are so flexible that when migrating towards the cell division site they may move from one Z position to another. As TIRF microscopy could only image the most top layer of a cell (Yu et al., 2011), it is possible that the "polar moving" actin cables actually represent cables coming from other layers. Rather, the second explanation is that these polar moving events are genuine. It is possible that formin initially nucleates actin filaments into random orientations and a fraction of them moves towards the poles. It is possible that the medially localized myosins cause the speed difference between the polar moving and the equatorial moving actin cables. Future experiments should distinguish these two possibilities.

TIRF microscopy data also suggest that mitotic actin cables are dynamic and exhibit a variety of behaviors: translocation; buckling; whipping, breakage and compaction. Interestingly, we also observed elongation of actin cables in the cell middle by TIRF microscopy. This is consistent with findings in other organisms, suggesting that actin flow and *de novo* nucleation in the cell middle may coexist (Alsop et al., 2009; Chen et al., 2008; Zhou and Wang, 2008). Currently, the fractions of F-actin filaments originated from the non-medial region and the medial region are unclear.

### 3.3.3 Cofilin-Adf1p may participate in the reorganization of non-medial F-actin cables

Interestingly, in some cases, the long non-medially assembled F-actin cables appeared to disassemble before they incorporated into the actomyosin ring in the synchronized *cdc25*-22 cells. This disassembly phenomenon was not observed in P*nmt1*-*wee1*-50 *adf1*-1 mutant at 36$^{o}$C, indicating that cofilin-Adf1p may participate in the reorganization of long actin cables into

the assembling actomyosin ring.

### 3.3.4 Formin-Cdc12p is responsible for nucleating the non-medial F-actin cables

In this thesis, we also found that formin-Cdc12p was responsible for nucleating the non-medial actin cables. Previously, formin-For3p was considered responsible for all F-actin cables in fission yeast (Feierbach and Chang, 2001; Kamasaki et al., 2005; Kovar et al., 2011). However, although actin cables were absent in most of the interphase *for3*Δ cells, we observed F-actin cables in mitotic *for3*Δ cells either by LAGFP or phalloidin staining. Thus, F-actin cables in fission yeast could be divided into two groups according to their nucleator and the cell cycle stage: interphase F-actin cables nucleated by formin-For3p and mitotic F-actin cables nucleated by other protein(s). Later, we proved that formin-Cdc12p was responsible for nucleating majority of the non-medial actin cables since *cdc12*Δ cells possessed fewer mitotic F-actin cables. Double deletion of both For3p and Cdc12p led to the complete abolishment of mitotic F-actin cables, indicating that Cdc12p together with For3p were responsible for nucleating the mitotic F-actin cables. It is possible that both For3p nucleated and Cdc12p nucleated F-actin cables contribute to actomyosin ring assembly. Future experiments should check the difference between these two kinds of actin cables (Skoumpla et al., 2007). Quantifying the contribution by each of these F-actin cable populations and comparing the controlling mechanisms of these two formins would also be interesting (Yonetani and Chang, 2010; Yonetani et al., 2008). Moreover, future experiments should also examine whether For3p could replace Cdc12p during actomyosin ring assembly. Overexpressing For3p or targeting it to the cell middle earlier may help to answer this question.

We have shown genetically that formin-Cdc12p was responsible for nucleating majority of the non-medial F-actin cables. However, previous studies showed that the low-expression-level protein Cdc12p only localized in the cell middle (Chang et al., 1997; Wu et al., 2003; Wu et al., 2006; Yonetani et al., 2008). Only one recent study suggested that formin-Cdc12p also localized to

"speckles" throughout the cell (Coffman et al., 2009). The elegant work by Coffman et al. used three tandem YFPs (3YFP) to tag formin-Cdc12p. Compared to the single fluorophore tagged Cdc12p, this fusion protein increased the signal to noise ratio under the same microscopy set up. Coffman et al. showed that, although the number of Cdc12p speckle decreased several folds during mitosis progression, Cdc12p speckles still present in the cell throughout mitosis. To check whether Cdc12p speckles colocalize with non-medial actin cables, double color imaging was performed in synchronized *cdc25*-22 cells expressing Cdc12p-3Venus and LAmCh. Results show that non-medially localized formin-Cdc12p speckles colocalized with non-medial actin cables, supporting our conclusion that formin-Cdc12p was responsible for nucleation of the non-medial F-actin cables. Moreover, our result together with the previous study on Cdc12p speckles (Coffman et al., 2009), suggest that caution should be used when studying the localization of a protein, as the current microscopy set up may not identify the low concentration sites. Future experiments would also be interesting to investigate the dynamics of formin-Cdc12p speckles on the non-medial F-actin cables.

### 3.3.5 Both ring assembly pathways are not essential for non-medial F-actin cable assembly

Interestingly, previous work has shown that actomyosin ring assembly in fission yeast proceeds through either of the two pathways: the Mid1p node-dependent pathway and the SIN-dependent pathway (Hachet and Simanis, 2008; Huang et al., 2008; Mishra and Oliferenko, 2008). However, we showed that non-medial F-actin cables were not affected in cells lacking one or both pathways. In cells devoid of both pathways, non-medially assembled F-actin cables from both ends "bump" into each other and move towards one side of the cell, resulting in no F-actin accumulation in the cell middle. Taken together, our data suggest that the previously established ring assembly pathways mainly participate in the organization of F-actin cables into the forming actomyosin ring but not the nucleation events of these F-actin cables.

### 3.3.6 The essentiality of cortical flow and medial *de novo* nucleation

It is unknown whether assembly of F-actin at the non-medial region or the cell middle alone is sufficient for actomyosin ring assembly. Future studies should target all formin-Cdc12p to the cell middle, or inhibit F-actin nucleation ability of formin-Cdc12p at either region during mitosis to answer this question (Carvalho and Pellman, 2004; Magidson et al., 2006). Interestingly, a recent work suggests that *de novo* F-actin assembly by the formin-Cdc12p nodes at the division site is more crucial than the non-medially assembled F-actin cables in fission yeast cytokinesis (Coffman et al., 2013). Researchers utilized a truncated Cdc12p (Δ503-Cdc12p, the first 503 AAs truncated) as the sole source of formin-Cdc12p and expressed it from *cdc12* promoter at its native locus. In the *for3*Δ Δ503-*cdc12* double mutant, Δ503-Cdc12p medial node localization was affected, suggesting no *de novo* nucleation by nodes at the division site. Moreover, actomyosin ring assembly was significantly impaired but non-medial F-actin cable assembly and migration was normal in the double mutant. Therefore, it is proposed that *de novo* assembly of F-actin filaments by formin-Cdc12p nodes at the division site are more important than the cortical flow of non-medially assembled actin cables. However, rather than only nucleating actin filaments from the nodes, it is highly possible that Cdc12p also has other functions at the division site during actomyosin ring assembly (Yonetani and Chang, 2010). By abolishing the medial node localization of Cdc12p, the other functions of Cdc12p may also be affected. Therefore, from the existing experimental data it is not enough to conclude that non-medial actin cables are not effective and reliable for actomyosin ring assembly. More work has to be done to address the importance of both sources of F-actin during actomyosin ring assembly.

### 3.3.7 The necessity of more EM studies

As mentioned above, significant amount of non-medially assembled F-actin cables migrate towards and incorporate into the actomyosin ring during mitosis. However, previous EM studies showed that the direction of F-actin cables switched between interphase and mitosis (Kamasaki et al., 2005). The pointed ends point towards the cell middle in interphase but point towards the tips during mitosis. The orientation of mitotic actin cables from this EM data

seemed to be at odds with our finding that actin cables are assembled in the non-medial region and migrate toward the division site. *In vitro* studies showed that if one end of an actin filament was immobilized, the F-actin filament could curve like an "S" shape due to continuous polymerization (Kovar et al., 2006). Hence, it is possible that the mitotic actin cable in this EM study actually represent the curving part of a migrating non-medial actin cable. Another EM study (Kamasaki et al., 2007) by the same group also showed that, in early mitosis, F-actin filaments in the actomyosin ring were parallel and could be divided into two semicircular populations of opposite directionality. During later stages, the actomyosin ring contained fewer actin filaments with mix directionality. This EM data are hard interpret, as we now know that non-medially assembled actin cables exist during cytokinesis. Further experiments should analyze more EM data to confirm the directionality of F-actin cables in mitosis and the directionality of F-actin filaments in the actomyosin ring. As EM has a low contrast, it may be helpful to correlate light microscopy with EM to study F-actin cables. Tagging lifeact with APEX might be helpful for this purpose (Martell et al., 2012).

### 3.3.8 Non-medial F-actin cables might contribute to the early stages of actomyosin ring assembly

During the course of studying the relationship between non-medial F-actin cables and the medially localized nodes, we fortuitously found that, in 23.8% of the synchronized *cdc25*-22 cells, Cdc12p-3Venus nodes were not detected at the division site while medial F-actin and non-medially located Cdc12p-3Venus speckles were easily found. This result is consistent with previous studies showing that formin-Cdc12p only localized to the nodes at 0.4 ± 0.9 min or 1.0 ± 2.5 min (mean ± SD) after SPB separation (Coffman et al., 2009; Wu et al., 2003; Wu and Pollard, 2005). Taken together, it is possible that non-medially assembled F-actin cables or medially assembled F-actin filaments nucleated by Cdc12p speckles contribute early to the assembly of fission yeast actomyosin ring. Future studies should determine the temporal relationship between these different sources of F-actin in the actomyosin ring.

### 3.3.9 Both Myo2p and Myo51p contribute to actomyosin ring assembly

Lastly, we studied the migration of the non-medially assembled F-actin cables. Our analysis of cells defective in Myo2p (type II myosin), Myo51p (type V myosin) and Rng3p (myosin activator/chaperone) showed that a combination of Myo2p and Myo51p functions may contribute to F-actin accumulation in the cell middle during cytokinesis. Mitotic F-actin cables in *myo2*-E1 *myo51*Δ double mutants were dispersed throughout the cell at 36$^{o}$C while *myo2*-E1 cells alone could still accumulate a certain amount of actin cables (Moseley and Goode, 2006). Further experiments showed that F-actin cables were much less dynamic in *myo2*-E1 *myo51*Δ cells comparing to those in the single mutants, which is consistent with the finding in mammalian cells that type II myosin is important for cortical actin flow (Zhou and Wang, 2008). This is the first study showing Myo51p contributes to actomyosin ring assembly (East and Mulvihill, 2011; Motegi et al., 2001; Win et al., 2001). However, how these two myosins function together during cytokinesis is still unknown. It is also unclear whether these two myosins are "pushing" the non-medial F-actin cables from the non-medial region or "pulling" the non-medial actin cables into the assembling actomyosin ring once they reach the medial region of the cell (Moseley and Goode, 2006). Future experiments should focus on understanding the detailed mechanisms.

In summary, this thesis has provided evidences for a novel mechanism for fission yeast actomyosin ring assembly during cytokinesis (see Illustration 6). This equatorial migration of non-medially assembled F-actin cables bears similarity to the "cortical actin flow" mechanism in higher eukaryotic cells (Alsop et al., 2009; Cao and Wang, 1990b; Chen et al., 2008; Guha et al., 2005; Zhou and Wang, 2008). Owing to the conservation of actomyosin ring assembly apparatuses/mechanisms between fission yeast and higher eukaryotes such as animals, future experiments in fission yeast should provide a more complete understanding of eukaryotic cytokinesis.

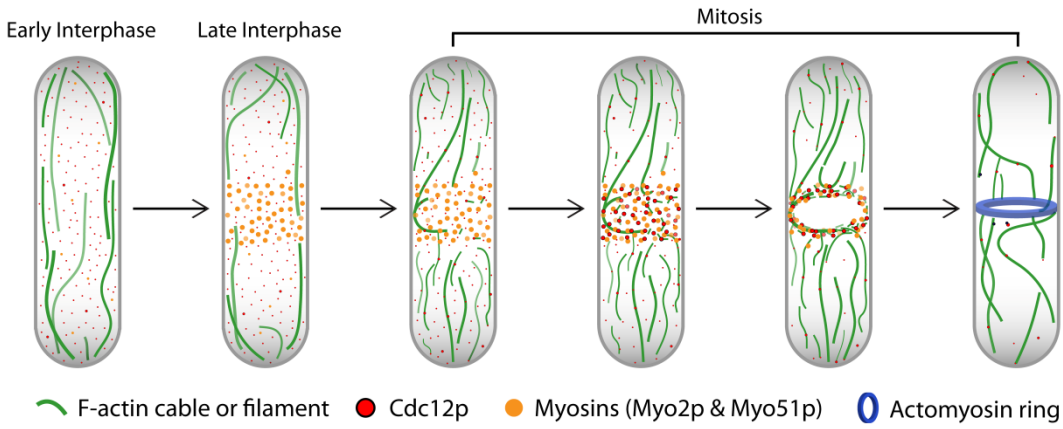


**Illustration 6**. Actomyosin ring assembly in fission yeast.

In interphase, F-actin filaments in the actin cables are nucleated by formin-For3p. Shortly before cells enter mitosis, some ring proteins, including myosins but not formin-Cdc12p, form a broad band of nodes in the cell center. At the onset of mitosis, non-medially assembled F-actin cables/filaments are nucleated by formin-Cdc12p throughout the cell. These non-medial actin cables migrate towards the cell center and start to accumulate before the appearance of formin-Cdc12p nodes. Long actin cables could be severed by cofilin-Adf1p during this migration/integration process. Medial accumulation of F-actin cable/filament could be uneven and may accumulate as linear/astral structures similar to the "Leading Cable Model" at the early stage of ring assembly. Shortly after non-medial actin cables/filaments start to accumulate, formin-Cdc12p nodes form. Then *de novo* nucleation of F-actin filaments by formin-Cdc12p nodes happens in the medial region of the cell, as proposed by the "Search-Capture-Pull-Release Model". By the mutual interactions between myosins, F-actin cables/filaments and some other actomyosin ring components, a contractile actomyosin is assembled. The long-term accumulation of F-actin cables/filaments in the cell middle depends on Myo2p and Myo51p.

# CHAPTER IV ACTIN MUTANTS AND CHARACTERIZATION OF ACTIN MUTANT *act1*-j28

## 4.1 INTRODUCTION

In many eukaryotes, actin is an essential gene and is involved in many cellular processes, such as muscle contraction, cell division, cell migration, cell polarity, endocytosis, transcription regulation etc. To study the cellular functions of actin, drugs such as phalloidin, Latrunculin A, Cytochalasin D and Jasplakinolide are commonly used to disturb the actin cytoskeleton. However, these chemicals usually affect overall actin in a general manner, which lead to a complex phenotype hard to explain. To study one specific aspect of actin function, actin mutant that is exclusively defective in one individual actin-requiring process would be of great value. In our recent work (Subramanian et al., 2013), we generated and characterized 39 novel temperature sensitive actin mutants by a new reverse genetic method (Tang et al., 2011) in fission yeast. In this pool of actin mutants, some mutants showed special cytokinesis defects while others displayed either polarity phenotypes or a mixture of defects. It would be helpful to carefully characterize these actin mutants to unravel the mechanisms causing these mutant phenotypes.

This chapter describes the preliminary characterization of one of the actin mutants isolated from the screen, *act1*-j28. This mutant, a temperature sensitive allele of actin, was defective in cytokinesis and failed to form an actomyosin ring. Overexpression of a putative 12 transmembrane protein was found to be able to suppress this actin mutant.

## 4.2 RESULTS

### 4.2.1 Characterization of actin mutant *act1*-j28

*act1*-j28 is one of the cytokinesis defect mutants isolated from our random mutagenesis screen (Subramanian et al., 2013; Tang et al., 2011). *act1*-j28 cells after overnight growth in YES plate at 36$^{o}$C were elongated and dumbbell shaped (Figure 19 A), a typical phenotype observed in other cytokinetic mutants (Balasubramanian et al., 1994; Chang et al., 1997; Kitayama et al., 1997). *act1*-j28 contains two point mutations, Phe200Ser

(subdomain 4 of G-actin) and Gly308Ser (subdomain 3 of G-actin). Both mutations are located in regions where no obvious secondary structure was found (Figure 19 B, left) and exposed on the surface of G-actin (Figure 19 B, right). As with the case of some actin mutants, it was hard to stain this mutant with phalloidin to visualize F-actin structures (Figure 19 C). We also found that lifeact-GFP suppressed *act1*-j28 mutant phenotype at restrictive temperature (data not shown). DAPI staining showed that *act1*-j28 cells were multinucleate under restrictive temperature (Figure 19 D). Fragmented cell wall was found in the cell middle of *act1*-j28 by Aniline Blue staining (Figure 19 D). To examine the formation of actomyosin ring in *act1*-j28, immunofluorescence staining of Cdc4p (one of the early node and actomyosin ring components) in *act1*-j28 cells was carried out. Complete Cdc4p rings could not be seen at 36$^{o}$C in *act1*-j28 (Figure 19 E). Although Cdc4p was found to localize to node-like structures in the cell middle, interestingly some cable-like structures were also found in the medial region in late mitotic *act1*-j28 cells (Figure 19 E, enlarged image). Cdc12p-3Venus localization was also unaffected in *act1*-j28 at 36°C (data not shown).

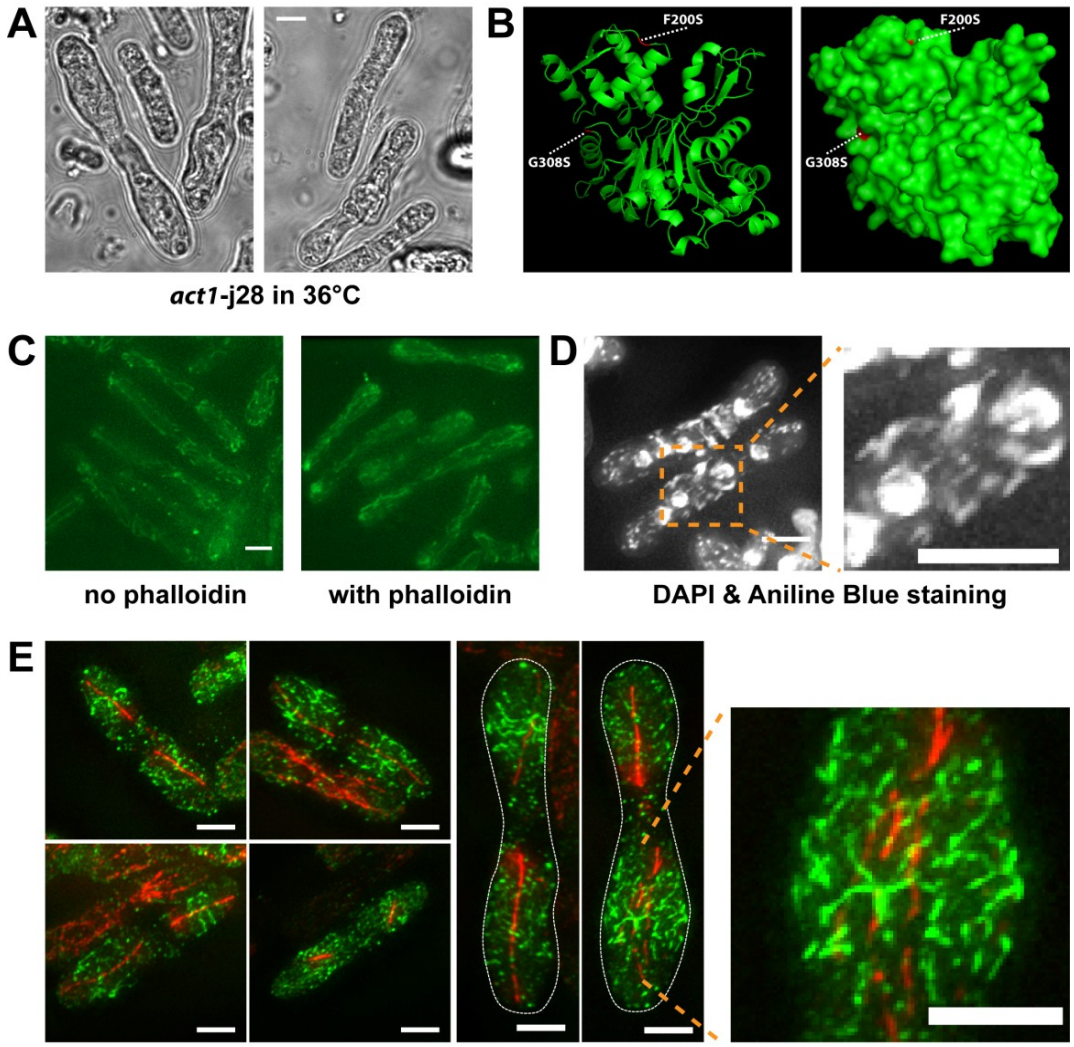


**Figure 19.** Characterization of actin mutant *act1*-j28.

(A) Bright field images of *act1*-j28 mutant cells from 36°C YES plate. (B) Ribbon (left) and surface (right) diagrams of budding yeast actin (PDB: 1YAG) with the corresponding mutated sites of fission yeast mutant *act1*-j28 highlighted in red shown by PyMOL. Both mutations (F200S & G308S) are on the surface of the actin structure. (C) *act1*-j28 cells stained with Alexa-488 phalloidin. Control cells (left) were not stained. The fluorescent structures in both images were from mitochondria autofluorescence. (D) *act1*-j28 cells stained with DAPI and Aniline Blue. On the right is an enlarged image of the highlighted yellow dotted region. (E) Immunofluorescence staining of mitotic *act1*-j28 cells by Anti-Cdc4p (green) and Anti-TAT1 antibodies (red). Part of an *act1*-j28 cell was enlarged on the right. In Figures B-D, *act1*-j28 cells were shifted up to 36°C for 6.7 h and fixed with paraformaldehyde. Images in Figures B-D were processed by deconvolution. Bars, 5 μm.

### 4.2.2 High copy suppressor screen for actin mutant *act1*-j28

From previous analysis, it was established that actin mutant *act1*-j28 was a nice cytokinesis mutant and further characterizing this mutant could aid better understanding of actin function during cytokinesis. To achieve this goal, we carried out a high copy suppressor screen (Forsburg, 2001; Subramanian et al., 2013) for *act1*-j28 (see methods for details). 11 individual transformations were performed; potential suppressor plasmids were recovered and sequenced. One plasmid containing *act1*+ gene was recovered twice (from different transformations, plasmid 1-1 & plasmid 2-2, 1468840-1477961 on chromosome II). Interestingly, 3 plasmids isolated from different transformations contained an overlapping region in chromosome II. Two of them (plasmid 4-16 & plasmid 5-3) contained exactly the same DNA fragment (4251853-4260611). The other one (plasmid 2-10) spanned a region from 4255224 to 4262844. The overlapping region (4255224-4260611) of these three plasmids contained only one protein coding gene (*SPBC1652.02*) and a predicted antisense RNA (on the antisense strand of SPBC1652.02). To confirm the suppression, empty plasmid, plasmid 2-2 (*act1*+) and plasmid 2-10 (*SPBC1652.02*+) were retransformed back to either wt cells or *act1*-j28 cells and suppression was checked under restrictive temperature (Figure 20 A). Wt cells carrying any of the three plasmids could grow normally on YES plates in both permissive temperature and restrictive temperature (Figure 20 A). *act1*-j28 cells with empty plasmids could grow at permissive temperature but were lethal at restrictive temperature (Figure 20 A). However, *act1*-j28 cells with either plasmid 2-2 (*act1*+) or plasmid 2-10 (*SPBC1652.02*+) could survive at restrictive temperature and no obvious difference was observed between these two plasmids (Figure 20 A). To further examine the morphology of these rescued cells, cells were checked by microscopy. Strikingly, it was found that both plasmid 2-2 (*act1*+) or plasmid 2-10 (*SPBC1652.02*+) could rescue the morphology of *act1*-j28 to a great extent (Figure 20 B and C). This result suggests that plasmid 2-10 (*SPBC1652.02*+) could rescue *act1*-j28 to the same extent as plasmid 2-2 (*act1*+). This potential suppressor gene *SPBC1652.02* encodes a predicted APC (amino acid-polyamine-organocation) amino acid transporter. This protein contains 594 AAs and are named Aap1p. There were limited studies on *aap1* gene.

From PomBase (http://www.pombase.org/), it was known that this *aap1* gene was not essential (Hayles et al., 2013; Kim et al., 2010). *aap1*Δ cells had a normal cell morphology as wt cells in glucose rich medium (Hayles et al., 2013). Orfeome Localization Data showed that when overexpressed, Aap1p-YFP localized to ER and cell membrane. Moreover, cell morphology was unaffected by overexpression (Matsuyama et al., 2006). Interestingly, TMHMM Server v.2.0 predicted that Aap1p contained 12 transmembrane regions; N (1-72 AAs) and C-terminal (519-594 AAs) were at the cytosolic side of the cell membrane (Figure 20 D). SMART (a Simple Modular Architecture Research Tool) predicted that amino acid permease domain of Aap1p started from 73 to 527 AAs. Multi-sequence alignment showed that *aap1* was highly conserved from bacteria to human beings (Figure 20 E). Orthologues of Aap1p in budding yeast were able to transport a variety of amino acids (Jauniaux and Grenson, 1990; Van Zeebroeck et al., 2009). Furthermore, in each organism, this gene has many paralogs. *aap1* gene has 10 paralogs in fission yeast and some of them showed similar localizations in Orfeome Localization Data (data not shown). Taken together, we found Aap1p to be a high copy suppressor for *act1*-j28.

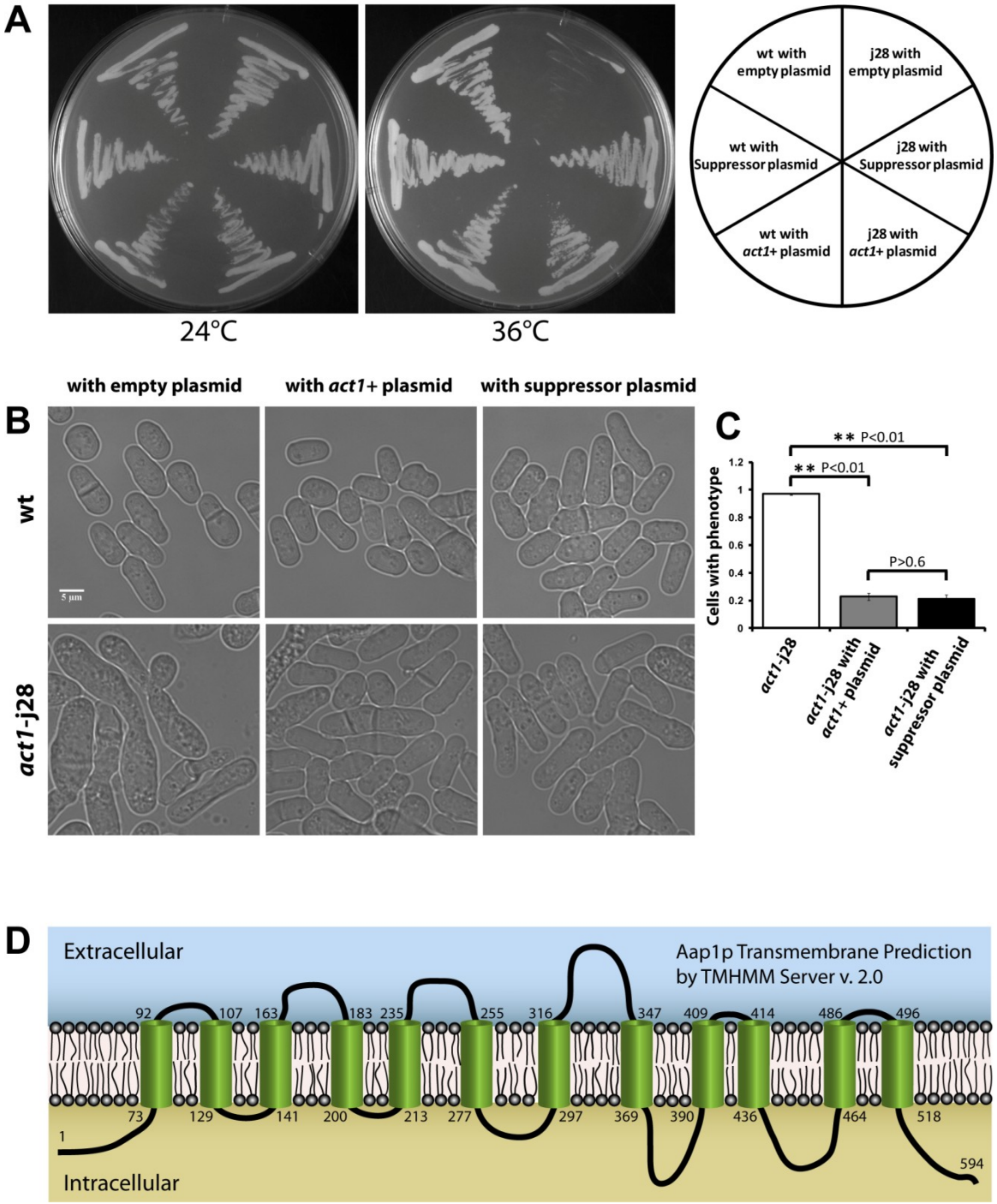
A
24°C
36°C
wt with empty plasmid
j28 with empty plasmid
wt with Suppressor plasmid
j28 with Suppressor plasmid
wt with act1+ plasmid
j28 with act1+ plasmid
B
with empty plasmid
with act1+ plasmid
with suppressor plasmid
wt
act1-j28
5 µm
C
** P<0.01
** P<0.01
P>0.6
Cells with phenotype
1.2
1
0.8
0.6
0.4
0.2
0
act1-j28
act1-j28 with act1+ plasmid
act1-j28 with suppressor plasmid
D
Extracellular
Aap1p Transmembrane Prediction by TMHMM Server v. 2.0
92
107
163
183
235
255
316
347
409
414
486
496
73
129
141
200
213
277
297
369
390
436
464
518
1
594
Intracellular

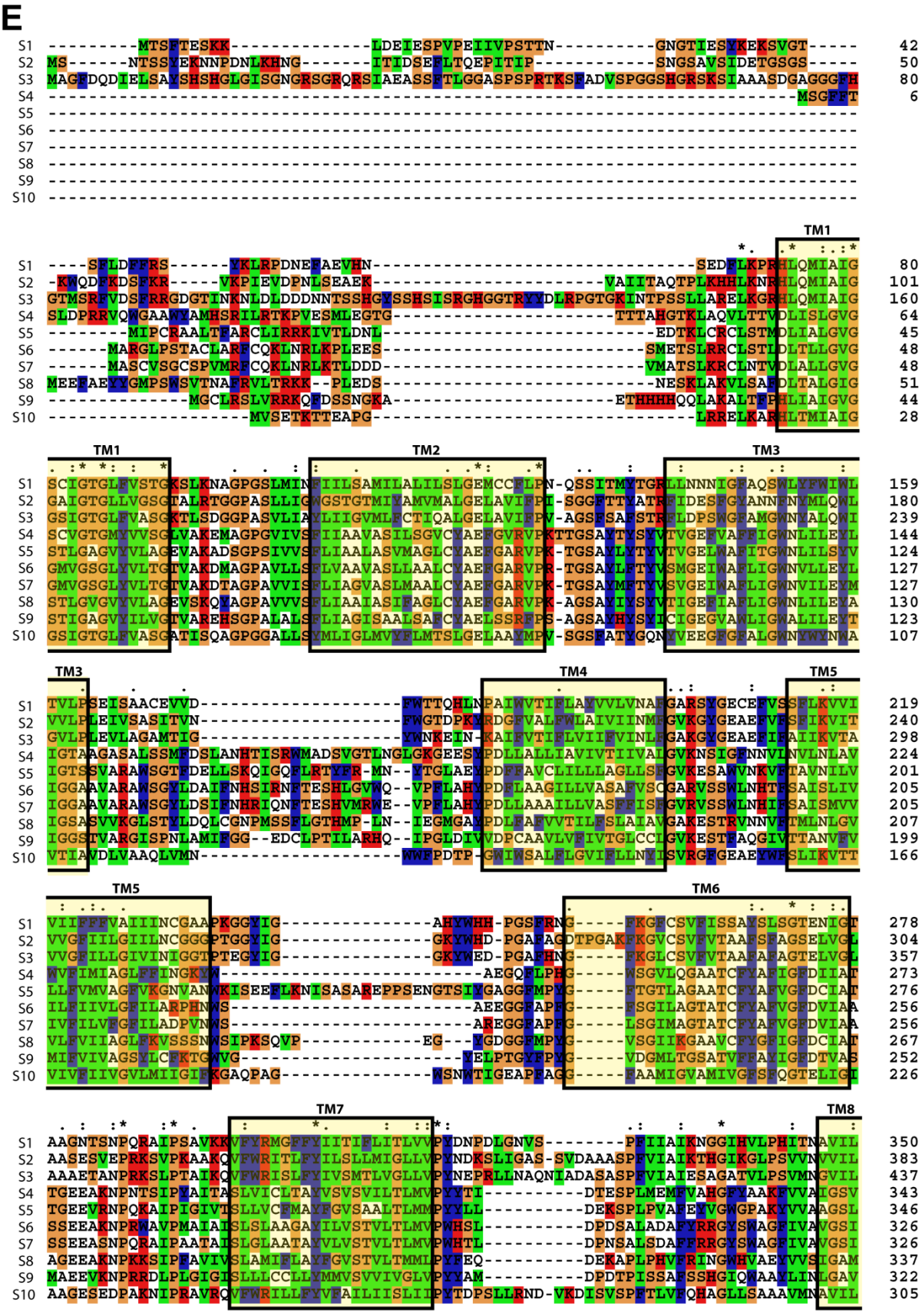
E
TM1
TM2
TM3
TM4
TM5
TM6
TM7
TM8

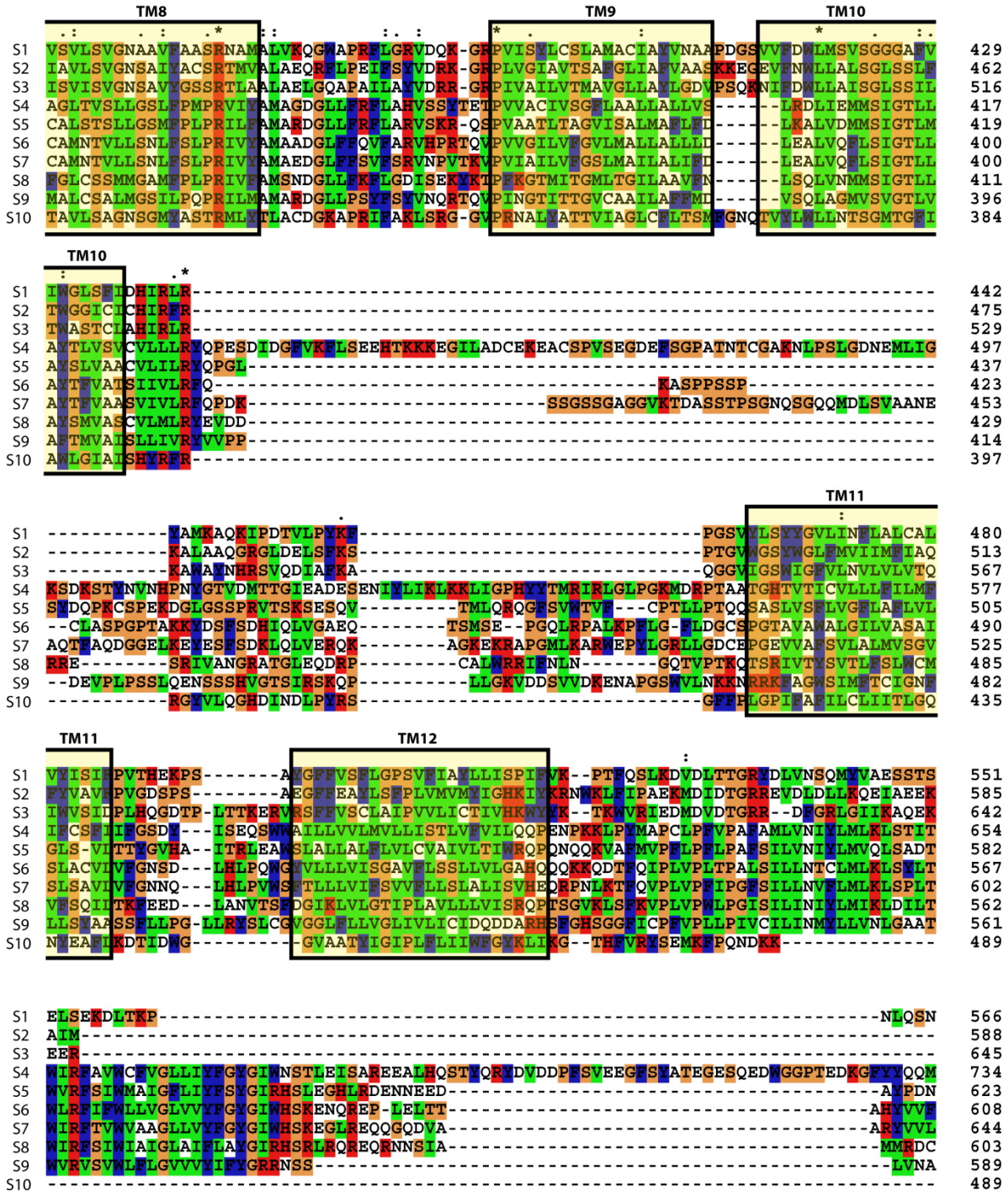
TM8
TM9
TM10
TM10
TM11
TM11
TM12
S1
S2
S3
S4
S5
S6
S7
S8
S9
S10

**Figure 20.** High copy suppressor screen for actin mutant *act1*-j28.

(A) Plasmids containing either the *act1*+ gene (plasmid 2-2) or the potential suppressor gene (plasmid 2-10) suppressed the temperature sensitivity of *act1*-j28 mutant cells in 36°C. wt cells with empty plasmid, *act1*+ plasmid or the suppressor gene plasmid were used as control. All cells were grew on leu- first, then replicated to YES and put in either 24°C or 36°C for 2 days before imaging. (B) Cells with indicated genotype were checked under microscopy. All cells were from YES plate as mentioned in Figure A. Bars, 5 μm. (C) Quantitation of cells from Figure B. Error bars show means ± SD of three independent experiments (N = 200 cells / bar). **P<0.01. (D) Schematic showing the predicted transmembrane regions of Aap1p from TMHMM Server v.2.0. (E) Amino acid sequence alignment of Aap1p with 9 orthologues from other species by ClustalX. Transmembrane regions were indicated above the alignment. Amino acid number of each orthologue was labeled on the right. Number S1-S10 on the left represents fission yeast NP_596769.2, budding yeast NP_012965.3, *Neurospora crassa* XP_960090.1, *Homo sapien*s NP_066000.2, chimpanzee XP_003311666.1, mouse NP_659101.2, zebra fish NP_919408.2, fly NP_649019.2, *Arabidopsis thaliana* NP_198510.2 and *E. coli* AAA60532.1, respectively. " * " indicates identical residues. " : " indicates conserved substitutions. " . " indicates semi-conserved substitutions.

### 4.2.3 Localization of potential *act1*-j28 suppressor Aap1p

A previous study showed Aap1p localized to the ER and cell membrane when overexpressed (Matsuyama et al., 2006). However, it was necessary to check the localization of Aap1p expressed under its endogenous promoter control. By tagging Aap1p with GFP at its C-terminus, we expressed this fusion protein from its native locus. Surprisingly, Aap1p-GFP was found to localize to cell membrane, vesicle-like structures, ring-like structure and septum-like structure (Figure 21 A and B). To check when Aap1p localized to the cell middle, single plane time-lapse spinning disk images were taken as Aap1p-GFP signal did not survive 4D imaging. Results showed that Aap1p-GFP localized to the cell middle early before nuclear division (Figure 21 C, upper panel). Aap1p-GFP localized to a septum-like structure as well (Figure 21 C, lower panel).

As Aap1p localized to the cell middle in early mitosis, we tested whether Aap1p was a node component. Cells coexpressing Aap1p-GFP and Rlc1p-tdTomato showed that Aap1p-GFP did not colocalize with Rlc1p-tdTomato nodes (Figure 21 D, arrow). Furthermore, Aap1p-GFP signal did not completely colocalize with the compact Rlc1p-tdTomato ring in some cells (Figure 21 D, asterisk). In these Rlc1p-tdTomato ring containing cells, instead of forming a compact Aap1p ring, Aap1p-GFP accumulated as a broad band in the cell middle (Figure 21 D, asterisk).

To confirm whether Aap1p ring colocalized with F-actin ring, mitotic cells coexpressing LAmCh and Aap1p-GFP were examined. Imaris 3D reconstruction showed that Aap1p-GFP ring colocalized with LAmCh labeled F-actin ring in some cells (Figure 21 E, left cell). However, in some other cases, Aap1p-GFP ring was absent in cells possessing a LAmCh labeled actin ring (Figure 21 E, right cell). These data indicate that Aap1p may localize to the ring in a later stage.

To further determine the exact time when Aap1p localized to the ring, cells coexpressing the cell cycle marker mCh-Atb2p and Aap1p-GFP were analyzed. This experiment showed unambiguously that Aap1p-GFP only compacted into

a full ring after the mitotic spindle was disassembled (Figure 21 F).

As Aap1p was identified as a potential actin mutant suppressor in this thesis, we then checked whether Aap1p localization depended on F-actin cytoskeleton. Aap1p-GFP cells were treated with 50 μM LatA for 10 min. Results showed that the localization of Aap1p-GFP was unaffected when F-actin cytoskeleton was disrupted (Figure 21 G). Interestingly, the number of Aap1p-GFP vesicle-like structure was lower after LatA treatment (Figure 21 G).

Collectively, we found that Aap1p-GFP localized to the cell medial region in early mitosis, after mitotic spindle disassembly it coalesced into a ring-like structure colocalizing with the actomyosin ring. Aap1p-GFP also localized to a septum-like structure after actomyosin ring constriction.

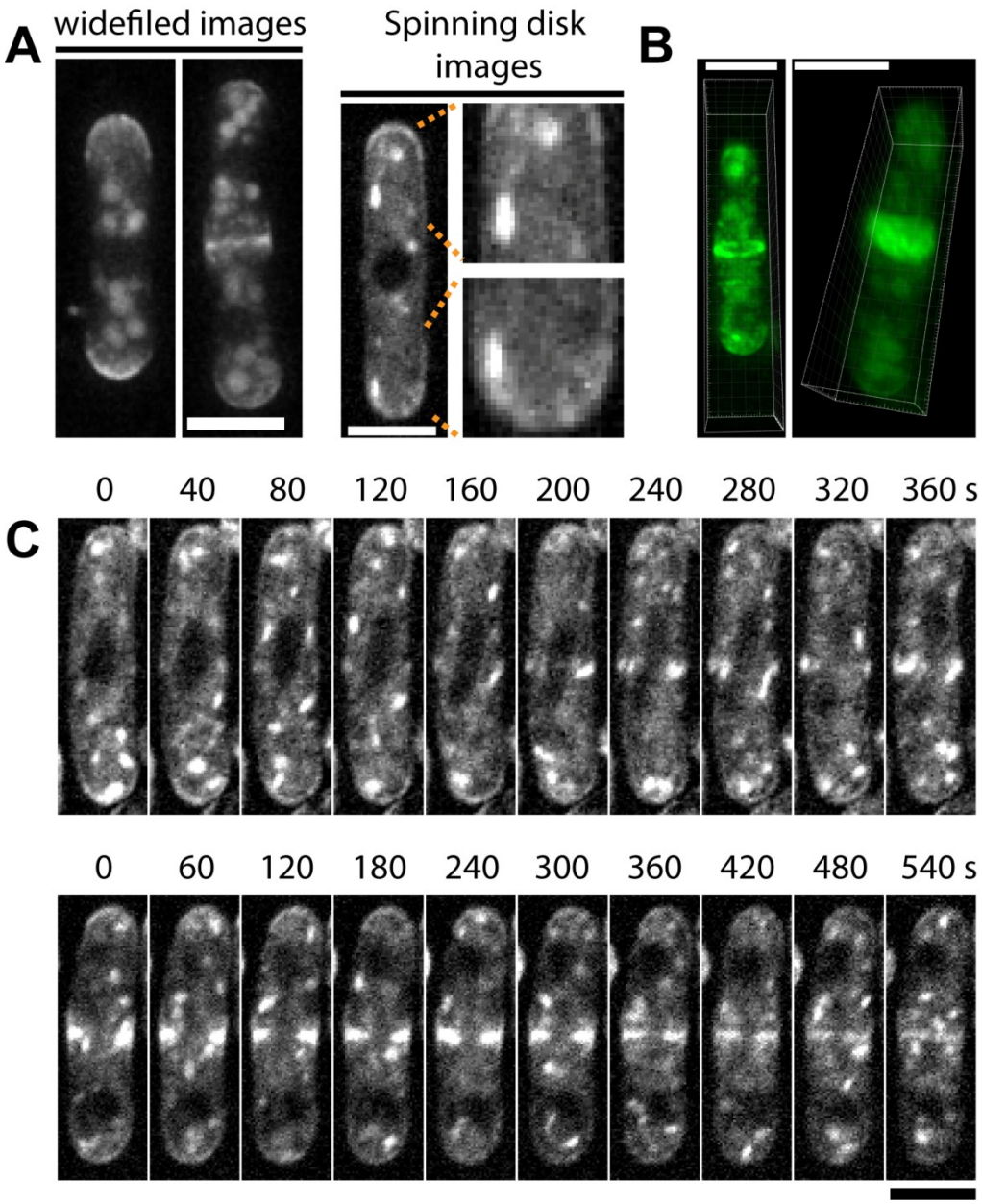
A
widefiled images
Spinning disk images
B
C
0 40 80 120 160 200 240 280 320 360 s
0 60 120 180 240 300 360 420 480 540 s

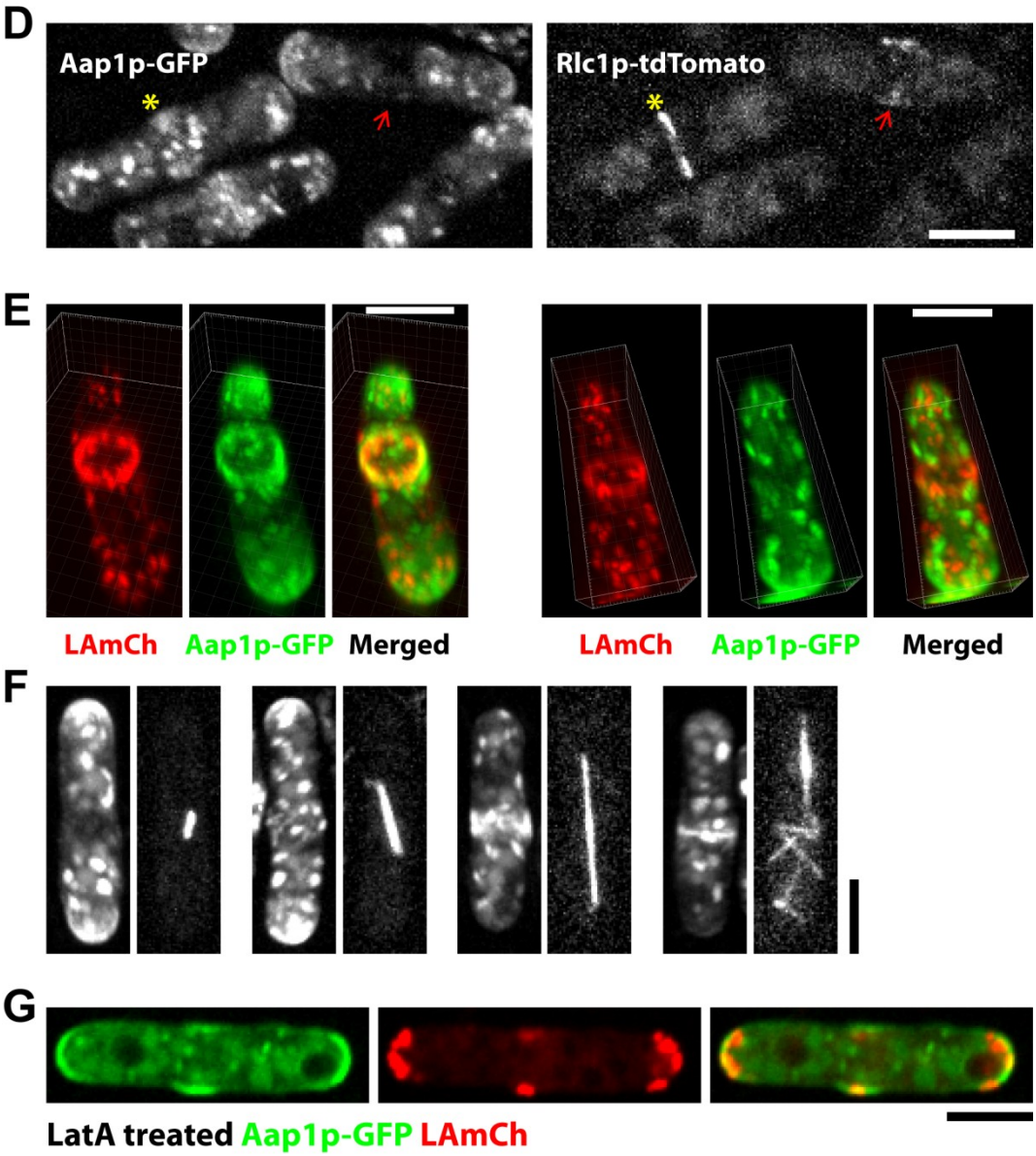


**Figure 21.** Localization of potential *act1*-j28 suppressor Aap1p.

(A) Widefield and spinning disk images of Aap1p-GFP cells. (B) Representative imaris 3D reconstructed images of Aap1p-GFP cells showing a ring-like structure and septum-like structure. (C) Single plane time-lapse images of Aap1p-GFP. (D) Spinning disk images of Aap1p-GFP Rlc1p-tdTomato. Yellow asterisks show the position of an actin ring. Red arrows show the position of nodes. (E) Imaris images of Aap1p-GFP LAmCh cells. (F) Spinning disk maximum-intensity projected images of mitotic Aap1p-GFP mCh-Atb2p cells. (G) 50 μM LatA treated Aap1p-GFP LAmCh cell. Bars, 5 μm.

## 4.3 DISCUSSION

In this chapter, an interesting cytokinetic mutant *act1*-j28 was characterized by DAPI, Aniline Blue and Cdc4p antibody staining under restrictive temperature. We established that *act1*-j28 contained double point mutations (F200S & G308S, regarding to amino acid sequence) within the open reading frame of *act1* gene. Both the mutations were on the surface of the G-actin structure and located in the linker regions between the α-helixes. Further experiments would be important to determine which mutation is more responsible for this mutant phenotype. It would also be interesting to purify this mutant actin protein and perform *in vitro* polymerization assays to determine the polymerization ability.

As *act1*-j28 was a cytokinetic mutant, genetic interactions between *act1*-j28 and other ring mutants was tested (Subramanian et al., 2013). This experiment suggests that *act1*-j28 genetically interacts with *cdc3*-124 but not *cdc15*-140, *rng2*-D5, *rng3*-65, *cdc8*-110, *myo2*-E1, *cdc4*-8 or *cdc12*-112. Learning more about this genetic interaction might help to understand the cause of the mutant phenotype.

During the characterization process, it was found that *act1*-j28 could not be stained by phalloidin under restrictive temperature. However, LAGFP strongly suppressed the mutant phenotype due to unknown reasons hence lifeact was not suitable for studying actin dynamics for *act1*-j28. Future experiments should use other probes such as Utr-CH to monitor actin dynamics in this mutant or use EM to study F-actin cytoskeleton in fixed *act1*-j28 mutant cells.

As potential suppressor genes are easy to be identified (simply blast the sequencing results against the whole fission yeast genome and search for overlapping genes) after recovering the library plasmids from the high copy suppressors, high copy suppressor screens were done for *act1*-j28. Aap1p was identified as a potential suppressor for *act1*-j28. As a predicted antisense RNA (SPBC1652.02) was on the antisense strand of the overlapping region of the suppressor plasmids, a frameshift mutation in the ORF of the *aap1* gene would be necessary to confirm the suppression by Aap1p.

Aap1p is a putative 12 transmembrane protein that localizes to the cell membrane and vesicle-like structures throughout cell cycle. It localizes to the cell medial region early before nucleus division. After anaphase, Aap1p localizes to ring-like structures and septum-like structures. Moreover, Aap1p ring/septum localization does not depend on F-actin, indicating other mechanisms may exist to recruit/maintain this protein to the cell middle during mitosis. In addition, Aap1p localization mimics the cell wall 1,3-beta-glucan synthase Cps1p localization (Cortes et al., 2002; Liu et al., 2002). Taken together, it could be possible that Aap1p is related to the coordination between cell membrane, actomyosin ring and cell wall. Future experiments should address this possibility. Moreover, it would be interesting to check whether plasmid 2-10 (contains *aap1* gene) could suppress other actin mutants.

Overexpression of Aap1p under *nmt1* promoter showed no obvious morphological defects (data not shown) and deletion of *aap1* gene seemed to have no obvious effect on cell morphology as well (Hayles et al., 2013; Kim et al., 2010). As Aap1p is highly conserved across kingdoms and has 10 paralogs in fission yeast, it would be intriguing to delete other paralogs bearing similar localizations in the background of *aap1* deletion.

Aap1p, as mentioned above, is predicted to have 12 transmembrane regions. Both N and C-terminal of Aap1p are predicted to be intracellular. To understand how this Aap1p protein suppresses the actin mutant *act1*-j28, it would be necessary to verify the physical interaction (if any) between actin and Aap1p biochemically. Furthermore, it would be interesting to purify the N and C-terminal of Aap1p from either *E. coli* or fission yeast for pull down assays to identify interaction partners of Aap1p.

Aap1p is predicted to have amino acid transport function, transporting amino acids from one side of the membrane to the other side. Because we identified Aap1p as a potential suppressor for the actin mutant *act1*-j28, it would be beneficial to screen for an *aap1* mutant that only defective in the amino acid transport or cytokinesis.

Finally, as actin mutations are related to diseases (Muller et al., 2012; Mundia et al., 2012; Wong et al., 2001), it should be fruitful to study and further characterize other 38 actin mutants from our previous genetic screen.

# CHAPTER V CONCLUSIONS AND FUTURE DIRECTIONS

This thesis explored the mechanisms of actomyosin ring assembly in fission yeast and characterized a novel fission yeast actin mutant *act1*-j28.

In the first part of this thesis, lifeact was for the first time successfully applied in living fission yeast cells to monitor F-actin dynamics (Riedl et al., 2008). Benefiting from this new technique and in combination with 3D time-lapse imaging, we found that F-actin cables could be assembled in the non-medial regions during mitosis and they migrate and incorporate into the assembling actomyosin ring. This finding disagrees with the existing fission yeast ring assembly models, in which longitudinal F-actin cables were considered dispensable during cytokinesis (Feierbach and Chang, 2001; Kovar et al., 2011; Mishra and Oliferenko, 2008; Vavylonis et al., 2008). However, by checking lifeact labeled F-actin dynamics in various mutants, careful phalloidin staining of the untagged cells and applying different actin monitoring probes in fission yeast, we conclude that non-medial F-actin cable assembly and migration occurs during cytokinesis. Meanwhile, we also provide evidence that non-medial F-actin cable assembly and medial F-actin nucleation co-exist in dividing fission yeast cells.

We also found that F-actin cables, in terms of cell cycle stages and nucleators, could be divided into two categories: interphase F-actin cables and mitotic F-actin cables. Interphase F-actin cables are nucleated by formin-For3p. The majority of mitotic F-actin cables are nucleated by formin-Cdc12p. Unlike previously reported (Feierbach and Chang, 2001), *for3*Δ cells possess mitotic F-actin cables. Mitotic non-medial F-actin cables are nucleated by formin-Cdc12p but not by formin-For3p. Consistent with a recent study (Coffman et al., 2009), Formin-Cdc12p was found to localize in the non-medial region as speckles. These non-medially localized speckles colocalize with non-medial F-actin cables and move rapidly along these cables.

Interestingly, we also noticed that non-medial F-actin cables are not assembled

through the two previously established ring assembly pathways: Mid1p-dependent pathway and Cdc15p-dependent pathway (Hachet and Simanis, 2008; Huang et al., 2008). We conclude that these two pathways may control the formation of the ring precursor spot or nodes.

Another striking finding in this thesis is that Myo51p (type V myosin) and Myo2p (type II myosin) function together during cytokinesis. It is possible that these myosins participate in actomyosin ring assembly through affecting F-actin cable movement/compaction.

The first part of this thesis is of considerable significance as it is the first study to successfully monitor mitotic F-actin dynamics in living fission yeast cells. Our data has provided clear evidence that fission yeast cells are utilizing a similar mechanism to recruit F-actin in the actomyosin ring as mammalian cells (Cao and Wang, 1990a; Cao and Wang, 1990b), demonstrating for the first time that non-medial F-actin cables are involved in actomyosin ring assembly.

However, it is still unknown if the non-medial F-actin cables are necessary for actomyosin ring assembly. It is also unknown how the two myosins (Myo51p and Myo2p) function together during cytokinesis. To address the first question, future studies should attempt to target all formin-Cdc12p to the non-medial region or restrict all of them in the cell middle (Dixon et al., 2012). Future work should also focus on finding a *cdc12* mutant defective in the activation mechanism or analyzing the truncated versions of formin-Cdc12p (Yonetani and Chang, 2010). Lastly, to know more about the detail mechanism how Myo51p and Myo2p work together, further studies need to analyze more carefully about the special relationship between these two myosins during actomyosin ring assembly. Superresolution microscopy may be useful for this purpose (Coltharp and Xiao, 2012; Shao et al., 2011; Willig et al., 2007; Xu et al., 2012; York et al., 2011).

The second part of this thesis shows preliminary data characterizing a novel fission yeast actin mutant *act1*-j28. This mutant shows a typical cytokinetic

mutant phenotype at restrictive temperature and fragmented cell wall near the division site.

High copy suppressor screen identified a single gene (*SPBC1652.02+*) might be the suppressor for this *act1*-j28 mutant. Aap1p is predicted to be a 12 transmembrane protein involved in amino acid transport. Our preliminary data shows that Aap1p-GFP localizes to cell membrane, vesicles, ring-like structure and septum-like structure in fission yeast. Aap1p-GFP does not colocalize with nodes, localizes to the cell middle before nucleus division and then condenses into a ring-like structure after anaphase. The Aap1p ring-like structure colocalizes with lifeact labeled F-actin ring in later mitosis and the localization of Aap1p is not dependent on F-actin.

Taken together, the second part of the thesis characterizes a novel actin mutant *act1*-j28 and identifies Aap1p as a potential suppressor. This finding might be interesting as Aap1p might play a role in late mitosis linking the F-actin ring and cell membrane. However, this second part is still at its early stage, more work is yet to be done. Future work should focus on studying the mechanism of how Aap1p suppress the *act1*-j28 mutant phenotype and whether Aap1p plays a role in cytokinesis.

## REFERENCES


Aizawa, H., M. Sameshima, and I. Yahara. 1997. A green fluorescent protein-actin fusion protein dominantly inhibits cytokinesis, cell spreading, and locomotion in Dictyostelium. *Cell structure and function*. 22:335-345.

Alsop, G.B., W. Chen, M. Foss, K.F. Tseng, and D. Zhang. 2009. Redistribution of actin during assembly and reassembly of the contractile ring in grasshopper spermatocytes. *PloS one*. 4:e4892.

Andersen, E.F., N.S. Asuri, and M.C. Halloran. 2011. In vivo imaging of cell behaviors and F-actin reveals LIM-HD transcription factor regulation of peripheral versus central sensory axon development. *Neural development*. 6:27.

Arabidopsis Genome, I. 2000. Analysis of the genome sequence of the flowering plant Arabidopsis thaliana. *Nature*. 408:796-815.

Arai, R., and I. Mabuchi. 2002. F-actin ring formation and the role of F-actin cables in the fission yeast Schizosaccharomyces pombe. *Journal of cell science*. 115:887-898.

Arai, R., K. Nakano, and I. Mabuchi. 1998. Subcellular localization and possible function of actin, tropomyosin and actin-related protein 3 (Arp3) in the fission yeast Schizosaccharomyces pombe. *European journal of cell biology*. 76:288-295.

Arasada, R., and T.D. Pollard. 2011. Distinct roles for F-BAR proteins Cdc15p and Bzz1p in actin polymerization at sites of endocytosis in fission yeast. *Curr Biol*. 21:1450-1459.

Asakura, T., T. Sasaki, F. Nagano, A. Satoh, H. Obaishi, H. Nishioka, H. Imamura, K. Hotta, K. Tanaka, H. Nakanishi, and Y. Takai. 1998. Isolation and characterization of a novel actin filament-binding protein from Saccharomyces cerevisiae. *Oncogene*. 16:121-130.

Balasubramanian, M.K., E. Bi, and M. Glotzer. 2004. Comparative analysis of cytokinesis in budding yeast, fission yeast and animal cells. *Curr Biol*. 14:R806-818.

Balasubramanian, M.K., D.M. Helfman, and S.M. Hemmingsen. 1992. A new tropomyosin essential for cytokinesis in the fission yeast S. pombe.

*Nature*. 360:84-87.

Balasubramanian, M.K., B.R. Hirani, J.D. Burke, and K.L. Gould. 1994. The Schizosaccharomyces pombe cdc3+ gene encodes a profilin essential for cytokinesis. *The Journal of cell biology*. 125:1289-1301.

Balasubramanian, M.K., R. Srinivasan, Y. Huang, and K.H. Ng. 2012. Comparing contractile apparatus-driven cytokinesis mechanisms across kingdoms. *Cytoskeleton*. 69:942-956.

Ballestrem, C., B. Wehrle-Haller, and B.A. Imhof. 1998. Actin dynamics in living mammalian cells. *Journal of cell science*. 111 ( Pt 12):1649-1658.

Bardin, A.J., and A. Amon. 2001. Men and sin: what's the difference? *Nat Rev Mol Cell Biol*. 2:815-826.

Bathe, M., and F. Chang. 2010. Cytokinesis and the contractile ring in fission yeast: towards a systems-level understanding. *Trends in microbiology*. 18:38-45.

Bennett, M.D. 1977. The time and duration of meiosis. *Philosophical transactions of the Royal Society of London. Series B, Biological sciences*. 277:201-226.

Berepiki, A., A. Lichius, J.Y. Shoji, J. Tilsner, and N.D. Read. 2010. F-actin dynamics in Neurospora crassa. *Eukaryot Cell*. 9:547-557.

Berro, J., V. Sirotkin, and T.D. Pollard. 2010. Mathematical modeling of endocytic actin patch kinetics in fission yeast: disassembly requires release of actin filament fragments. *Mol Biol Cell*. 21:2905-2915.

Bray, D., and J.G. White. 1988. Cortical flow in animal cells. *Science*. 239:883-888.

Bretschneider, T., S. Diez, K. Anderson, J. Heuser, M. Clarke, A. Muller-Taubenberger, J. Kohler, and G. Gerisch. 2004. Dynamic actin patterns and Arp2/3 assembly at the substrate-attached surface of motile cells. *Curr Biol*. 14:1-10.

Burkel, B.M., G. von Dassow, and W.M. Bement. 2007. Versatile fluorescent probes for actin filaments based on the actin-binding domain of utrophin. *Cell Motil Cytoskeleton*. 64:822-832.

Campellone, K.G., and M.D. Welch. 2010. A nucleator arms race: cellular control of actin assembly. *Nat Rev Mol Cell Biol*. 11:237-251.

Cao, L.G., and Y.L. Wang. 1990a. Mechanism of the formation of contractile ring in dividing cultured animal cells. I. Recruitment of preexisting actin filaments into the cleavage furrow. *The Journal of cell biology*. 110:1089-1095.

Cao, L.G., and Y.L. Wang. 1990b. Mechanism of the formation of contractile ring in dividing cultured animal cells. II. Cortical movement of microinjected actin filaments. *The Journal of cell biology*. 111:1905-1911.

Carnahan, R.H., and K.L. Gould. 2003. The PCH family protein, Cdc15p, recruits two F-actin nucleation pathways to coordinate cytokinetic actin ring formation in Schizosaccharomyces pombe. *The Journal of cell biology*. 162:851-862.

Carvalho, P., and D. Pellman. 2004. Mitotic spindle: laser microsurgery in yeast cells. *Curr Biol*. 14:R748-750.

Cerutti, L., and V. Simanis. 1999. Asymmetry of the spindle pole bodies and spg1p GAP segregation during mitosis in fission yeast. *Journal of cell science*. 112 ( Pt 14):2313-2321.

Chang, F. 1999. Movement of a cytokinesis factor cdc12p to the site of cell division. *Curr Biol*. 9:849-852.

Chang, F., D. Drubin, and P. Nurse. 1997. cdc12p, a protein required for cytokinesis in fission yeast, is a component of the cell division ring and interacts with profilin. *The Journal of cell biology*. 137:169-182.

Chen, Q., S. Nag, and T.D. Pollard. 2012. Formins filter modified actin subunits during processive elongation. *Journal of structural biology*. 177:32-39.

Chen, Q., and T.D. Pollard. 2011. Actin filament severing by cofilin is more important for assembly than constriction of the cytokinetic contractile ring. *The Journal of cell biology*. 195:485-498.

Chen, Q., and T.D. Pollard. 2013. Actin filament severing by cofilin dismantles actin patches and produces mother filaments for new patches. *Curr Biol*. 23:1154-1162.

Chen, W., M. Foss, K.F. Tseng, and D. Zhang. 2008. Redundant mechanisms recruit actin into the contractile ring in silkworm spermatocytes. *PLoS Biol*. 6:e209.

Chin, J.W., T.A. Cropp, J.C. Anderson, M. Mukherji, Z. Zhang, and P.G. Schultz. 2003. An expanded eukaryotic genetic code. *Science*. 301:964-967.

Clayton, J.E., M.R. Sammons, B.C. Stark, A.R. Hodges, and M. Lord. 2010. Differential regulation of unconventional fission yeast myosins via the actin track. *Curr Biol*. 20:1423-1431.

Coffman, V.C., A.H. Nile, I.J. Lee, H. Liu, and J.Q. Wu. 2009. Roles of formin nodes and myosin motor activity in Mid1p-dependent contractile-ring assembly during fission yeast cytokinesis. *Mol Biol Cell*. 20:5195-5210.

Coffman, V.C., J.A. Sees, D.R. Kovar, and J.Q. Wu. 2013. The formins Cdc12 and For3 cooperate during contractile ring assembly in cytokinesis. *The Journal of cell biology*. 203:101-114.

Collins, A., A. Warrington, K.A. Taylor, and T. Svitkina. 2011. Structural organization of the actin cytoskeleton at sites of clathrin-mediated endocytosis. *Curr Biol*. 21:1167-1175.

Coltharp, C., and J. Xiao. 2012. Superresolution microscopy for microbiology. *Cellular microbiology*. 14:1808-1818.

Cooper, J.A. 1987. Effects of cytochalasin and phalloidin on actin. *The Journal of cell biology*. 105:1473-1478.

Cortes, J.C., J. Ishiguro, A. Duran, and J.C. Ribas. 2002. Localization of the (1,3)beta-D-glucan synthase catalytic subunit homologue Bgs1p/Cps1p from fission yeast suggests that it is involved in septation, polarized growth, mating, spore wall formation and spore germination. *Journal of cell science*. 115:4081-4096.

Deibler, M., J.P. Spatz, and R. Kemkemer. 2011. Actin fusion proteins alter the dynamics of mechanically induced cytoskeleton rearrangement. *PloS one*. 6:e22941.

Delgado-Alvarez, D.L., O.A. Callejas-Negrete, N. Gomez, M. Freitag, R.W. Roberson, L.G. Smith, and R.R. Mourino-Perez. 2010. Visualization of F-actin localization and dynamics with live cell markers in Neurospora crassa. *Fungal genetics and biology : FG & B*. 47:573-586.

Didelot, X., and M.C. Maiden. 2010. Impact of recombination on bacterial evolution. *Trends in microbiology*. 18:315-322.

Ding, D.Q., Y. Chikashige, T. Haraguchi, and Y. Hiraoka. 1998. Oscillatory nuclear movement in fission yeast meiotic prophase is driven by astral microtubules, as revealed by continuous observation of chromosomes and microtubules in living cells. *Journal of cell science*. 111 ( Pt 6):701-712.

Dixon, A.S., J.E. Constance, T. Tanaka, T.H. Rabbitts, and C.S. Lim. 2012. Changing the subcellular location of the oncoprotein Bcr-Abl using rationally designed capture motifs. *Pharmaceutical research*. 29:1098-1109.

dos Remedios, C.G., D. Chhabra, M. Kekic, I.V. Dedova, M. Tsubakihara, D.A. Berry, and N.J. Nosworthy. 2003. Actin binding proteins: regulation of cytoskeletal microfilaments. *Physiological reviews*. 83:433-473.

Doyle, A., R. Martin-Garcia, A.T. Coulton, S. Bagley, and D.P. Mulvihill. 2009. Fission yeast Myo51 is a meiotic spindle pole body component with discrete roles during cell fusion and spore formation. *Journal of cell science*. 122:4330-4340.

Doyle, T., and D. Botstein. 1996. Movement of yeast cortical actin cytoskeleton visualized in vivo. *Proceedings of the National Academy of Sciences of the United States of America*. 93:3886-3891.

Duraiswami, S. 1953. Studies on the cytology of yeasts. VIII. Karyokinesis and cytokinesis in a diploid brewery yeast. *La Cellule*. 55:379-395.

East, D.A., and D.P. Mulvihill. 2011. Regulation and function of the fission yeast myosins. *Journal of cell science*. 124:1383-1390.

Edwards, K.A., M. Demsky, R.A. Montague, N. Weymouth, and D.P. Kiehart. 1997. GFP-moesin illuminates actin cytoskeleton dynamics in living tissue and demonstrates cell shape changes during morphogenesis in Drosophila. *Developmental biology*. 191:103-117.

Edwards, K.A., R.A. Montague, S. Shepard, B.A. Edgar, R.L. Erikson, and D.P. Kiehart. 1994. Identification of Drosophila cytoskeletal proteins by induction of abnormal cell shape in fission yeast. *Proceedings of the National Academy of Sciences of the United States of America*. 91:4589-4593.

Fankhauser, C., A. Reymond, L. Cerutti, S. Utzig, K. Hofmann, and V.

Simanis. 1995. The S. pombe cdc15 gene is a key element in the reorganization of F-actin at mitosis. *Cell*. 82:435-444.

Feierbach, B., and F. Chang. 2001. Roles of the fission yeast formin for3p in cell polarity, actin cable formation and symmetric cell division. *Curr Biol*. 11:1656-1665.

Feierbach, B., F. Verde, and F. Chang. 2004. Regulation of a formin complex by the microtubule plus end protein tea1p. *The Journal of cell biology*. 165:697-707.

Feng, Z., W. Ning Chen, P. Vee Sin Lee, K. Liao, and V. Chan. 2005. The influence of GFP-actin expression on the adhesion dynamics of HepG2 cells on a model extracellular matrix. *Biomaterials*. 26:5348-5358.

Ferguson, S.M., A. Raimondi, S. Paradise, H. Shen, K. Mesaki, A. Ferguson, O. Destaing, G. Ko, J. Takasaki, O. Cremona, O.T. E, and P. De Camilli. 2009. Coordinated actions of actin and BAR proteins upstream of dynamin at endocytic clathrin-coated pits. *Developmental cell*. 17:811-822.

Forsburg, S.L. 2001. The art and design of genetic screens: yeast. *Nature reviews. Genetics*. 2:659-668.

Fujiwara, T., M. Bandi, M. Nitta, E.V. Ivanova, R.T. Bronson, and D. Pellman. 2005. Cytokinesis failure generating tetraploids promotes tumorigenesis in p53-null cells. *Nature*. 437:1043-1047.

Furge, K.A., Q.C. Cheng, M. Jwa, S. Shin, K. Song, and C.F. Albright. 1999. Regions of Byr4, a regulator of septation in fission yeast, that bind Spg1 or Cdc16 and form a two-component GTPase-activating protein with Cdc16. *The Journal of biological chemistry*. 274:11339-11343.

Furge, K.A., K. Wong, J. Armstrong, M. Balasubramanian, and C.F. Albright. 1998. Byr4 and Cdc16 form a two-component GTPase-activating protein for the Spg1 GTPase that controls septation in fission yeast. *Curr Biol*. 8:947-954.

Garcia-Cortes, J.C., and D. McCollum. 2009. Proper timing of cytokinesis is regulated by Schizosaccharomyces pombe Etd1. *The Journal of cell biology*. 186:739-753.

Golden, A. 2000. Cytoplasmic flow and the establishment of polarity in C. elegans 1-cell embryos. *Current opinion in genetics & development*.

10:414-420.

Gomez-Lopez, S., R.G. Lerner, and C. Petritsch. 2013. Asymmetric cell division of stem and progenitor cells during homeostasis and cancer. *Cellular and molecular life sciences : CMLS*.

Green, R.A., E. Paluch, and K. Oegema. 2012. Cytokinesis in animal cells. *Annual review of cell and developmental biology*. 28:29-58.

Guertin, D.A., L. Chang, F. Irshad, K.L. Gould, and D. McCollum. 2000. The role of the sid1p kinase and cdc14p in regulating the onset of cytokinesis in fission yeast. *The EMBO journal*. 19:1803-1815.

Guha, M., M. Zhou, and Y.L. Wang. 2005. Cortical actin turnover during cytokinesis requires myosin II. *Curr Biol*. 15:732-736.

Guizetti, J., L. Schermelleh, J. Mantler, S. Maar, I. Poser, H. Leonhardt, T. Muller-Reichert, and D.W. Gerlich. 2011. Cortical constriction during abscission involves helices of ESCRT-III-dependent filaments. *Science*. 331:1616-1620.

Hachet, O., and V. Simanis. 2008. Mid1p/anillin and the septation initiation network orchestrate contractile ring assembly for cytokinesis. *Genes Dev*. 22:3205-3216.

Hansen, W.J., N.J. Cowan, and W.J. Welch. 1999. Prefoldin-nascent chain complexes in the folding of cytoskeletal proteins. *The Journal of cell biology*. 145:265-277.

Hayles, J., V. Wood, L. Jeffery, K.L. Hoe, D.U. Kim, H.O. Park, S. Salas-Pino, C. Heichinger, and P. Nurse. 2013. A genome-wide resource of cell cycle and cell shape genes of fission yeast. *Open biology*. 3:130053.

Heese, M., U. Mayer, and G. Jurgens. 1998. Cytokinesis in flowering plants: cellular process and developmental integration. *Current opinion in plant biology*. 1:486-491.

Higgs, H.N., and K.J. Peterson. 2005. Phylogenetic analysis of the formin homology 2 domain. *Mol Biol Cell*. 16:1-13.

Hoffmann, C., G. Gaietta, A. Zurn, S.R. Adams, S. Terrillon, M.H. Ellisman, R.Y. Tsien, and M.J. Lohse. 2010. Fluorescent labeling of tetracysteine-tagged proteins in intact cells. *Nature protocols*. 5:1666-1677.

Hou, M.C., D.A. Guertin, and D. McCollum. 2004. Initiation of cytokinesis is

controlled through multiple modes of regulation of the Sid2p-Mob1p kinase complex. *Molecular and cellular biology*. 24:3262-3276.

Hu, C.K., M. Coughlin, and T.J. Mitchison. 2012. Midbody assembly and its regulation during cytokinesis. *Mol Biol Cell*. 23:1024-1034.

Huang, Y., H. Yan, and M.K. Balasubramanian. 2008. Assembly of normal actomyosin rings in the absence of Mid1p and cortical nodes in fission yeast. *The Journal of cell biology*. 183:979-988.

Iwano, M., H. Shiba, K. Matoba, T. Miwa, M. Funato, T. Entani, P. Nakayama, H. Shimosato, A. Takaoka, A. Isogai, and S. Takayama. 2007. Actin dynamics in papilla cells of Brassica rapa during self- and cross-pollination. *Plant physiology*. 144:72-81.

Jauniaux, J.C., and M. Grenson. 1990. GAP1, the general amino acid permease gene of Saccharomyces cerevisiae. Nucleotide sequence, protein similarity with the other bakers yeast amino acid permeases, and nitrogen catabolite repression. *European journal of biochemistry / FEBS*. 190:39-44.

Johnson, A.E., D. McCollum, and K.L. Gould. 2012. Polar opposites: Fine-tuning cytokinesis through SIN asymmetry. *Cytoskeleton*. 69:686-699.

Johnson, H.W., and M.J. Schell. 2009. Neuronal IP3 3-kinase is an F-actin-bundling protein: role in dendritic targeting and regulation of spine morphology. *Mol Biol Cell*. 20:5166-5180.

Jordan, S.N., and J.C. Canman. 2012. Rho GTPases in animal cell cytokinesis: an occupation by the one percent. *Cytoskeleton*. 69:919-930.

Jourdain, I., E.A. Brzezinska, and T. Toda. 2013. Fission yeast Nod1 is a component of cortical nodes involved in cell size control and division site placement. *PloS one*. 8:e54142.

Jourdain, I., H.C. Dooley, and T. Toda. 2012. Fission yeast sec3 bridges the exocyst complex to the actin cytoskeleton. *Traffic*. 13:1481-1495.

Jurgens, G. 2005. Plant cytokinesis: fission by fusion. *Trends in cell biology*. 15:277-283.

Kaksonen, M., Y. Sun, and D.G. Drubin. 2003. A pathway for association of receptors, adaptors, and actin during endocytic internalization. *Cell*. 115:475-487.

Kaksonen, M., C.P. Toret, and D.G. Drubin. 2006. Harnessing actin dynamics for clathrin-mediated endocytosis. *Nat Rev Mol Cell Biol*. 7:404-414.

Kamasaki, T., R. Arai, M. Osumi, and I. Mabuchi. 2005. Directionality of F-actin cables changes during the fission yeast cell cycle. *Nature cell biology*. 7:916-917.

Kamasaki, T., M. Osumi, and I. Mabuchi. 2007. Three-dimensional arrangement of F-actin in the contractile ring of fission yeast. *The Journal of cell biology*. 178:765-771.

Kanbe, T., T. Akashi, and K. Tanaka. 1994. Changes in the Distribution of F-Actin in the Fission Yeast Schizosaccharomyces-Pombe by Arresting Growth in Distilled Water - Correlative Studies with Fluorescence and Electron-Microscopy. *J Electron Microsc*. 43:20-24.

Karagiannis, J., A. Bimbo, S. Rajagopalan, J. Liu, and M.K. Balasubramanian. 2005. The nuclear kinase Lsk1p positively regulates the septation initiation network and promotes the successful completion of cytokinesis in response to perturbation of the actomyosin ring in Schizosaccharomyces pombe. *Mol Biol Cell*. 16:358-371.

Kim, D.U., J. Hayles, D. Kim, V. Wood, H.O. Park, M. Won, H.S. Yoo, T. Duhig, M. Nam, G. Palmer, S. Han, L. Jeffery, S.T. Baek, H. Lee, Y.S. Shim, M. Lee, L. Kim, K.S. Heo, E.J. Noh, A.R. Lee, Y.J. Jang, K.S. Chung, S.J. Choi, J.Y. Park, Y. Park, H.M. Kim, S.K. Park, H.J. Park, E.J. Kang, H.B. Kim, H.S. Kang, H.M. Park, K. Kim, K. Song, K.B. Song, P. Nurse, and K.L. Hoe. 2010. Analysis of a genome-wide set of gene deletions in the fission yeast Schizosaccharomyces pombe. *Nature biotechnology*. 28:617-623.

Kitayama, C., A. Sugimoto, and M. Yamamoto. 1997. Type II myosin heavy chain encoded by the myo2 gene composes the contractile ring during cytokinesis in Schizosaccharomyces pombe. *The Journal of cell biology*. 137:1309-1319.

Kost, B., P. Spielhofer, and N.H. Chua. 1998. A GFP-mouse talin fusion protein labels plant actin filaments in vivo and visualizes the actin cytoskeleton in growing pollen tubes. *The Plant journal : for cell and molecular biology*. 16:393-401.

Kovar, D.R., E.S. Harris, R. Mahaffy, H.N. Higgs, and T.D. Pollard. 2006.

Control of the assembly of ATP- and ADP-actin by formins and profilin. *Cell*. 124:423-435.

Kovar, D.R., J.R. Kuhn, A.L. Tichy, and T.D. Pollard. 2003. The fission yeast cytokinesis formin Cdc12p is a barbed end actin filament capping protein gated by profilin. *The Journal of cell biology*. 161:875-887.

Kovar, D.R., V. Sirotkin, and M. Lord. 2011. Three's company: the fission yeast actin cytoskeleton. *Trends in cell biology*. 21:177-187.

Kovar, D.R., J.Q. Wu, and T.D. Pollard. 2005. Profilin-mediated competition between capping protein and formin Cdc12p during cytokinesis in fission yeast. *Mol Biol Cell*. 16:2313-2324.

Krapp, A., S. Schmidt, E. Cano, and V. Simanis. 2001. S. pombe cdc11p, together with sid4p, provides an anchor for septation initiation network proteins on the spindle pole body. *Curr Biol*. 11:1559-1568.

Kwok, E.Y., and M.R. Hanson. 2004. In vivo analysis of interactions between GFP-labeled microfilaments and plastid stromules. *BMC plant biology*. 4:2.

Laporte, D., V.C. Coffman, I.J. Lee, and J.Q. Wu. 2011. Assembly and architecture of precursor nodes during fission yeast cytokinesis. *The Journal of cell biology*. 192:1005-1021.

Laporte, D., N. Ojkic, D. Vavylonis, and J.Q. Wu. 2012. alpha-Actinin and fimbrin cooperate with myosin II to organize actomyosin bundles during contractile-ring assembly. *Mol Biol Cell*. 23:3094-3110.

Lee, I.J., V.C. Coffman, and J.Q. Wu. 2012. Contractile-ring assembly in fission yeast cytokinesis: Recent advances and new perspectives. *Cytoskeleton*. 69:751-763.

Li, R. 2013. The art of choreographing asymmetric cell division. *Developmental cell*. 25:439-450.

Li, Z., M.J. Trimble, Y.V. Brun, and G.J. Jensen. 2007. The structure of FtsZ filaments in vivo suggests a force-generating role in cell division. *The EMBO journal*. 26:4694-4708.

Liu, J., X. Tang, H. Wang, S. Oliferenko, and M.K. Balasubramanian. 2002. The localization of the integral membrane protein Cps1p to the cell division site is dependent on the actomyosin ring and the septation-inducing network in Schizosaccharomyces pombe. *Mol Biol*

*Cell*. 13:989-1000.

Lo Presti, L., F. Chang, and S.G. Martin. 2012. Myosin Vs organize actin cables in fission yeast. *Mol Biol Cell*. 23:4579-4591.

Lord, M., E. Laves, and T.D. Pollard. 2005. Cytokinesis depends on the motor domains of myosin-II in fission yeast but not in budding yeast. *Mol Biol Cell*. 16:5346-5355.

Lord, M., and T.D. Pollard. 2004. UCS protein Rng3p activates actin filament gliding by fission yeast myosin-II. *The Journal of cell biology*. 167:315-325.

Ma, X., M. Kovacs, M.A. Conti, A. Wang, Y. Zhang, J.R. Sellers, and R.S. Adelstein. 2012. Nonmuscle myosin II exerts tension but does not translocate actin in vertebrate cytokinesis. *Proceedings of the National Academy of Sciences of the United States of America*. 109:4509-4514.

Mabuchi, I., S. Tsukita, S. Tsukita, and T. Sawai. 1988. Cleavage furrow isolated from newt eggs: contraction, organization of the actin filaments, and protein components of the furrow. *Proceedings of the National Academy of Sciences of the United States of America*. 85:5966-5970.

Magidson, V., F. Chang, and A. Khodjakov. 2006. Regulation of cytokinesis by spindle-pole bodies. *Nature cell biology*. 8:891-893.

Marks, J., I.M. Hagan, and J.S. Hyams. 1986. Growth polarity and cytokinesis in fission yeast: the role of the cytoskeleton. *Journal of cell science. Supplement*. 5:229-241.

Martell, J.D., T.J. Deerinck, Y. Sancak, T.L. Poulos, V.K. Mootha, G.E. Sosinsky, M.H. Ellisman, and A.Y. Ting. 2012. Engineered ascorbate peroxidase as a genetically encoded reporter for electron microscopy. *Nature biotechnology*. 30:1143-1148.

Martin, B.R., B.N. Giepmans, S.R. Adams, and R.Y. Tsien. 2005a. Mammalian cell-based optimization of the biarsenical-binding tetracysteine motif for improved fluorescence and affinity. *Nature biotechnology*. 23:1308-1314.

Martin, S.G., and F. Chang. 2006. Dynamics of the formin for3p in actin cable assembly. *Curr Biol*. 16:1161-1170.

Martin, S.G., W.H. McDonald, J.R. Yates, 3rd, and F. Chang. 2005b. Tea4p

links microtubule plus ends with the formin for3p in the establishment of cell polarity. *Developmental cell*. 8:479-491.

Martin, S.G., S.A. Rincon, R. Basu, P. Perez, and F. Chang. 2007. Regulation of the formin for3p by cdc42p and bud6p. *Mol Biol Cell*. 18:4155-4167.

Matsuyama, A., R. Arai, Y. Yashiroda, A. Shirai, A. Kamata, S. Sekido, Y. Kobayashi, A. Hashimoto, M. Hamamoto, Y. Hiraoka, S. Horinouchi, and M. Yoshida. 2006. ORFeome cloning and global analysis of protein localization in the fission yeast Schizosaccharomyces pombe. *Nature biotechnology*. 24:841-847.

May, K.M., F.Z. Watts, N. Jones, and J.S. Hyams. 1997. Type II myosin involved in cytokinesis in the fission yeast, Schizosaccharomyces pombe. *Cell Motil Cytoskeleton*. 38:385-396.

McCollum, D., M.K. Balasubramanian, L.E. Pelcher, S.M. Hemmingsen, and K.L. Gould. 1995. Schizosaccharomyces pombe cdc4+ gene encodes a novel EF-hand protein essential for cytokinesis. *The Journal of cell biology*. 130:651-660.

McCollum, D., and K.L. Gould. 2001. Timing is everything: regulation of mitotic exit and cytokinesis by the MEN and SIN. *Trends in cell biology*. 11:89-95.

Mendes Pinto, I., B. Rubinstein, A. Kucharavy, J.R. Unruh, and R. Li. 2012. Actin depolymerization drives actomyosin ring contraction during budding yeast cytokinesis. *Developmental cell*. 22:1247-1260.

Mendes Pinto, I., B. Rubinstein, and R. Li. 2013. Force to divide: structural and mechanical requirements for actomyosin ring contraction. *Biophysical journal*. 105:547-554.

Miller, M.P., A. Amon, and E. Unal. 2013. Meiosis I: when chromosomes undergo extreme makeover. *Current opinion in cell biology*.

Minet, M., P. Nurse, P. Thuriaux, and J.M. Mitchison. 1979. Uncontrolled septation in a cell division cycle mutant of the fission yeast Schizosaccharomyces pombe. *Journal of bacteriology*. 137:440-446.

Mingorance, J., G. Rivas, M. Velez, P. Gomez-Puertas, and M. Vicente. 2010. Strong FtsZ is with the force: mechanisms to constrict bacteria. *Trends in microbiology*. 18:348-356.

Mishra, M., M. D'Souza V, K.C. Chang, Y. Huang, and M.K. Balasubramanian. 2005. Hsp90 protein in fission yeast Swo1p and UCS protein Rng3p facilitate myosin II assembly and function. *Eukaryot Cell*. 4:567-576.

Mishra, M., J. Kashiwazaki, T. Takagi, R. Srinivasan, Y. Huang, M.K. Balasubramanian, and I. Mabuchi. 2013. In vitro contraction of cytokinetic ring depends on myosin II but not on actin dynamics. *Nature cell biology*. 15:853-859.

Mishra, M., and S. Oliferenko. 2008. Cytokinesis: catch and drag. *Curr Biol*. 18:R247-250.

Moreno, S., A. Klar, and P. Nurse. 1991. Molecular genetic analysis of fission yeast Schizosaccharomyces pombe. *Methods Enzymol*. 194:795-823.

Morrell, J.L., G.C. Tomlin, S. Rajagopalan, S. Venkatram, A.S. Feoktistova, J.J. Tasto, S. Mehta, J.L. Jennings, A. Link, M.K. Balasubramanian, and K.L. Gould. 2004. Sid4p-Cdc11p assembles the septation initiation network and its regulators at the S. pombe SPB. *Curr Biol*. 14:579-584.

Moseley, J.B., and B.L. Goode. 2006. The yeast actin cytoskeleton: from cellular function to biochemical mechanism. *Microbiology and molecular biology reviews : MMBR*. 70:605-645.

Moseley, J.B., A. Mayeux, A. Paoletti, and P. Nurse. 2009. A spatial gradient coordinates cell size and mitotic entry in fission yeast. *Nature*. 459:857-860.

Motegi, F., R. Arai, and I. Mabuchi. 2001. Identification of two type V myosins in fission yeast, one of which functions in polarized cell growth and moves rapidly in the cell. *Mol Biol Cell*. 12:1367-1380.

Motegi, F., M. Mishra, M.K. Balasubramanian, and I. Mabuchi. 2004. Myosin-II reorganization during mitosis is controlled temporally by its dephosphorylation and spatially by Mid1 in fission yeast. *The Journal of cell biology*. 165:685-695.

Motegi, F., K. Nakano, and I. Mabuchi. 2000. Molecular mechanism of myosin-II assembly at the division site in Schizosaccharomyces pombe. *Journal of cell science*. 113 ( Pt 10):1813-1825.

Muller, M., A.J. Mazur, E. Behrmann, R.P. Diensthuber, M.B. Radke, Z. Qu, C. Littwitz, S. Raunser, C.A. Schoenenberger, D.J. Manstein, and H.G.

Mannherz. 2012. Functional characterization of the human alpha-cardiac actin mutations Y166C and M305L involved in hypertrophic cardiomyopathy. *Cellular and molecular life sciences : CMLS*. 69:3457-3479.

Mullins, J.M., and J.R. McIntosh. 1982. Isolation and initial characterization of the mammalian midbody. *The Journal of cell biology*. 94:654-661.

Mulvihill, D.P., C. Barretto, and J.S. Hyams. 2001. Localization of fission yeast type II myosin, Myo2, to the cytokinetic actin ring is regulated by phosphorylation of a C-terminal coiled-coil domain and requires a functional septation initiation network. *Mol Biol Cell*. 12:4044-4053.

Mundia, M.M., R.W. Demers, M.L. Chow, A.A. Perieteanu, and J.F. Dawson. 2012. Subdomain location of mutations in cardiac actin correlate with type of functional change. *PloS one*. 7:e36821.

Nakamura, T., M. Nakamura-Kubo, A. Hirata, and C. Shimoda. 2001. The Schizosaccharomyces pombe spo3+ gene is required for assembly of the forespore membrane and genetically interacts with psy1(+)-encoding syntaxin-like protein. *Mol Biol Cell*. 12:3955-3972.

Nakano, K., J. Imai, R. Arai, E.A. Toh, Y. Matsui, and I. Mabuchi. 2002. The small GTPase Rho3 and the diaphanous/formin For3 function in polarized cell growth in fission yeast. *Journal of cell science*. 115:4629-4639.

Nakano, K., and I. Mabuchi. 2006a. Actin-capping protein is involved in controlling organization of actin cytoskeleton together with ADF/cofilin, profilin and F-actin crosslinking proteins in fission yeast. *Genes to cells : devoted to molecular & cellular mechanisms*. 11:893-905.

Nakano, K., and I. Mabuchi. 2006b. Actin-depolymerizing protein Adf1 is required for formation and maintenance of the contractile ring during cytokinesis in fission yeast. *Mol Biol Cell*. 17:1933-1945.

Nakano, K., K. Satoh, A. Morimatsu, M. Ohnuma, and I. Mabuchi. 2001. Interactions among a fimbrin, a capping protein, and an actin-depolymerizing factor in organization of the fission yeast actin cytoskeleton. *Mol Biol Cell*. 12:3515-3526.

Naqvi, N.I., K. Eng, K.L. Gould, and M.K. Balasubramanian. 1999. Evidence

for F-actin-dependent and -independent mechanisms involved in assembly and stability of the medial actomyosin ring in fission yeast. *The EMBO journal*. 18:854-862.

Noegel, A.A., S. Rapp, F. Lottspeich, M. Schleicher, and M. Stewart. 1989. The Dictyostelium gelation factor shares a putative actin binding site with alpha-actinins and dystrophin and also has a rod domain containing six 100-residue motifs that appear to have a cross-beta conformation. *The Journal of cell biology*. 109:607-618.

Noguchi, T., and I. Mabuchi. 2001. Reorganization of actin cytoskeleton at the growing end of the cleavage furrow of Xenopus egg during cytokinesis. *Journal of cell science*. 114:401-412.

Normand, G., and R.W. King. 2010. Understanding cytokinesis failure. *Advances in experimental medicine and biology*. 676:27-55.

Nurse, P. 2002. Cyclin dependent kinases and cell cycle control (nobel lecture). *Chembiochem : a European journal of chemical biology*. 3:596-603.

Okada, K., H. Ravi, E.M. Smith, and B.L. Goode. 2006. Aip1 and cofilin promote rapid turnover of yeast actin patches and cables: a coordinated mechanism for severing and capping filaments. *Mol Biol Cell*. 17:2855-2868.

Osawa, M., D.E. Anderson, and H.P. Erickson. 2008. Reconstitution of contractile FtsZ rings in liposomes. *Science*. 320:792-794.

Padmanabhan, A., K. Bakka, M. Sevugan, N.I. Naqvi, V. D'Souza, X. Tang, M. Mishra, and M.K. Balasubramanian. 2011. IQGAP-related Rng2p organizes cortical nodes and ensures position of cell division in fission yeast. *Curr Biol*. 21:467-472.

Pang, K.M., E. Lee, and D.A. Knecht. 1998. Use of a fusion protein between GFP and an actin-binding domain to visualize transient filamentous-actin structures. *Curr Biol*. 8:405-408.

Paoletti, A., and F. Chang. 2000. Analysis of mid1p, a protein required for placement of the cell division site, reveals a link between the nucleus and the cell surface in fission yeast. *Mol Biol Cell*. 11:2757-2773.

Patkar, R.N., Y.K. Xue, G. Shui, M.R. Wenk, and N.I. Naqvi. 2012. Abc3-mediated efflux of an endogenous digoxin-like steroidal glycoside by Magnaporthe oryzae is necessary for host invasion during

blast disease. *PLoS pathogens*. 8:e1002888.

Peckova, H., and J. Lom. 1990. Growth, morphology and division of flagellates of the genus Trypanoplasma (Protozoa, Kinetoplastida) in vitro. *Parasitology research*. 76:553-558.

Pelham, R.J., Jr., and F. Chang. 2001. Role of actin polymerization and actin cables in actin-patch movement in Schizosaccharomyces pombe. *Nature cell biology*. 3:235-244.

Petersen, J., O. Nielsen, R. Egel, and I.M. Hagan. 1998. FH3, a domain found in formins, targets the fission yeast formin Fus1 to the projection tip during conjugation. *The Journal of cell biology*. 141:1217-1228.

Pichoff, S., and J. Lutkenhaus. 2002. Unique and overlapping roles for ZipA and FtsA in septal ring assembly in Escherichia coli. *The EMBO journal*. 21:685-693.

Pichoff, S., and J. Lutkenhaus. 2005. Tethering the Z ring to the membrane through a conserved membrane targeting sequence in FtsA. *Molecular microbiology*. 55:1722-1734.

Pollard, T.D. 2008. Progress towards understanding the mechanism of cytokinesis in fission yeast. *Biochemical Society transactions*. 36:425-430.

Pollard, T.D., and J.Q. Wu. 2010. Understanding cytokinesis: lessons from fission yeast. *Nat Rev Mol Cell Biol*. 11:149-155.

Prendergast, F.G., and K.G. Mann. 1978. Chemical and physical properties of aequorin and the green fluorescent protein isolated from Aequorea forskalea. *Biochemistry*. 17:3448-3453.

Quintero, O.A., M.M. DiVito, R.C. Adikes, M.B. Kortan, L.B. Case, A.J. Lier, N.S. Panaretos, S.Q. Slater, M. Rengarajan, M. Feliu, and R.E. Cheney. 2009. Human Myo19 is a novel myosin that associates with mitochondria. *Curr Biol*. 19:2008-2013.

Ray, S., K. Kume, S. Gupta, W. Ge, M. Balasubramanian, D. Hirata, and D. McCollum. 2010. The mitosis-to-interphase transition is coordinated by cross talk between the SIN and MOR pathways in Schizosaccharomyces pombe. *The Journal of cell biology*. 190:793-805.

Riedl, J., A.H. Crevenna, K. Kessenbrock, J.H. Yu, D. Neukirchen, M. Bista, F.

Bradke, D. Jenne, T.A. Holak, Z. Werb, M. Sixt, and R. Wedlich-Soldner. 2008. Lifeact: a versatile marker to visualize F-actin. *Nat Methods*. 5:605-607.

Riedl, J., K.C. Flynn, A. Raducanu, F. Gartner, G. Beck, M. Bosl, F. Bradke, S. Massberg, A. Aszodi, M. Sixt, and R. Wedlich-Soldner. Lifeact mice for studying F-actin dynamics. *Nat Methods*. 7:168-169.

Riedl, J., K.C. Flynn, A. Raducanu, F. Gartner, G. Beck, M. Bosl, F. Bradke, S. Massberg, A. Aszodi, M. Sixt, and R. Wedlich-Soldner. 2010. Lifeact mice for studying F-actin dynamics. *Nat Methods*. 7:168-169.

Rincon, S.A., Y. Ye, M.A. Villar-Tajadura, B. Santos, S.G. Martin, and P. Perez. 2009. Pob1 participates in the Cdc42 regulation of fission yeast actin cytoskeleton. *Mol Biol Cell*. 20:4390-4399.

Roberts-Galbraith, R.H., and K.L. Gould. 2008. Stepping into the ring: the SIN takes on contractile ring assembly. *Genes Dev*. 22:3082-3088.

Roberts-Galbraith, R.H., M.D. Ohi, B.A. Ballif, J.S. Chen, I. McLeod, W.H. McDonald, S.P. Gygi, J.R. Yates, 3rd, and K.L. Gould. 2010. Dephosphorylation of F-BAR protein Cdc15 modulates its conformation and stimulates its scaffolding activity at the cell division site. *Molecular cell*. 39:86-99.

Rosenberg, J.A., G.C. Tomlin, W.H. McDonald, B.E. Snydsman, E.G. Muller, J.R. Yates, 3rd, and K.L. Gould. 2006. Ppc89 links multiple proteins, including the septation initiation network, to the core of the fission yeast spindle-pole body. *Mol Biol Cell*. 17:3793-3805.

Russell, P., and P. Nurse. 1986. cdc25+ functions as an inducer in the mitotic control of fission yeast. *Cell*. 45:145-153.

Saha, S., and T.D. Pollard. 2012. Anillin-related protein Mid1p coordinates the assembly of the cytokinetic contractile ring in fission yeast. *Mol Biol Cell*. 23:3982-3992.

Schell, M.J., C. Erneux, and R.F. Irvine. 2001. Inositol 1,4,5-trisphosphate 3-kinase A associates with F-actin and dendritic spines via its N terminus. *The Journal of biological chemistry*. 276:37537-37546.

Schmidt, M., B. Bowers, A. Varma, D.H. Roh, and E. Cabib. 2002. In budding yeast, contraction of the actomyosin ring and formation of the primary septum at cytokinesis depend on each other. *Journal of cell science*.

115:293-302.

Schmidt, S., M. Sohrmann, K. Hofmann, A. Woollard, and V. Simanis. 1997. The Spg1p GTPase is an essential, dosage-dependent inducer of septum formation in Schizosaccharomyces pombe. *Genes Dev*. 11:1519-1534.

Scott, B.J., E.M. Neidt, and D.R. Kovar. 2011. The functionally distinct fission yeast formins have specific actin-assembly properties. *Mol Biol Cell*. 22:3826-3839.

Sedzinski, J., M. Biro, A. Oswald, J.Y. Tinevez, G. Salbreux, and E. Paluch. 2011. Polar actomyosin contractility destabilizes the position of the cytokinetic furrow. *Nature*. 476:462-466.

Shao, L., P. Kner, E.H. Rego, and M.G. Gustafsson. 2011. Super-resolution 3D microscopy of live whole cells using structured illumination. *Nat Methods*. 8:1044-1046.

Sheahan, M.B., C.J. Staiger, R.J. Rose, and D.W. McCurdy. 2004. A green fluorescent protein fusion to actin-binding domain 2 of Arabidopsis fimbrin highlights new features of a dynamic actin cytoskeleton in live plant cells. *Plant physiology*. 136:3968-3978.

Singh, N.S., N. Shao, J.R. McLean, M. Sevugan, L. Ren, T.G. Chew, A. Bimbo, R. Sharma, X. Tang, K.L. Gould, and M.K. Balasubramanian. 2011. SIN-inhibitory phosphatase complex promotes Cdc11p dephosphorylation and propagates SIN asymmetry in fission yeast. *Curr Biol*. 21:1968-1978.

Skoumpla, K., A.T. Coulton, W. Lehman, M.A. Geeves, and D.P. Mulvihill. 2007. Acetylation regulates tropomyosin function in the fission yeast Schizosaccharomyces pombe. *Journal of cell science*. 120:1635-1645.

Smertenko, A.P., M.J. Deeks, and P.J. Hussey. 2010. Strategies of actin reorganisation in plant cells. *Journal of cell science*. 123:3019-3028.

Smith, M.G., S.R. Swamy, and L.A. Pon. 2001. The life cycle of actin patches in mating yeast. *Journal of cell science*. 114:1505-1513.

Snaith, H.A., J. Thompson, J.R. Yates, 3rd, and K.E. Sawin. 2011. Characterization of Mug33 reveals complementary roles for actin cable-dependent transport and exocyst regulators in fission yeast exocytosis. *Journal of cell science*. 124:2187-2199.

Sohrmann, M., C. Fankhauser, C. Brodbeck, and V. Simanis. 1996. The dmf1/mid1 gene is essential for correct positioning of the division septum in fission yeast. *Genes Dev*. 10:2707-2719.

Sohrmann, M., S. Schmidt, I. Hagan, and V. Simanis. 1998. Asymmetric segregation on spindle poles of the Schizosaccharomyces pombe septum-inducing protein kinase Cdc7p. *Genes Dev*. 12:84-94.

Sparks, C.A., M. Morphew, and D. McCollum. 1999. Sid2p, a spindle pole body kinase that regulates the onset of cytokinesis. *The Journal of cell biology*. 146:777-790.

Stark, B.C., T.E. Sladewski, L.W. Pollard, and M. Lord. 2010. Tropomyosin and myosin-II cellular levels promote actomyosin ring assembly in fission yeast. *Mol Biol Cell*. 21:989-1000.

Stirling, P.C., J. Cuellar, G.A. Alfaro, F. El Khadali, C.T. Beh, J.M. Valpuesta, R. Melki, and M.R. Leroux. 2006. PhLP3 modulates CCT-mediated actin and tubulin folding via ternary complexes with substrates. *The Journal of biological chemistry*. 281:7012-7021.

Subramanian, D., J. Huang, M. Sevugan, R.C. Robinson, M.K. Balasubramanian, and X. Tang. 2013. Insight into actin organization and function in cytokinesis from analysis of fission yeast mutants. *Genetics*. 194:435-446.

Takaine, M., O. Numata, and K. Nakano. 2009. Fission yeast IQGAP arranges actin filaments into the cytokinetic contractile ring. *The EMBO journal*. 28:3117-3131.

Takemoto, D., D.A. Jones, and A.R. Hardham. 2003. GFP-tagging of cell components reveals the dynamics of subcellular re-organization in response to infection of Arabidopsis by oomycete pathogens. *The Plant journal : for cell and molecular biology*. 33:775-792.

Tanaka, K., T. Yonekawa, Y. Kawasaki, M. Kai, K. Furuya, M. Iwasaki, H. Murakami, M. Yanagida, and H. Okayama. 2000. Fission yeast Eso1p is required for establishing sister chromatid cohesion during S phase. *Molecular and cellular biology*. 20:3459-3469.

Tang, X., J. Huang, A. Padmanabhan, K. Bakka, Y. Bao, B.Y. Tan, W.Z. Cande, and M.K. Balasubramanian. 2011. Marker reconstitution mutagenesis: a simple and efficient reverse genetic approach. *Yeast*. 28:205-212.

Toi, H., K. Fujimura-Kamada, K. Irie, Y. Takai, S. Todo, and K. Tanaka. 2003. She4p/Dim1p interacts with the motor domain of unconventional myosins in the budding yeast, Saccharomyces cerevisiae. *Mol Biol Cell*. 14:2237-2249.

Tokunaga, M., N. Imamoto, and K. Sakata-Sogawa. 2008. Highly inclined thin illumination enables clear single-molecule imaging in cells. *Nat Methods*. 5:159-161.

Uehara, R., G. Goshima, I. Mabuchi, R.D. Vale, J.A. Spudich, and E.R. Griffis. 2010. Determinants of myosin II cortical localization during cytokinesis. *Curr Biol*. 20:1080-1085.

Vallen, E.A., J. Caviston, and E. Bi. 2000. Roles of Hof1p, Bni1p, Bnr1p, and myo1p in cytokinesis in Saccharomyces cerevisiae. *Mol Biol Cell*. 11:593-611.

van den Ent, F., and J. Lowe. 2006. RF cloning: a restriction-free method for inserting target genes into plasmids. *Journal of biochemical and biophysical methods*. 67:67-74.

van der Honing, H.S., L.S. van Bezouwen, A.M. Emons, and T. Ketelaar. 2011. High expression of Lifeact in Arabidopsis thaliana reduces dynamic reorganization of actin filaments but does not affect plant development. *Cytoskeleton*. 68:578-587.

Van Zeebroeck, G., B.M. Bonini, M. Versele, and J.M. Thevelein. 2009. Transport and signaling via the amino acid binding site of the yeast Gap1 amino acid transceptor. *Nature chemical biology*. 5:45-52.

Vavylonis, D., J.Q. Wu, S. Hao, B. O'Shaughnessy, and T.D. Pollard. 2008. Assembly mechanism of the contractile ring for cytokinesis by fission yeast. *Science*. 319:97-100.

Vidali, L., C.M. Rounds, P.K. Hepler, and M. Bezanilla. 2009. Lifeact-mEGFP reveals a dynamic apical F-actin network in tip growing plant cells. *PloS one*. 4:e5744.

Vishwasrao, H.D., P. Trifilieff, and E.R. Kandel. 2012. In vivo imaging of the actin polymerization state with two-photon fluorescence anisotropy. *Biophysical journal*. 102:1204-1214.

Wachtler, V., S. Rajagopalan, and M.K. Balasubramanian. 2003. Sterol-rich plasma membrane domains in the fission yeast Schizosaccharomyces

pombe. *Journal of cell science*. 116:867-874.

Waddle, J.A., T.S. Karpova, R.H. Waterston, and J.A. Cooper. 1996. Movement of cortical actin patches in yeast. *The Journal of cell biology*. 132:861-870.

Wang, H., and D. Vavylonis. 2008. Model of For3p-mediated actin cable assembly in fission yeast. *PloS one*. 3:e4078.

Wang, J., and D.A. Richards. 2011. Spatial regulation of exocytic site and vesicle mobilization by the actin cytoskeleton. *PloS one*. 6:e29162.

Westphal, M., A. Jungbluth, M. Heidecker, B. Muhlbauer, C. Heizer, J.M. Schwartz, G. Marriott, and G. Gerisch. 1997. Microfilament dynamics during cell movement and chemotaxis monitored using a GFP-actin fusion protein. *Curr Biol*. 7:176-183.

Willig, K.I., B. Harke, R. Medda, and S.W. Hell. 2007. STED microscopy with continuous wave beams. *Nat Methods*. 4:915-918.

Win, T.Z., Y. Gachet, D.P. Mulvihill, K.M. May, and J.S. Hyams. 2001. Two type V myosins with non-overlapping functions in the fission yeast Schizosaccharomyces pombe: Myo52 is concerned with growth polarity and cytokinesis, Myo51 is a component of the cytokinetic actin ring. *Journal of cell science*. 114:69-79.

Winder, S.J., and K.R. Ayscough. 2005. Actin-binding proteins. *Journal of cell science*. 118:651-654.

Wloka, C., and E. Bi. 2012. Mechanisms of cytokinesis in budding yeast. *Cytoskeleton*. 69:710-726.

Wong, K.C., N.I. Naqvi, Y. Iino, M. Yamamoto, and M.K. Balasubramanian. 2000. Fission yeast Rng3p: an UCS-domain protein that mediates myosin II assembly during cytokinesis. *Journal of cell science*. 113 ( Pt 13):2421-2432.

Wong, W.W., T.C. Doyle, P. Cheung, T.M. Olson, and E. Reisler. 2001. Functional studies of yeast actin mutants corresponding to human cardiomyopathy mutations. *Journal of muscle research and cell motility*. 22:665-674.

Wu, J.Q., J.R. Kuhn, D.R. Kovar, and T.D. Pollard. 2003. Spatial and temporal pathway for assembly and constriction of the contractile ring in fission yeast cytokinesis. *Developmental cell*. 5:723-734.

Wu, J.Q., and T.D. Pollard. 2005. Counting cytokinesis proteins globally and locally in fission yeast. *Science*. 310:310-314.

Wu, J.Q., V. Sirotkin, D.R. Kovar, M. Lord, C.C. Beltzner, J.R. Kuhn, and T.D. Pollard. 2006. Assembly of the cytokinetic contractile ring from a broad band of nodes in fission yeast. *The Journal of cell biology*. 174:391-402.

Xu, K., H.P. Babcock, and X. Zhuang. 2012. Dual-objective STORM reveals three-dimensional filament organization in the actin cytoskeleton. *Nat Methods*. 9:185-188.

Xu, Y., J.B. Moseley, I. Sagot, F. Poy, D. Pellman, B.L. Goode, and M.J. Eck. 2004. Crystal structures of a Formin Homology-2 domain reveal a tethered dimer architecture. *Cell*. 116:711-723.

Yan, H., and M.K. Balasubramanian. 2012. Meiotic actin rings are essential for proper sporulation in fission yeast. *Journal of cell science*. 125:1429-1439.

Yang, H.C., and L.A. Pon. 2002. Actin cable dynamics in budding yeast. *Proceedings of the National Academy of Sciences of the United States of America*. 99:751-756.

Yi, J., X.S. Wu, T. Crites, and J.A. Hammer, 3rd. 2012. Actin retrograde flow and actomyosin II arc contraction drive receptor cluster dynamics at the immunological synapse in Jurkat T cells. *Mol Biol Cell*. 23:834-852.

Yonetani, A., and F. Chang. 2010. Regulation of cytokinesis by the formin cdc12p. *Curr Biol*. 20:561-566.

Yonetani, A., R.J. Lustig, J.B. Moseley, T. Takeda, B.L. Goode, and F. Chang. 2008. Regulation and targeting of the fission yeast formin cdc12p in cytokinesis. *Mol Biol Cell*. 19:2208-2219.

York, A.G., A. Ghitani, A. Vaziri, M.W. Davidson, and H. Shroff. 2011. Confined activation and subdiffractive localization enables whole-cell PALM with genetically expressed probes. *Nat Methods*. 8:327-333.

Young, M.E., J.A. Cooper, and P.C. Bridgman. 2004. Yeast actin patches are networks of branched actin filaments. *The Journal of cell biology*. 166:629-635.

Yu, J.H., A.H. Crevenna, M. Bettenbuhl, T. Freisinger, and R. Wedlich-Soldner.

2011. Cortical actin dynamics driven by formins and myosin V. *Journal of cell science*. 124:1533-1541.

Zhang, D., A. Vjestica, and S. Oliferenko. 2010. The cortical ER network limits the permissive zone for actomyosin ring assembly. *Curr Biol*. 20:1029-1034.

Zhou, M., and Y.L. Wang. 2008. Distinct pathways for the early recruitment of myosin II and actin to the cytokinetic furrow. *Mol Biol Cell*. 19:318-326.